Aalto University

School of Science

Master's Programme in Life Science Technologies

Satu Pallasaho

Retinal Pigment Epithelium Heating Treatment for Age-Related Macular Degeneration

Master's Thesis

Espoo, July 29, 2019

Supervisor: Ari Koskelainen, Professor

Thesis advisors: Teemu Turunen, MS.c. (Tech.)

Marja Pitkänen, MS.c. (Tech.)

Aalto-yliopisto
Perustieteiden
korkeakoulu

Abstract of the Master's Thesis

Author: Satu Pallasaho

Title of the thesis: Retinal Pigment Epithelium Heating Treatment for Age-Related Macular Degeneration

Study program: Life Science Technologies

Supervisor: Prof. Ari Koskelainen

Major or minor/code: Biomedical Engineering / SCI3059

Thesis advisors: M.Sc. Teemu Turunen, M.Sc. Marja Pitkänen

Date: 29.7.2019 **Number of pages:** 109 + 7 **Language:** English

Age-related macular degeneration (AMD) is a degenerative disease of the retina. The pathogenesis of AMD is not known, but several mechanisms have been proposed. This Master's thesis introduces theories related to reduced nutrient and oxygen delivery to retina, chronic inflammation, oxidative stress and malfunction of mechanisms maintaining protein homeostasis.

Laser heating treatment of the retina is promising treatment modality for AMD. Heating of retina has been observed to induce several changes in the retinal cells. One of the observed changes is the heat shock response. During the heat shock response, cells produce heat shock proteins (HSPs) that maintain protein homeostasis, inhibit the inflammatory response and prevent cell death. Heat shock induction after laser heating may offer a novel therapeutic approach to prevent the progression of AMD.

The treatment temperature and duration have to be selected carefully. The temperature needs to be sufficiently high to induce a heat shock response but low enough to prevent cell death. With a longer treatment duration, a lower temperature is needed. This Master's thesis utilizes electroretinography (ERG) based method to assess retinal temperature during treatment. The purpose of this Master's thesis was to study how laser heating treatment affects the retinal function in mice.

We found substantial variation in power needed to reach the same temperature increase in different mice. This finding supports the usage of temperature determination method during heating treatment. Histological analysis revealed increased HSP expression and signs of cell death within the heated area. The amount of HSP correlated with the used heating laser power.

Keywords: Retinal laser treatment, pigment epithelium, heat shock protein, age-related macular degeneration, electroretinography

Aalto-yliopisto
Perustieteiden
korkeakoulu

Diplomityön tiivistelmä

Tekijä: Satu Pallasaho

Työn nimi: Pigmenttiepiteelin lämmitys silmänpohjan ikärappeuman hoitona

Koulutusohjelma: Life Science Technologies

Valvoja: Prof. Ari Koskelainen

Pää tai sivuaine/koodi: Biomedical Engineering / SCI3059

Työn ohjaaja(t): DI Teemu Turunen, DI Marja Pitkänen

Päivämäärä: 29.7.2019 **Sivumäärä:** 109 + 7 **Kieli:** Englanti

Silmänpohjan ikärappeuma on silmän verkkokalvoa rappeuttava sairaus. Sairauden syntymekanismia ei tunneta, mutta siitä on esitetty useita teorioita. Tässä työssä esitellään silmänpohjan ikärappeuman syntyyn liittyviä teorioita, jotka käsittelevät muutoksia verkkokalvon ravinteiden ja hapen saannissa, kroonista tulehdusreaktiota, oksidatiivista stressiä ja solujen proteiinitasapainon säätelytekijöiden häiriöitä.

Verkkokalvon lämmittäminen laserilla on lupaava hoitomuoto silmänpohjan ikärappeumalle. Verkkokalvon lämmityksen on havaittu aiheuttavan useita muutoksia verkkokalvon soluissa. Eräs havaituista muutoksista on lämpöshokkireaktio, jossa solut tuottavat lämpöshokkiproteiineja. Lämpöshokkiproteiinit ylläpitävät solun proteiinitasapainoa, säätelevät tulehdusreaktiota sekä ehkäisevät solukuolemia. Lämpöshokkiproteiinien eritys lämmityshoidon jälkeen saattaa tarjota uuden hoitomuodon silmänpohjan ikärappeuman etenemisen pysäyttämiseksi.

Hoidon aikainen verkkokalvon lämpötila ja hoidon kesto on valittava huolellisesti. Lämpötilan on oltava tarpeeksi korkea aiheuttaakseen lämpöshokkireaktion, mutta riittävän matala solukuolemien välttämiseksi. Pidemmillä lämmityksen kestoilla sopiva lämpötila on alhaisempi. Tässä työssä käytettiin elektroretinografiaan (ERG) perustuvaa lämpötilan arviointimenetelmää, joka mahdollistaa verkkokalvon lämpötilan arvioinnin hoidon aikana. Työn tavoitteena on tutkia, millaisia vaikutuksia laserhoidolla on verkkokalvoon.

Havaitsimme hiirten välillä merkittävää vaihtelua tehossa, joka tarvittiin samansuuruisen lämpötilannousun aikaansaamiseksi. Tämä havainto tukee lämpötilanarviointimenetelmän käyttöä lämmityshoidon aikana. Histologinen analyysi paljasti lämpöshokkiproteiinien määrän lisääntyneen lämmitetyllä alueella sekä merkkejä solukuolemista. Lämpöshokkiproteiinien määrän korreloi käytetyn lämmityslaserin tehon kanssa.

Avainsanat: Verkkokalvon laserhoito, pigmenttiepiteeli, lämpöshokkiproteiini, silmänpohjan ikärappeuma, elektroretinografia

Foreword

The Master's thesis was written as a part of ongoing research in the Department of Neuroscience and Biomedical Engineering (NBE) of Aalto University. The writing process has been demanding but highly rewarding. Therefore, it is somewhat bittersweet that it is ending. I hope that the future will bring me equally satisfactory challenges.

I am grateful to my supervisor Ari Koskelainen for giving me the opportunity to work in his pioneering research group and providing this exciting Master's thesis topic. Especially, I want to thank my instructors Marja Pitkänen and Teemu Turunen for introducing me to the world of retinal research. I am grateful for their willingness to share their expertise in experimental research. They have helped me in many ways throughout the writing process.

I also want to express my gratitude to Mooud Amirkavei for her invaluable help in the staining and imaging of the tissue samples and Ossi Kaikkonen for his technical support regarding the heating device. For their advice in immunohistochemistry, I want to thank Helder André, Soile Nymark, Teemu Ihalainen, and Julia Johansson.

In addition, I am grateful for my parents for supporting me in every step of my studies. I warmly thank my partner Markus for always being there for me and our cat Winston for an extremely relaxed writing company.

Table of Contents

Abbreviations

ADP	Adenosine diphosphate
ALS	Amyotrophic lateral sclerosis
AMD	Age-related macular degeneration
AMPK	Adenosine monophosphate-activated protein kinase
ANOVA	Analysis of variance
APOE	Apolipoprotein E
AREDS	Age-Related Eye Disease Study
ATP	Adenosine triphosphate
bFGF	Basic fibroblast growth factor
C3	Complement factor 3
CFH	Complement factor H
CFI	Complement factor I
cGMP	Cyclic guanosine monophosphate
CNV	Choroidal neovascularization
CRP	C-reactive protein
CTD	C-terminal transactivation domain of HSF
DAMP	Danger-associated molecular pattern
DBD	DNA-binding domain of HSF
DNA	Deoxyribonucleic acid
ERG	Electroretinography
GHS	Glutathione
GSSG	Oxidized glutathione
hESC	Human embryonic stem cell
HIER	Heat-induced epitope retrieval
HIF	Hypoxia-inducible factor
Hip	HSPA interacting protein

Hop	HSPA/HSPC organizing protein
HSE	Heat shock element
HSF	Heat shock factor
HSP	Heat shock protein
IL	Interleukin
iPSC	Induced pluripotent stem cell
IQR	Inter-quartile range
LZ1-3	Leucine zipper 1-3 domain of HSF
LZ4	Leucine zipper 4 domain of HSF
MDA	Malondialdehyde
miRNA	Micro-RNA
MMP	Matrix metalloproteinase
mtDNA	Mitochondrial DNA
NADPH	Nicotinamide adenine dinucleotide phosphate
NBD	Nucleotide-binding domain of HSP
nDNA	Nuclear DNA
NEF	Nucleotide exchange factor
NFκB	Nuclear factor-κB
NLR	Nucleotide-binding oligomerization domain-like receptor
NLRP3	Nucleotide-binding domain, leucine-rich-containing family, pyrin domain-containing-3
NSAID	Nonsteroidal anti-inflammatory drug
PAMP	Pathogen-associated molecular pattern
PDE	Phosphodiesterase
PEDF	Pigment epithelium-derived factor
PDT	Photodynamic therapy
PIER	Protease induced epitope retrieval
PRR	Pattern recognition receptor

PUFA	Polyunsaturated fatty acid
RD	Regulatory domain of HSF
RNA	Ribonucleic acid
ROS	Reactive oxygen species
RPE	Retinal pigment epithelium
RPESC	Retinal pigment epithelial stem cell
SBD	Substrate binding domain of HSP
SDM	Subthreshold diode micropulse photocoagulation
SEM	Standard error of the mean
SRT	Selective retinal therapy
STD	Standard deviation
TGF-β	Transforming growth factor
TIMP	Tissue inhibitor of metalloproteinase
TS-R	Thermal stimulation of the retina
TTM	B-wave time-to-maximum
TTT	Transpupillary thermotherapy
UPS	Ubiquitin-proteasome system
VEGF	Vascular endothelial growth factor
4-HNE	4-hydroxynonenal

Introduction

Vision is considered to be the most important sense of humans. It provides us the most of the information about the surrounding world since the majority of human sensory cells are located in the retina [1]. The leading cause of irreversible vision loss in people over 50 years old in western countries is age-related macular degeneration (AMD) [2]. AMD has detrimental effects on the quality of life. AMD patients suffer more often from depression compared to similarly aged people without AMD [3]. In addition, AMD increases the risk of falls and other injuries and reduces patients' ability to cope in everyday situations [4, 5].

AMD is a degenerative disease of the retina. The pathogenesis of AMD is not known in detail. However, AMD has been associated with changes in Bruch's membrane and choroidal blood flow, to chronic inflammation, to oxidative stress, and to the retinal accumulation of cellular debris. [6] The disease is divided into wet and dry forms, dry form being more common [7]. Currently, there is no treatment for dry AMD [8].

Laser heating of the retina is considered as a potential treatment for AMD. Laser heating treatments include cell death-inducing modalities as well as cell death avoiding subthreshold modalities. The aim of subthreshold treatments is to induce positive changes in retinal function by heating retinal pigment epithelium (RPE) cells. One of the observed heating-induced changes is the heat shock response in which RPE cells increase the expression of heat shock proteins (HSPs). In this Master's thesis, we studied a specific HSP-family, HSPA. HSPAs are molecular chaperones that assist in the correct folding of proteins, promote refolding and degradation of misfolded proteins and prevent the formation of harmful protein aggregates [9]. In addition, HSPAs are regulators of cell death and inflammation [10, 11]. All of these qualities may be useful in the treatment of AMD and, therefore, increased HSPA expression by laser heating may offer a novel therapeutic approach to prevent the progression of AMD.

Induction of heat shock response without causing cell death requires a careful selection of the treatment temperature and duration. The temperature needs to be sufficiently high to induce a heat shock response but low enough to prevent cell death. With a longer treatment duration, a lower temperature is needed. The retinal temperature during the treatment is affected by heating laser parameters and individual properties such as fundus pigmentation, choroidal blood flow and transparency of ocular media [12 - 14]. Therefore, the same laser parameters cannot be used to induce the same temperature elevation in all

patients and in all locations in the patient's retina. The lack of a method to estimate retinal temperature during treatment has thus slowed down the development of these treatments. This Master's thesis utilizes a temperature estimation method developed by Pitkänen et al. [15] to assess retinal temperature during heating treatment. This method is based on the temperature dependent properties of electroretinography (ERG) signal. ERG signal is caused by changes in a flow of ions in the extracellular space of retinal cells and is used clinically to evaluate the retinal function and to diagnose retinal disorders [16, 17].

The purpose of this Master's thesis was to study how laser heating treatment of the RPE affects the retinal function in mice. The extent of variation in treatment power needed to reach the same temperature elevation in different individuals was assessed and the accuracy of the temperature estimation method in temperatures above the temperatures to which the estimation method was calibrated was investigated. Moreover, the effect of laser treatment on retinal pigment epithelium HSPA content and cell viability was examined using immunostaining. In addition, the literature was reviewed to facilitate greater understanding of mechanisms of heat shock protein expression and function, AMD pathogenesis and current treatment modalities of AMD. The overall aim of this Master's thesis was to provide information for the ongoing research in the Department of Neuroscience and Biomedical Engineering (NBE) of Aalto University aiming to develop a novel subthreshold heating treatment for AMD.

The literature review of this Master's thesis begins by introducing the structure and operation of the human eye. The second chapter explores heat shock response and focuses on HSPA family. Chapter three introduces AMD and is followed by Chapter four that outlines possible mechanisms contributing to the development of AMD. Chapter five presents the main treatment methods for AMD. The literature review is followed by the experimental part of the thesis. Chapters six and seven describe the used methods and the acquired results. Finally, the results are discussed in Chapter eight.

1. Structure and Operation of Eye

To humans, vision provides more information about the surrounding world than the other senses together since about 70 percent of the human sensory cells are located in the eye. The eye is a highly specialized and adaptable organ. It allows us to see in versatile lighting conditions as well as to focus on objects at different distances. [1] This chapter presents the structure of the human eye focusing more deeply on the structure and operation of the retina and introduces the differences in the structure of the human and mouse eye.

1.1 Human Eye

Figure 1 presents the structure of the human eye. The eyeball consists of three layers. The outermost layer, fibrous tunic, consists of sclera and cornea. The sclera is a layer of dense connective tissue that supports the eye. The transparent cornea covers the anterior part of the eyeball. Its curved shape helps to focus incoming light onto the retina. The middle layer, vascular tunic, consists of the choroid, ciliary body, and iris. The highly vascularized choroid covers most of the inner surface of the sclera. It provides nutrition for the innermost layer and prevents reflection of light by absorbing it. The ciliary body and the iris are located in the anterior part of the eye. The iris has opening in the middle called pupil and the muscles of iris adjust the size of the pupil thereby controlling the amount of light entering the eye. The innermost layer consists of the retina which lines posterior parts of the eyeball. It contains photoreceptor cells capable of sensing light. [18]

The area at the center of the retina is named after its yellowish pigments as macula lutea (in Latin *macula* “a small flat spot”, *lute-* “yellowish”). The center of the macula is referred to as the fovea. The fovea is the area of the highest visual acuity. [18] Optic disk is the location where the optic nerve exits the eye and the retinal blood vessels enter the eye. The optic disk lacks photoreceptor cells and therefore no visual sensation can arise from this region. [19]

The transparent lens is located behind the pupil and iris. The ciliary body changes the shape of the lens to focus the incoming light to the retina. Lens divides the interior part of the eyeball into two cavities. The posterior cavity contains transparent gel, vitreous humor. The anterior cavity is divided into the anterior chamber and posterior chamber and is filled with aqueous humor, a transparent fluid that nourishes lens and cornea. [18]

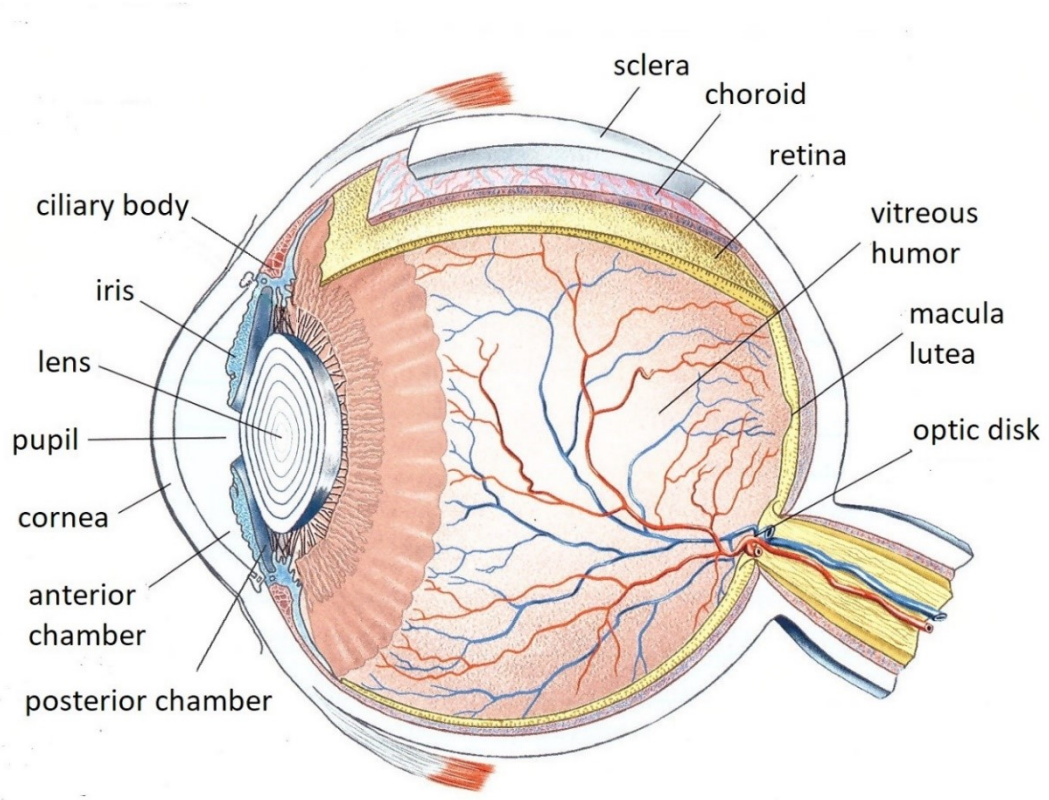

Figure 1. *Structure of the human eye. [1, modified]*

1.2 Human Retina

The retina contains several different types of cells that are organized into layers. Figure 2 presents the structure of the retina. The outermost layer of the retina is retinal pigment epithelium (RPE). Photoreceptors, the light-sensing cells of the retina, are located proximal to the pigment epithelium. They transmit the information of light into bioelectrical signals in a process referred to as phototransduction. Photoreceptors consist of outer and inner segments. Outer segments contain photopigments that absorb incoming light. Inner segments, in turn, contain cell organelles such as nucleus, mitochondria and Golgi complex and form the outer nuclear layer of the retina. The information of light is transmitted from photoreceptors to bipolar cells via synapses located in the outer plexiform layer. Bipolar cell nuclei form the inner nuclear layer. Bipolar cells pass the information of light to ganglion cells via synapses located in the inner plexiform layer. The cell bodies of ganglion cells are located in the ganglion cell layer. Ganglion cell axons form optic nerve that forwards the information to the rest of the brain. [19]

Horizontal cells and amacrine cells modify retinal signaling via lateral connections [19]. Horizontal cells receive information from photoreceptor cells and are responsible for lateral inhibition of bipolar cells [20]. Amacrine cells have various functions in the information processing of the retina [21]. They receive information from bipolar cells and form synaptic connections back to bipolar cells, amacrine cells and ganglion cells [19].

The retina has a high metabolism and it consumes most oxygen per unit weight of the human tissues. It receives oxygen from two different circulatory systems: choroidal and retinal vessels. Retinal vessels supply oxygen and nutrients to the inner parts of the retina. [22] The outer retina receives nutrients and oxygen from the choroid. Photoreceptors are the most oxygen-consuming cells in the retina: they consume over 90 % of the oxygen delivered to the retina. In order to meet this high oxygen demand, the choroid has a especially high blood flow. The choroidal blood flow per unit tissue weight is ten-fold higher than in the brain. [23]

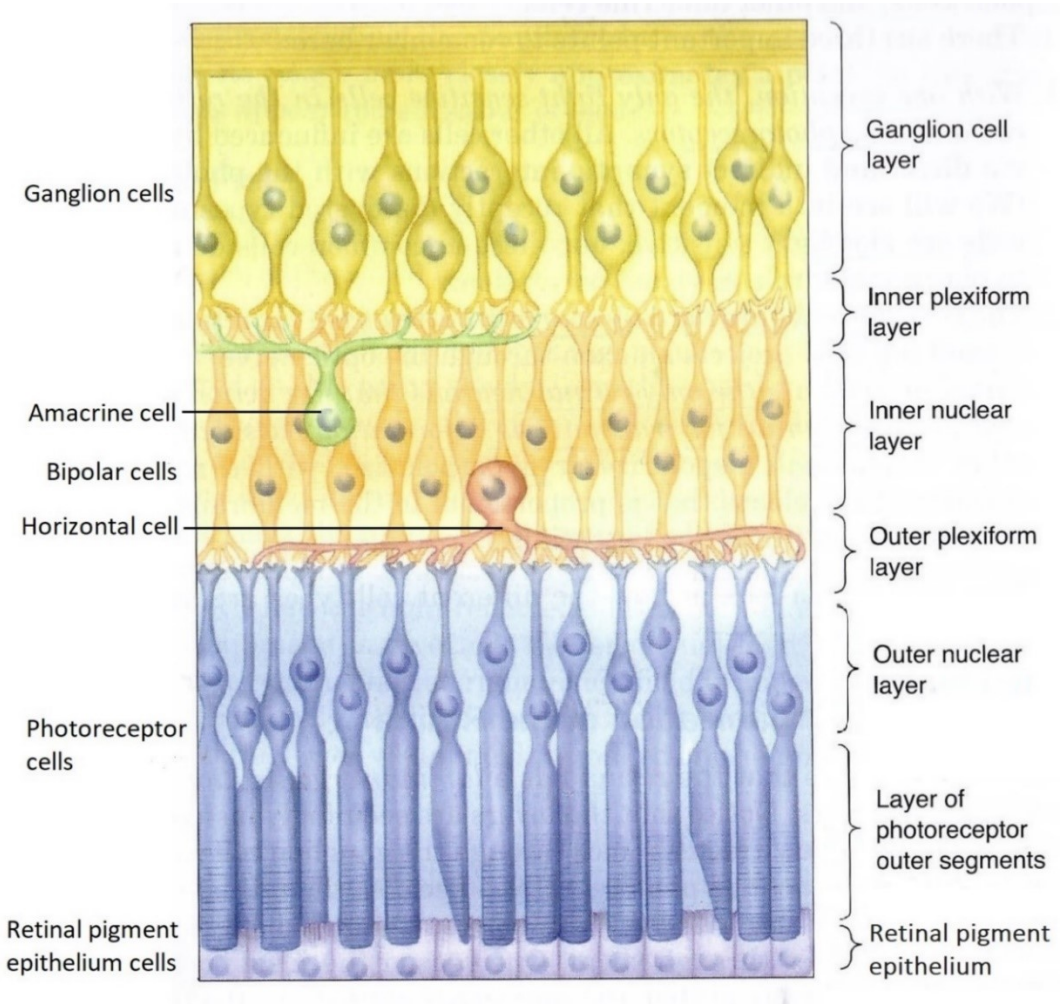

Figure 2. *The laminar structure of the retina. [18, modified]*

1.2.1 Photoreceptor Cells

Photoreceptors are divided into rods and cones. Rods are specialized to function in dim light whereas cones are less sensitive to light and thus function in brighter lighting conditions. The human retina contains three types of cones. Each of them is sensitive to a different spectrum of light allowing discrimination of colors. [18] Cones are divided to short-wavelength, medium-wavelength and long-wavelength cones that are the most sensitive to light with wavelength approximately 430 nm, 530 nm and 560 nm respectively [19]. This chapter focuses mainly on the rod cells because they were essential in the experimental part of this Master's thesis.

Figure 3 shows the structure of photoreceptor cells. Photoreceptor cells are divided into outer and inner segments. Photopigments are located in the outer segment whereas components necessary for the metabolism of the cell such as cell nucleus, Golgi complex and mitochondria are located in the inner segment. The synaptic terminal is located at the end of the inner segment. [18]

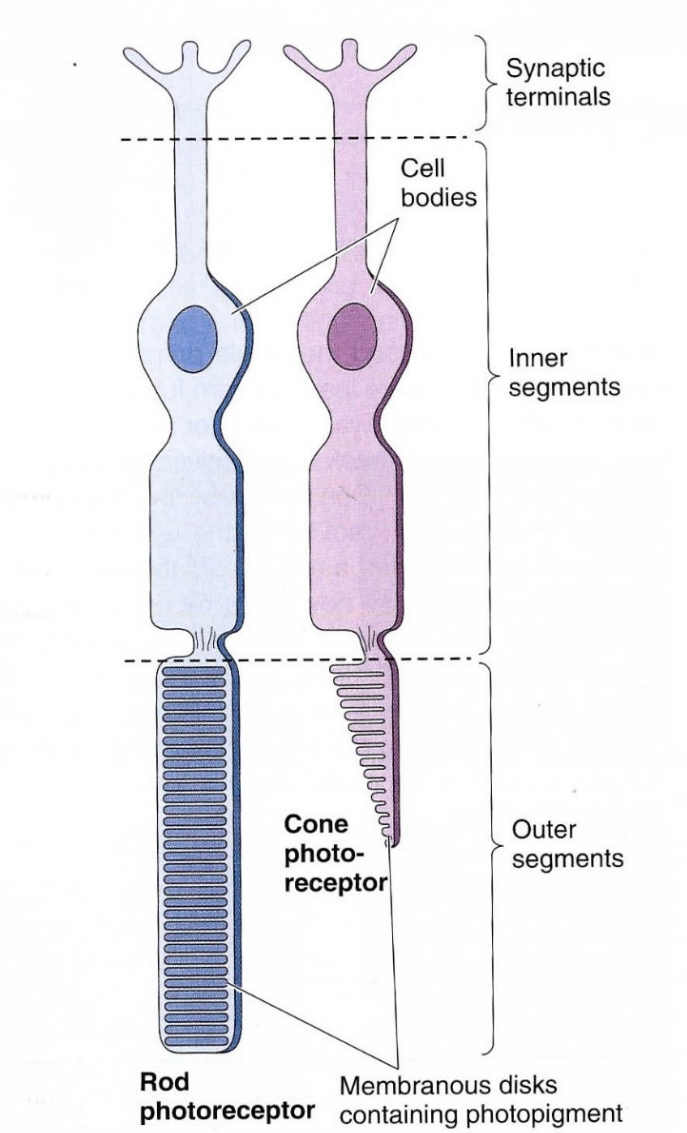

Figure 3. *Photoreceptor cell structure. [19, modified]*

All neurons, including photoreceptors, actively maintain ion concentration differences between intracellular and extracellular fluid. These differences are important for cell viability. The differences in ion concentration between the intracellular and extracellular fluids creates an electrical potential difference across the plasma membrane that is referred to as the membrane potential. In the resting state of the cell, the intracellular fluid has negative potential compared to the extracellular fluid. This resting state potential difference is referred to as resting membrane potential, and by convention, it has a negative value. [19]

Membrane potential can change in response to alterations in the permeability of the cell membrane to ions [19]. The phospholipid bilayer of the plasma membrane is impermeable to ions but ions can move through the cell membrane via ion channels formed by proteins embedded in the membrane. The opening of ion channels can be regulated by binding of ligand molecules, membrane potential or mechanical stimulus. Cell can also move ions against their electrochemical gradient using exchangers and pumps. [21] Changes in membrane permeability can lead to hyperpolarization where membrane potential becomes more negative or to depolarization where membrane potential becomes less negative compared to the resting membrane potential [19].

Resting membrane potential of a typical neuron is -65 mV whereas resting membrane potential of rod in complete darkness is approximately -30 mV. This difference in resting membrane potential is a result of photoreceptor dark current. The dark current is caused by the inflow of cations such as Na^+ and Ca^{2+} through cyclic guanosine monophosphate (cGMP) gated channels that are located in the outer segment. [19] This inflow is compensated by the outflow of K^+ ions through K^+ selective ion channels in the inner segment [18]. Na^+ ions are returned to extracellular space and K^+ ions to intracellular space by Na^+/K^+ pumps located in the inner segment cell membrane [21]. The dark current maintains rod cell depolarization [18]. In the depolarized state of the cell, L-type calcium channels located near the synaptic terminal are open letting Ca^{2+} ions into the cell. The open state of the L-type calcium channels facilitates intracellular calcium concentration that results in the release of neurotransmitter glutamate at the synaptic terminal. [21]

Figure 4 shows a schematic presentation of the rod light response. When a photon arrives to a rod cell, it may be absorbed by a photopigment molecule, rhodopsin, in the rod outer segment. This absorption activates the photopigment molecule and is the first step in phototransduction. [19] The activation results in a conformation change in rhodopsin which allows it to induce separation of α-subunit from G-protein transducin. Transducin α-subunit, in turn, activates phosphodiesterase (PDE) that hydrolyzes cGMP molecules and therefore causes a decrease in the cytoplasmic concentration of cGMP. The probability of cGMP gated ion channels being in open state increases when cGMP molecules are bound to them. Therefore, the decrease in cytoplasmic cGMP concentration leads to a higher probability of cGMP-gated ion channels being in a closed state. [24] Closure of cGMP gated channels in the outer segment reduces dark current by preventing the inflow of Na^+ and Ca^{2+} ions. [19] However, the outflow of K^+ ions from the inner segment continues resulting in hyperpolarization of the cell. This hyperpolarization leads to the closure of L-type Ca^{2+} channels and decrease in outer segment intracellular calcium concentration which results

in a reduction in the release of glutamate to the synaptic cleft. [21] The reduction of glutamate release is detected by bipolar cells [19].

In addition to the inner segment, outer segment calcium concentration decreases after the closure of cGMP channels. Closure of cGMP channels prevents the inflow of Ca^{2+} ions through them. However, photoreceptor outer segment actively removes calcium ions and this removal continues during photoexcitation resulting in a decrease in the outer segment calcium level. [21] This reduction results in the accelerated synthesis of cGMP by activation of guanylate cyclase. After photoexcitation, rhodopsin, transducin and PDE are deactivated and the photoreceptor cell returns to its resting state. [24]

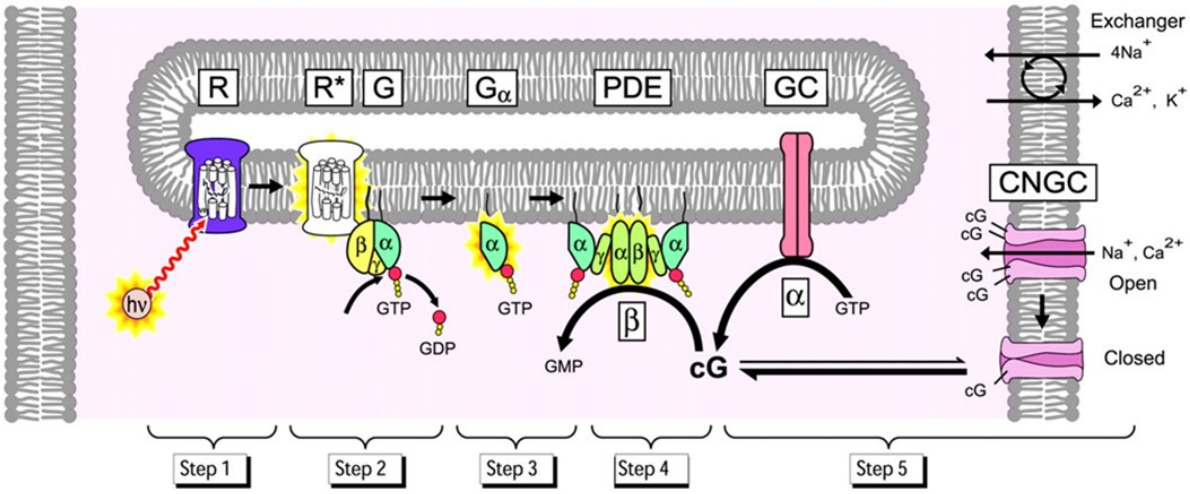

Figure 4. *Schematic presentation of the phototransduction cascade. Abbreviations used in the figure are: photon (hv), rhodopsin (R), activated rhodopsin (R*), transducin (G), α subunit of transducin (G_α), phosphodiesterase (PDE), cGMP (cG), cGMP-gated channel (CNGC), guanylate cyclase (GC). [25]*

1.2.2 Bipolar Cells

Bipolar cells can be divided into ON and OFF cells based on their response to the reduction of glutamate release from photoreceptors. ON bipolar cells respond to the reduction in glutamate by depolarizing whereas OFF bipolar cells respond by hyperpolarizing. The difference in response is caused by the presence of different glutamate receptors in the bipolar cell membrane. The receptors of OFF bipolar cells are ligand-gated ion channels, which have a higher probability to be open when glutamate is bound to them. When open, these ion channels facilitate the inward movement of Na^+ ions depolarizing the cell. However, the light-induced reduction of glutamate release from photoreceptor cells causes

these ion channels to close leading to hyperpolarization of the cell. In contrast, ON bipolar cells have glutamate receptors that cause hyperpolarization when glutamate is bound to them. Therefore, these cells depolarize when glutamate release from photoreceptor cells decreases. [19]

In addition to having direct synaptic connections to photoreceptor cell, bipolar cells are also connected to other photoreceptors via horizontal cells. When a photoreceptor cell hyperpolarizes in response to light, also the horizontal cells connected to it hyperpolarize. Therefore, when light is shone to the eye, ON bipolar cell may receive a depolarizing signal via direct connection to photoreceptor cell and additional hyperpolarizing signal via horizontal cells connected to other hyperpolarized photoreceptor cells. This lateral inhibition is one of the mechanisms that allow information processing at the outer plexiform layer of the retina. [19]

1.2.3 Retinal Pigment Epithelium

The retinal pigment epithelium (RPE) consists of a single layer of epithelial cells that contain high amounts of pigment granules. These granules carry melanin and are therefore referred to as melanosomes. [7] The RPE melanosome content varies topographically. The amount is lowest in the macular area and increases towards the periphery of the retina. [26] Topographical changes may arise from the topographical development of RPE that causes posterior and peripheral RPE to undergo differentiation at different times and locations. In addition, the variation of melanosome content among patches of cells and differences between cells can be remarkable. [27]

RPE cells are attached to the anterior layer of Bruch's membrane. The apical surface of RPE cells faces the photoreceptor outer segments and the basolateral surface faces the Bruch's membrane. RPE has close structural connections with photoreceptors by fingerlike processes that extend in between photoreceptor outer segments. [7]

RPE has multiple important metabolic and supportive functions. It participates in the renewal of photoreceptor by phagocytosing and degrading the tips of photoreceptor outer segments. The shedding is balanced by the continuous growth of outer segments at their base. [28] In addition, RPE supports photoreceptor function by regenerating bleached visual pigments as well as transporting molecules and ions between photoreceptors and the choroid [28, 29]. Moreover, RPE expresses growth factors and secretes components

that create a specific extracellular matrix, interphotoreceptor matrix that is important for the maintenance of photoreceptor cells [28, 30].

1.2.4 Bruch's Membrane

Bruch's membrane is a connective tissue that lies between RPE and choroid. It has three layers: two collagenous layers and elastic layer in between them. [31] Bruch's membrane has several functions. It regulates the diffusion of molecules and ions between choroid and RPE. In addition, it provides physical support for RPE cell adhesion and surface for migration. Moreover it acts as a barrier that restricts the migration of choroidal cells preventing blood vessel growth to the retina. [7]

Transport through Bruch's membrane occurs via passive diffusion. The diffusion rate is affected by the composition of membrane and concentrations of particles on both sides of the membrane. Changes in the Bruch's membrane related to age, genetics, environmental factors, and disease state affect its permeability to different substances. [7]

1.3 Mouse Eye

In this Master's thesis, the effect of retinal laser heating treatment was studied with mice. The structure of the mouse eye is highly similar to the human eye. Figure 5 illustrates schematic presentations of human and mouse eye cross-sections. Differences between the mouse and human eye include the lack of macula, smaller eye diameter as well as larger pupil diameter and lens size compared to the diameter of the eye. In addition, the mouse has only two cone pigments corresponding to short-wavelength and medium-wavelength pigments found in humans. The absence of long-wavelength pigment results in the reduced ability of the mouse to see long-wavelength light compared to humans. [32]

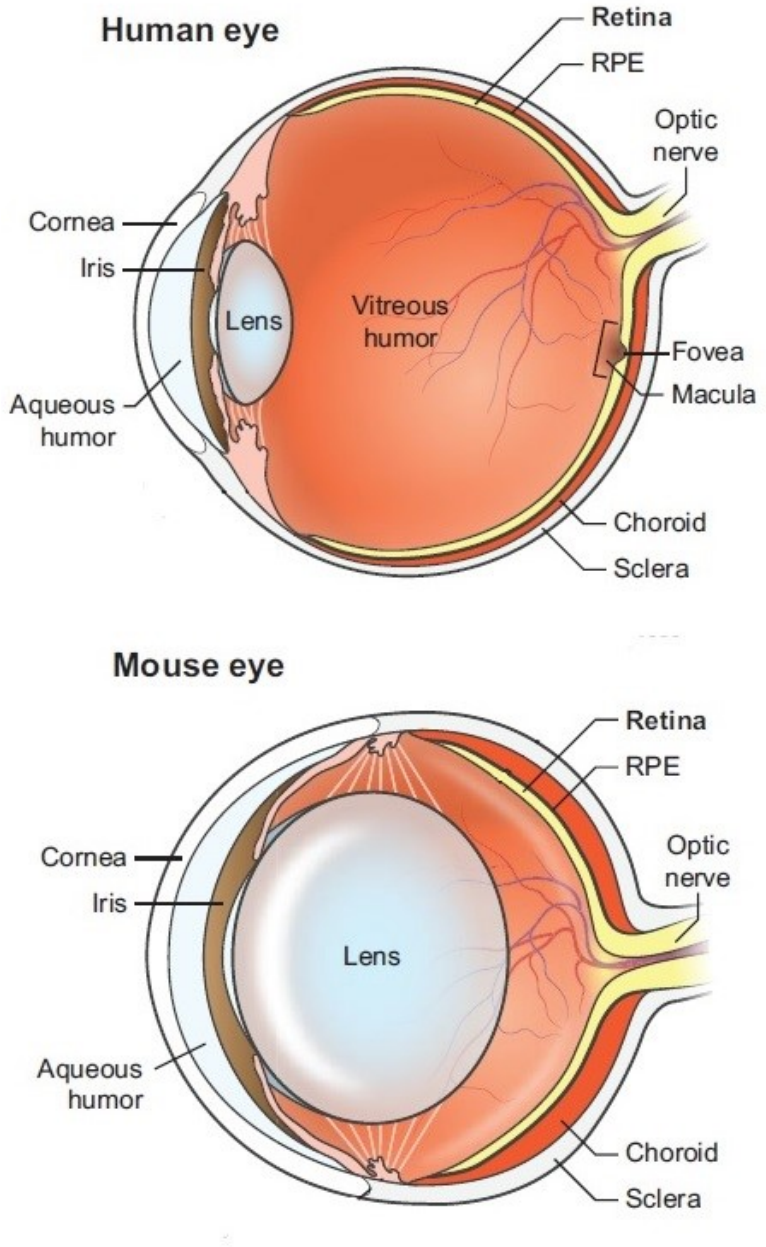

Figure 5. *Schematic presentation of the structure of human and mouse eye. [32, modified]*

The retinal structure of mice is similar to humans. The most prominent difference in the mouse retina compared to the human retina is the lack of macula. [33] Approximately 97 % and 95 % of the photoreceptors are rods in mouse and human retina, respectively [19, 34]. In the human retina, most of the cone cells are located in the fovea and their proportion reduces significantly to the periphery. The human central fovea does not contain rods. [19] However, the rod to cone ratio of peripheral parts of the human macula is similar to the central mouse retina [33].

In addition, the photoreceptor cell density of mouse central retina is greater than in human macula. This results in the higher phagocytic load of mouse central RPE compared to the human macula. Moreover, the central region of both mouse and human retina has higher photoreceptor cell density and thinner Bruch's membrane compared to the peripheral retina. However, the magnitudes of these differences between central and peripheral retina are larger in humans. [33]

2. Heat Shock Response

Cells of homothermic species, such as human, have specialized to function in a specific temperature. Deviation from this temperature affects various cellular functions and thus poses a threat to their survival. Even a small increase in temperature can lead to protein unfolding and aggregation. Moreover, temperature increase damages cytoskeleton and affects nuclear processes. The extent of defects depends on the magnitude and duration of temperature elevation. Accumulation of these defects can lead to cell death. In order to cope with increased temperature, cells have developed a specific cellular response mechanism, heat shock response. In heat shock response, the cell increases the synthesis of protein repairing chaperones, heat shock proteins (HSPs). [35] HSPs are also produced in response to other protein-damaging stress stimuli such as ischemia, nutrient deprivation, irradiation and infection [36].

The structure of HSPs is highly conserved across species which suggest that they play a vital role in cellular survival. They are present in various cellular locations such as cytosol, mitochondria, endoplasmic reticulum, and nucleus. [37] HSPs are divided into following families based on their molecular weight: HSPA (HSP70), HSPH (HSP110), HSPC (HSP90), DNAJ (HSP40), HSPB (small HSPs) and chaperonin families HSPD (HSP60) and HSPE (HSP10). [38] There are several different naming conventions for HSPs. The nomenclature proposed by Kampinga et al. [39] is used in this Master's thesis.

2.1 HSPA Family

HSPA family is the most widely studied class of HSPs. It contains at least 13 proteins that are listed in Table 1. [40] HSPA family members differ from each other by amino acid sequence, expression level and subcellular localization [41]. Some of the HSPA family members are expressed constitutively whereas others are expressed in response to stress [40]. Stress-inducible members of HSPA family are HSPA1A, HSPA1B, HSPA6, HSPA7, and HSPA14 [36]. It has been proposed that the purpose of these proteins is to repair damages caused by abnormal conditions whereas the other HSPA family members have house-keeping functions [41].

HSPA1A and HSPA1B are the most studied members of the HSPA family [41]. They are the major stress-inducible members of HSPA family. Together HSPA1A and HSPA1B are also

sometimes referred to as HSP70-1 or HSP70. The amino acid sequence of these two proteins is very similar differing only by two amino acids. [36]

Table 1. *Members of HSPA family [36, 39, 41]*

Protein name	**Other names**	**Localization**	**Stress-induced**
HSPA1A	HSP70-1, HSP72, HSPA1, HSP70, HSP1-a, HSP70-1A, HSP70i	Cytosol, nucleus, lysosomes, cell membrane, extracellular exosomes	Yes
HSPA1B	HSPA70-2, HSP70-1, HSP72, HSP70, HSP1-b, HSP70-1B	Cytosol, nucleus, lysosomes, extracellular exosomes	Yes
HSPA1L	Hum70t, Hsp-hom, Hsp70-hom, HSP70-1L, HSP70-1t	Cytosol, nucleus	No
HSPA2	HSP70-3, HSP70-2, HSP70.2	Cytosol, nucleus, lysosomes, cell membrane, extracellular exosomes	No
HSPA5	HSP70-5, BIP, GRP78, MIF2	Endoplasmic reticulum, extracellular exosomes	No
HSPA6	HSP70-6, HSP70B’	Cytosol, nucleus, extracellular exosomes	Yes
HSPA7	HSP70-7, HSP70B	Blood microparticles, extracellular exosomes	Yes
HSPA8	HSC70, HSC71, HSP71, HSP70-8, HSP73	Cytosol, nucleus, lysosomes, cell membrane, extracellular exosomes	No
HSPA9	HSP70-9, GRP75, mtHsp75, Mortalin, HSPA9B, MOT, MOT2, PBP74, mot-2, mtHsp70	Mitochondria, nucleus	No
HSPA12A	HSP70-12A, FLJ13874, KIAA0417	Intracellular, extracellular exosomes	No
HSPA12B	HSP70-12B, RP23-32L15.1, 2700081N06Rik	Intracellular, blood plasma	No
HSPA13	HSP70-13, Stch	ER, extracellular exosomes	No
HSPA14	HSP70-14, HSP70L1, MGC131990	Cytosol, membrane	Yes

The HSPA family members contain two domains: the nucleotide-binding domain (NBD) at their N-terminal and the substrate-binding domain (SBD) at their C-terminal. NBD has ATPase activity whereas SBD contains peptide binding cleft and lid regions. The two domains are connected by a linker. [42] In addition, eukaryotic cytosolic HSPAs contain EEVD motif in their C-terminal region. EEVD motif is involved in binding of co-chaperones and other HSPs. Specialized HSPAs such as HSPA5 and HSPA9, located mainly in the endoplasmic reticulum (ER) and mitochondria, respectively, lack EEVD motif. However, these HSPAs contain localization signal in their N-terminal. In addition, the C-terminal of HSPA5 contains a sequence that prevents it from leaving the ER. [36]

The members of the HSPA family function as molecular chaperones. They assist in the correct folding of newly synthesized proteins, promote refolding of misfolded proteins, prevent aggregation and solubilize aggregated proteins. Natively folded cytosolic proteins typically adopt conformation where their hydrophobic parts are left inside the protein whereas hydrophilic parts face the cytosol. Therefore, HSPAs are able to recognize misfolded proteins by their exposed hydrophobic surfaces. [9] In addition, HSPAs assist in the transportation of proteins between cellular compartments, participate in the assembly of multi-protein complexes, control the activity of vide variety of regulatory proteins and have immunomodulatory functions [9, 36, 41]. The function of HSPAs is supported by members of DNAJ and HSPC families as well as several co-chaperones such as HSPA interacting protein (Hip) and HSPA/HSPC organizing protein (Hop) [36].

The mechanism how HSPA assists proteins in a non-native state to fold into the native state is unclear [9]. However, Figure 6 presents one possible model where DNAJs, HSPCs and co-chaperones aid HSPA in the refolding of non-natively folded proteins. In the first step of this model, DNAJ binds to non-native polypeptides to prevent their aggregation. DNAJ forms a complex with Hip and transfer the non-native proteins to HSPAs. In the ATP bound state, the lid region of SBD is open causing low substrate affinity and high exchange rate. The second step begins with the binding of the complex containing the polypeptide, DNAJ, and Hip to the HSPA. DNAJs interact with the ATPase domain of HSPA. This interaction induces conformation change that stimulates ATP hydrolysis to ADP and closure of the lid. Hip prevents the dissociation of ADP from HSPA. When the lid is closed, the substrate has high affinity and slow exchange rate and DNAJ dissociates from the complex. In the third step, Hop couples HSPC to the HSPA to allow the participation of HSPC to the unfolding. Release of ADP and Hip from the HSPA is mediated by the interaction of nucleotide exchange factors (NEFs) such as Bag-1. The release of ADP allows binding of a new ATP molecule to the HSPA and the HSPA returns to the low-affinity state releasing the unfolded protein. The unfolded protein can then fold into native protein or be rebound to HSPA. [36]

Moreover, it has been proposed that by binding to non-native proteins HSPAs are able to reduce the amount of free non-native proteins sufficiently low to prevent aggregation and therefore give proteins time to fold to their native state [9].

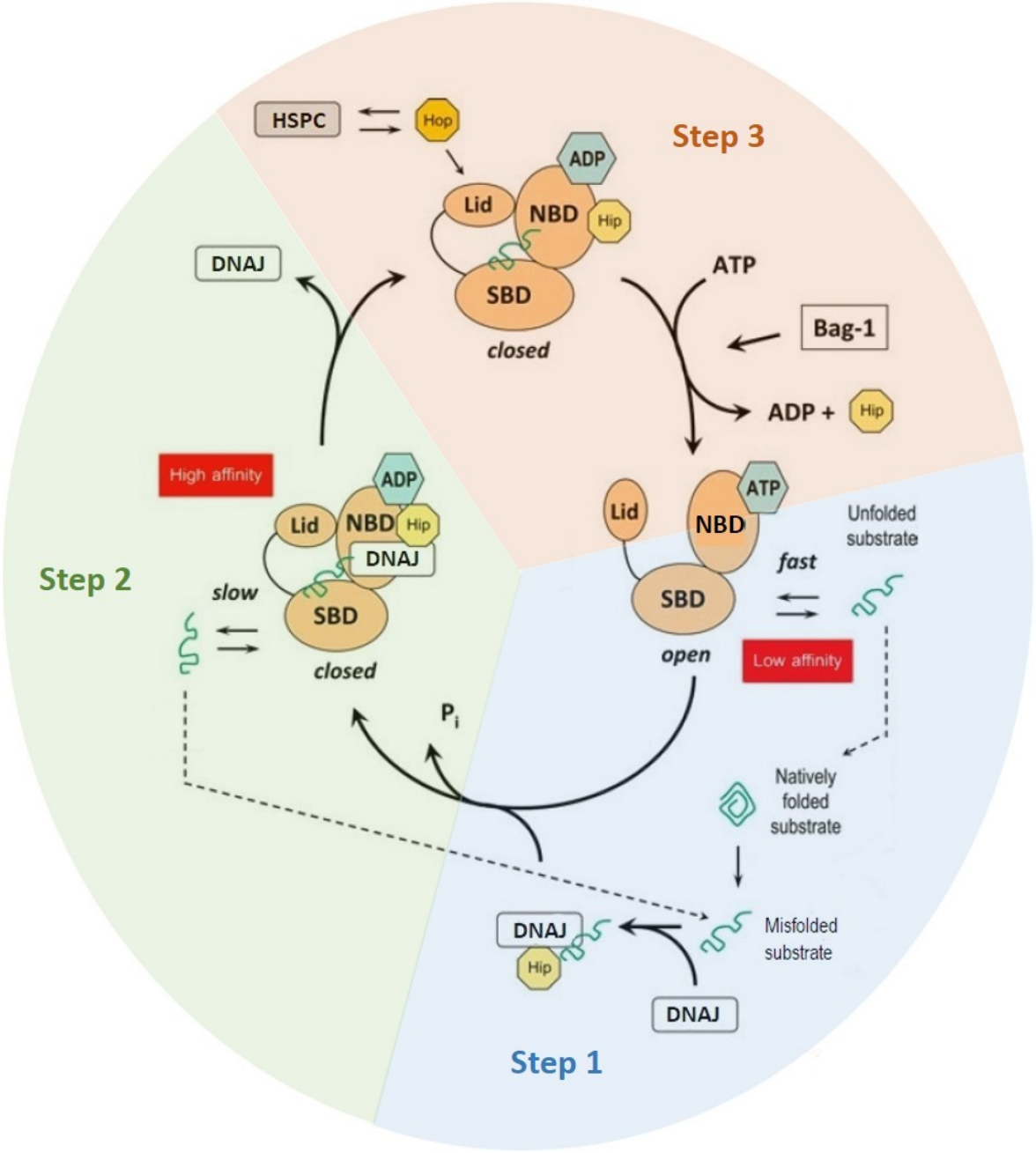

Figure 6. *Proposed HSPA chaperone reaction cycle [36, modified]*

HSPA has also antiapoptotic properties [11]. Apoptosis is a cell death pathway where the cell activates intracellular death mechanisms and kills itself in a controlled manner [43]. Apoptosis can occur via two pathways: intrinsic pathway (also referred to as mitochondrial pathway) and extrinsic pathway (also referred to as death receptors pathway). Both pathways are mediated by caspases. [11] Caspases are intracellular proteolytic enzymes [43]. In the intrinsic pathway, intracellular stress signals induce the production or activation of pro-apoptotic molecules that induce the release of apoptogenic molecules such as cytochrome c from mitochondria. The release of apoptogenic molecules results in the activation of caspases. The extrinsic pathway is activated through death receptors located in the plasma membrane leading to the activation of caspases. Several HSPs, including HSPA, have been shown to prevent apoptosis by blocking caspase activation. [11]

In addition, HSPA has anti-inflammatory properties. HSPA inhibits inflammatory response by preventing the activation of nuclear factor-κB (NFκB) [10]. NFκB proteins are gene regulatory proteins that have a central role in the initiation of inflammatory response [43]. NFκB is normally bound to its inhibitory protein IκB. However, in response to noxious stimuli IκB is phosphorylated by IκB kinase and NFκB is released. Activated NFκB translocates to the nucleus and initiates activation of several inflammation-related genes. HSPA prevents activation of NFκB by interacting with IκB kinase. [10]

2.2 Regulation of Heat Shock Response

The heat shock response is mainly regulated via transcriptional control that is mediated via heat shock factors (HSFs). The mammalian HSF protein family contains four members: HSF-1, HSF-2, HSF-3 and HSF-4. In addition to promoting cellular survival under stress, HSFs have important regulatory functions related to development and lifespan. HSF-1 is the master regulator of heat shock response in vertebrates. Also, HSF-2 and HSF-3 seem to be related to the transcriptional regulation of heat shock response but their role is uncertain. [44]

Figure 7 shows a schematic presentation of the HSF-1-mediated transcriptional control of the heat shock response. The HSF-1 protein domains from N-terminal to C-terminal are DNA-binding domain (DBD), leucine zipper 1-3 (LZ1-3), regulatory domain (RD), leucine zipper 4 (LZ4) and C-terminal transactivation domain (CTD). HSF-1 is constitutively expressed. In the absence of stress stimulus, HSF-1 is kept in an inactive, monomeric form. This form is maintained by multiple post-translational modifications and intramolecular binding of LZ1-3 and LZ4 domains. [45] The HSF-1 function is also repressed by chaperone interactions such as binding of DNAJ and HSPA to the CTD-domain. Also, HSPC together

with co-chaperones participates in the repression but their exact interaction site is not known. [45, 46]

When a cell is under proteotoxic stress, the amount of non-native proteins increases. These non-native proteins compete for HSP with HSF. As a higher portion of HSP chaperones is bound to the non-native proteins, the HSF-1s are dissociated from chaperones. [47] In addition, the interaction between LZ1-3 and LZ4 domains is disrupted and the regulatory domain becomes hyperphosphorylated leading to the activation of HSF-1. Activated HSF-1 enters the nucleus where it homotrimerizes. The inactive HSF-1 present in the nucleus can also activate upon stress and form trimers. [45] Homotrimerized HSF-1 molecules bind to specific gene sequences, heat shock elements (HSEs) that are located upstream of heat shock genes and increase the transcription of heat shock genes [47]. The HSF-1 function is inhibited by a negative feedback loop where HSPA and DNAJ bind to the C-terminal transactivation domain [46]. HSF-1 dissociates from the DNA, is dephosphorylated and returns to the cytoplasm. Finally, it binds to the HSPC multichaperone complex to resume its inactivated form. [45, 46] In addition to promoting chaperone transcription, HSF-1 regulates genes related to protein degradation, ion transportation, signal transduction, energy generation, vesicular transport and cytoskeleton formation [46].

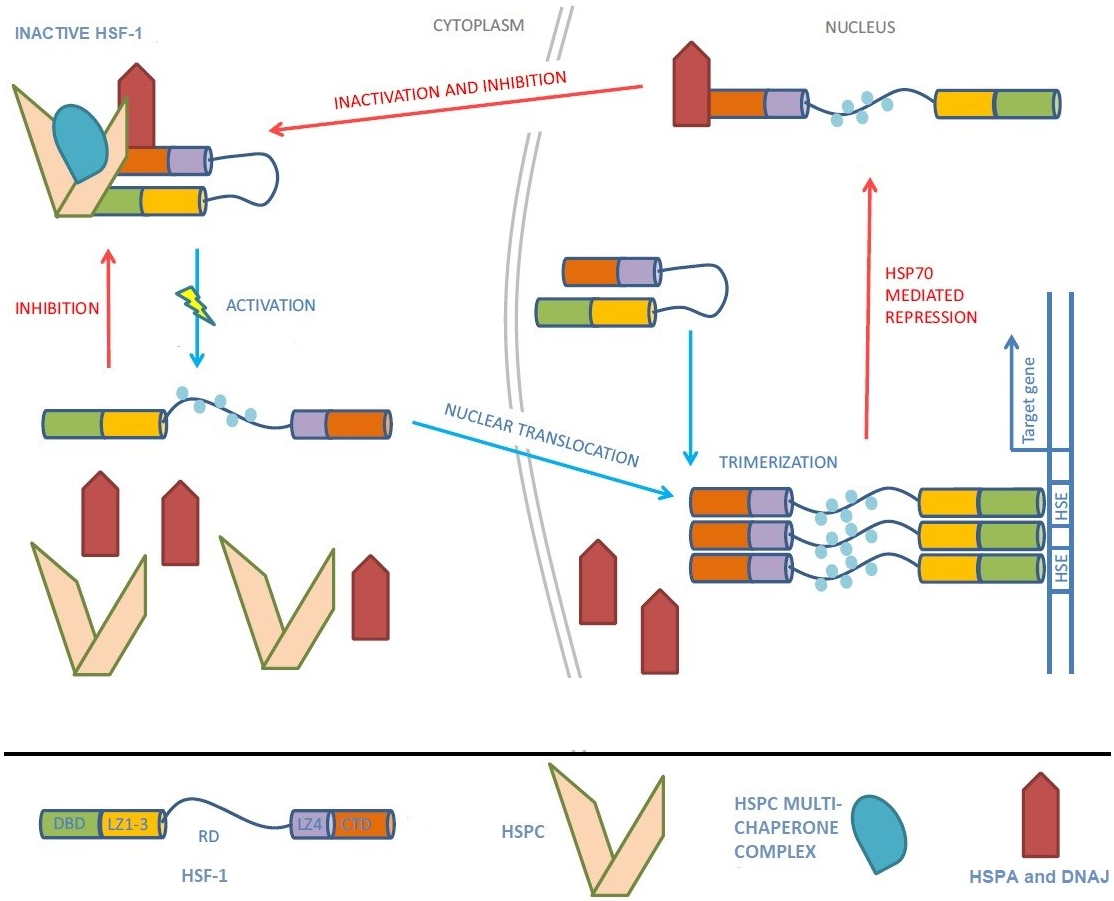

Figure 7. *HSF-1-mediated transcriptional control of heat shock response. [45, modified]*

Moreover, HSPs are regulated post-transcriptionally and post-translationally. [36] The post-transcriptional regulation is mediated via micro-RNAs (miRNAs) that regulate the stability and translation of messenger RNAs [36, 43]. The post-translational modifications of HSPs are not well known. Some of their amino acids are phosphorylated but the effect of phosphorylation remains unknown. [36] Additionally, the function of HSPs is regulated by various co-chaperones [48].

2.3 Heat Shock Response and Disease

Changes in HSP expression are associated with several pathological states. HSPA correlates positively with various inflammation markers and serum HSPA levels increase with increasing degrees of inflammation [49]. The plasma concentration of HSPA increases with the progression of disease stages in heart failure patients and therefore HSPA could serve as a potential biomarker for the early detection of heart failure. Additionally, the high expression level of HSPA is related to a variety of human cancers. HSPA is important in

tumorigenesis and promotes cancer cell survival. HSPA overexpression in cancer cells often correlates to metastases and poor clinical outcome. Other diseases associated with changes in HSPA levels include fatty liver disease, diabetes, stroke, asthma, and renal disease. [36] In addition, the concentration of HSPA decreases with age leading to impaired protein quality control [50]. This change has been linked to age-related diseases such as Alzheimer's disease, Parkinson's disease, amyotrophic lateral sclerosis (ALS) and age-related macular degeneration [51].

Due to the relationship between heat shock protein expression and disease, modulation of heat shock response is seen as a potential treatment method in multiple diseases. In cancer, where HSPA overexpression relates to the cancer cell survival, the objective has been the inhibition of HSPA function. Several pharmacological agents have been studied and are discussed in more detail in the review by Radons [36]. On the other hand, in diseases related to the toxicity from misfolded and aggregated proteins, the focus has been in upregulation of HSPs. HSP upregulation is thought to protect cells from the disease-associated accumulation of misfolded proteins and protein aggregates. [48]

The amplification of the heat shock response has been attempted using several different pharmacological agents. One approach is the induction of stress to the cell. For example, the amount of HSPs is increased by the inhibition of the proteasomal system because it leads to an increased amount of misfolded proteins that compete for HSPs with HSF-1s. Also, inhibition of HSP90 can lead to increased HSF-1 activation. [48] However, high levels of HSP90 inhibitors are cytotoxic [46]. HSP90 inhibitors include geldanamycin, some coumarin antibiotics, (–)-epigallo-catechin-3-gallate, gedunin, AEG3482, ITZ-1 and 17-AAG [46, 52].

In addition, HSP synthesis is enhanced by co-inducers. Known co-inducers include aspirin and hydroxylamine derivatives such as bimoclomol and arimoclomol. Bimoclomol amplifies the HSF-1 activation by prolonging the binding of HSF-1 to the heat shock elements. [48] Other pharmacological agents used to modulate heat shock response include celastrol, HSF1A, riluzole, non-steroidal anti-inflammatory drugs and several anti-ulcer drugs such as geranylgeranylacetone, carbenoxolone, zinc l-carnosine, and rebamipide. However, the mechanism how these agents promote heat shock response is not known in detail. [46]

3. Age-Related Macular Degeneration

Age-related macular degeneration (AMD) is a degenerative disease of the retina that leads to the loss of central vision [53]. AMD is the most common cause of irreversible vision loss in the people over 50 years old in Western countries [2]. It was estimated in 2014 that by 2020 the global number of people with AMD is around 200 million and increases to nearly 300 million by 2040 [54].

AMD affects mainly the macular area. However, AMD-like retinal abnormalities have been observed also in the peripheral retina [55]. AMD affects choroid, Bruch's membrane, retinal pigment epithelium and neural retina [56]. The etiology and pathogenesis of AMD are not known in detail. It seems that the initial pathogenesis of AMD involves RPE degeneration which leads to the death of photoreceptor cells due to the close relationship between RPE and photoreceptors. [57] The most prominent risk factor of AMD is age. Other risk factors include smoking, high dietary intake of saturated fatty acids, obesity, some cardiovascular diseases, and family history. [29, 58] This chapter describes the signs and symptoms of AMD.

3.1 Signs of AMD

AMD is diagnosed based on visual dysfunction as well as ophthalmoscopically visible macular findings that include geographic atrophy, choroidal neovascularization (CNV) and sub-RPE depositions [28]. Geographic atrophy is characterized by photoreceptor degeneration around the fovea and is typically horseshoe-shaped [7]. Due to the close relationship between RPE and photoreceptors, this degeneration is most likely caused by impaired RPE function and RPE cell death [57].

CNV is a condition where abnormal, leaking blood vessels grow from the choroid to retina. [7] The choroidal blood vessel growth is regulated by growth-promoting pro-angiogenic factors such as vascular endothelial factor (VEGF) and growth-inhibiting anti-angiongenic factors such as pigment epithelium-derived factor (PEDF). Normally, there is a balance between these factors and it seems that CNV is caused by disturbances in this balance. Hypoxia, ischemia, local inflammation, and activation of the immune system increase the amount of pro-angiogenic factors and may, therefore, be related to the development of CNV. [22] Formation of new vessels in CNV usually leads to fluid accumulation and bleeding

below the retina causing macular edema, retinal detachment as well as scarring and thus result in a major decrease in central vision [29, 59].

Sub-RPE deposits can be divided by their morphology into two groups: drusen and basal deposits. Drusen are round-shaped, yellowish depositions of debris between the retinal pigment epithelium and Bruch's membrane [2, 59]. They can be found both in the macula and in the peripheral retina. Drusen are categorized based on their diameter as small (diameter smaller than 63 μm), medium (diameter from 63 to 124 μm) or large (diameter over 124 μm). They are also categorized as soft or hard depending on their appearance. [2] Hard drusen have discrete margins and they are usually located in the periphery of the retina. Soft drusen are typically larger than hard ones, have less distinct edges and are located in the macular area. [2, 59] Soft drusen usually appear during the late stages of the disease [29].

Minor amounts of small drusen are commonly found in people over 50 years and therefore they are considered to be part of normal aging [2]. However, their presence is a risk factor for AMD. Multiple larger drusen are considered as a sign of AMD. [59] Nevertheless, the mechanisms leading to the formation of drusen and the relation of drusen to the development of AMD are unknown. [29, 59] Drusen have many similarities with plaques and deposits observed in many age-related diseases such as Alzheimer's disease and atherosclerosis [60, 61]. Common components include amyloid beta, clusterin, vitronectin, amyloid P, apolipoprotein E, acute phase reactants and complement components [61]. Similarities suggest that these diseases share common pathologic pathways [60].

Basal deposits are divided into basal linear deposits and basal laminar deposits. Basal linear deposits have high lipid content and they are located in the Bruch's membrane. Basal laminar deposits, in turn, are located between the RPE and Bruch's membrane. Basal laminar deposits contain high amounts of long spaced collagen whereas basal linear deposits contain primarily membranous debris. [7]

3.2 AMD Classification

Based on the prevalence of visual dysfunction and characteristic macular findings, AMD can be classified into early, intermediate or advanced (also referred to as late) AMD. Early AMD is characterized by the presence of a few medium-sized drusen or retinal pigmentary abnormalities. In intermediate AMD, the retina has at least one large drusen, several

medium drusen or geographic atrophy that does not extend to the center of the macula. Advanced AMD can be further divided into either wet (also referred to as neovascular or exudative) or dry (also referred to as non-neovascular, atrophic or nonexudative) form. [2] Approximately 10-15 % of the AMD patients have a wet form of the disease. Dry AMD is characterized by the presence of drusen and geographic atrophy whereas wet AMD is characterized by CNV. [7] The same patient can have both of the forms at the same time either in the same eye or in different eyes. Furthermore, dry AMD can turn into wet AMD and vice versa. [28]

Early AMD is often asymptomatic and the vision loss is mild. However, the patient may experience gaps in the image, image distortion, blurred vision, decreased contrast sensitivity, abnormal light adaptation or decreased vision in dim lighting conditions. In dry AMD, the vision loss generally develops over the course of months or years starting with small blind spots in the vision and resulting in the loss of the central vision. In wet AMD major vision loss develops faster, over days or weeks, due to the sub-retinal hemorrhage or fluid accumulation that eventually leads to scarring of the retina. [2, 7, 62]

4. AMD Pathogenesis

Currently, the mechanism of AMD development is not known. However, several pathological factors such as the reduction of oxygen and nutrient transport to the retina, chronic oxidative stress, chronic inflammation and decline of protein degradation have been linked to the development of AMD. These factors are related to each other and most likely function together to induce AMD pathogenesis. This chapter reviews some of the possible mechanisms contributing to the development of AMD.

4.1 Reduced Nutrient and Oxygen Transport

Retina has one of the highest metabolic activities of human tissues. In order to meet the high consumption of oxygen and nutrients, the retina receives blood supply via two sources: choroidal capillaries and retinal vessels. Capillary network of the choroid is referred to as choriocapillaris. Choriocapillaris is mainly responsible for blood supply to the avascular outer retina and retinal vessels to the inner retina. [63] In addition, the movement of nutrients and oxygen to the outer retina is regulated by the permeability of Bruch's membrane [7].

Age affects both choriocapillaris and Bruch's membrane and it is possible that these age-related changes are related to the development of AMD. The thickness of the choroid as well as the density and lumen diameter of choriocapillaris decrease with age leading to reduced choroidal blood flow [6]. Further decrease in the choroidal blood flow correlates with the development of AMD [6, 64]. In addition, aging results in thickening of Bruch's membrane due to increased accumulation and cross-linking of collagen fibers as well as deposition of debris and lipids [7, 28]. These effects may relate to impaired ability to degrade extracellular matrix proteins such as collagen and elastin. Degradation of collagen and elastin is normally conducted by matrix metalloproteinases (MMPs). The function of MMPs is inhibited by tissue inhibitors of metalloproteinases (TIMPs), and in the aging retina, TIMP content increases. The increase of TIMP content can lead to sustained inhibition of MMPs and therefore, to reduced degradation of extracellular matrix proteins. [6] Subsequent thickening of the Bruch's membrane leads to changes in membrane permeability that reduce transport across the membrane [6, 7]. Furthermore, accumulation of drusen, retinal detachment, and macular edema increase the diffusion distance between choriocapillaris and retina and therefore hinder the movement of oxygen and nutrients. [64]

Inadequate supply of oxygen and nutrients has several adverse effects on the retinal function that may contribute to the development of AMD. Reduced delivery of oxygen to tissue causes a state of tissue oxygen deprivation referred to as hypoxia. The retina is particularly prone to hypoxia because of the high oxygen consumption of photoreceptor cells. Photoreceptors consume 90 to 100 % of the oxygen delivered by choriocapillaris and therefore even small changes in the choriocapillaris function or oxygen diffusion to the photoreceptors may induce hypoxia in retina. [6] Hypoxia can directly lead to RPE and photoreceptor cell death and, additionally, it causes CNV by generating the production of hypoxia-inducible factors (HIFs) that activate angiogenesis by promoting VEGF expression [6, 64]. Hypoxia might thus start a vicious cycle where VEGF production induces growth of leaky vessels that cause macular edema and retinal detachment. Edema and retinal detachment, in turn, increase the diffusion distance of oxygen which further promotes hypoxia and VEGF production. [64]

Besides regulating the movement of oxygen and nutrients between choriocapillaris and retina, Bruch's membrane regulates the survival of adjacent RPE and choriocapillaris by acting as a scaffold for these cells. Therefore, age-related changes in the Bruch's membrane may result in decreased cell adhesion and death of RPE cells, photoreceptors and choriocapillaris endothelial cells. [28]

4.2 Chronic Inflammation

Inflammation is the body's response to tissue damage. The aim of inflammation is to dispose pathogens, toxins or foreign material at the site of tissue damage, prevent the spreading of injury, initiate tissue recovery and restore tissue homeostasis. Inflammation is mediated by the innate immune system. The innate immune system, unlike the adaptive immune system, is a nonspecific defense mechanism. Therefore, it is not able to adapt or adjust its response. [18]

Even though the aim of inflammation is to protect the tissues, chronic or excessive inflammation can itself induce tissue damage. The chronic inflammatory response is hypothesized to contribute to retinal dysfunction and death in AMD. [65] Moreover, chronic inflammation may contribute to neuronal dysfunction and loss in various neurodegenerative diseases such as multiple sclerosis, Alzheimer's disease, Parkinson's disease, amyotrophic lateral sclerosis and Huntington's disease [59, 66].

4.2.1 Innate Immune System and Inflammation

When the innate immune system recognizes pathogens or tissue damage, it activates and promotes inflammation by secreting cytokines that attract immune system cells to the site of infection [67, 68]. This recognition is facilitated by pattern recognition receptors (PRRs). Ligands for these receptors, pathogen-associated molecular patterns (PAMPs), are expressed by invading micro-organisms but not by the host organism. In addition to pathogens, non-infectious factors such as trauma, excessive heat or cold, chemical insults, and radiation can cause tissue damage. In response to non-infectious tissue damage, dead cells release danger-associated molecular patterns (DAMPs) that bind to PRRs and facilitate activation of the innate immune system. [66, 69]

Nucleotide-binding oligomerization domain-like receptors (NLRs) are intracellular PRRs. In response to PAMP and DAMP danger signals, some of the NLRs form large cytoplasmic complexes referred to as inflammasomes. NLRP3 inflammasome (nucleotide-binding domain, leucine-rich-containing family, pyrin domain-containing-3) has the capability to respond to the widest range of different danger stimuli. Its activation has been linked to many autoinflammatory and autoimmune disorders. [67]

Innate immune system PRRs include C-reactive protein (CRP) that activates the complement system [7, 66]. The complement system consists of a group of proteins. It promotes inflammation, eliminates pathogens and enhances the immune response. In the normal state of the eye, the complement system is continuously activated to promote the elimination of potential pathogens. Intraocular complement regulatory proteins control the level of complement system activation. They maintain sufficient activation to eliminate potential pathogens and to prevent excessive complement activation than can lead to tissue damage. [7]

4.2.2 Inflammation and AMD

Retina has developed certain mechanisms to protect its delicate structure from inflammatory responses. RPE cells and endothelial cells of the choroidal capillaries form the blood-retina barrier that maintains the homeostasis of the retina [70]. Blood-retina barrier and the lack of lymphatic system create a physical barrier that prevents the entry and exit of immune system cells and larger molecules into and out of the retina. In addition, retinal cells such as RPE cells express immune-suppressive agents. Due to its ability to limit inflammatory responses, the retina is referred to as immune-privileged tissue. [71, 72] The

retina has its own local immune system that includes retinal innate immune cells and complement regulatory system. This system can be activated when retina suffers from noxious stimuli. [72] However, malfunction of inflammation regulation can lead to chronic and paranormal inflammatory response and immune-mediated damage in the retina [7].

The theory that chronic inflammation contributes to the development of AMD has been strengthened by the observation that alterations in immune system genes are strongly related to the development of AMD [73]. In addition, AMD-induced factors such as drusen and cell death cause inflammation [66, 74]. Moreover, AMD-induced lesions are associated with immune system cell recruitment and cytokines interleukin-1β (IL-1β) and interleukin-18 (IL-18) that promote inflammation [53, 65]. Nevertheless, it is unknown whether inflammation is the cause or result of AMD since cell death, drusen and macrophage recruitment may also result from inflammation [53, 65, 73].

4.2.2.1 Genetic Alterations

Several immune system related genetic alterations seem to be involved in the development of AMD. The best known genetic risk of AMD is Y402 (Tyr402-His) variant of the complement factor H (CFH) [73]. CFH is a regulator of the complement system. Its primary role is to differentiate between host organism and pathogen. Dysfunction of CFH might lead to excessive complement system activation and immune-mediated damage. Mutations in the gene coding for CFH have been associated with other diseases that involve local inflammation and drusen-like deposits, such as atypical hemolytic uremic syndrome, dense deposit disease, and atherosclerosis. [59]

Besides CFH, variations in other complement system-related genes such as in complement factors 3 (C3) and I (CFI) as well as in regulator of complement system activation clade G, member 1 (SERPING1) have been associated with AMD. In addition, genetic alterations of immune system regulators not related to complement system have been associated with AMD. These include chemokine receptor CX3CR1 and chemokine C–C motif ligand 2 (CCL-2, also referred to as monocyte chemotactic protein 1 (MCP-1)). [73]

4.2.2.2 Cell Death

Cells can die via various pathways that can be divided into anti-inflammatory and pro-inflammatory. In necrotic cell death, the cellular membrane is disrupted and cellular contents are released. These released constituents are able to stimulate the innate immune system and may, therefore, induce inflammation. [66] In contrast, in anti-inflammatory apoptosis the cellular membrane remains intact and cells are cleared by phagocytic cells. [65] However, if apoptotic cells are not properly cleared out by phagocytic cells, they undergo secondary necrosis. In secondary necrosis, the integrity of their membrane is disrupted which leads to the activation of the innate immune system. Microglia are the main phagocytic cells of the retina. If the amount of cells undergoing apoptotic cell death exceeds the phagocytic capability of microglia, apoptotic cells undergo secondary necrosis and induce local inflammation. This can be a result of either excessive amount of dying cells or a decrease in the amount of microglia. [66]

Inflammation can itself be the cause of cell death. Pyroptosis is a cell death pathway induced by the activation of NLRP3 inflammasome. Pyroptosis results in cell lysis and release of inflammatory cytokines to the extracellular space and is therefore pro-inflammatory. [65]

In addition, the AMD-induced RPE cell death may affect the regulation of immune response in the retina. RPE cells modulate the immune response of the eye by secreting various molecules. They include molecules that trigger immune cascade and production of pro-inflammatory mediators as well as molecules that block any possible excessive inflammatory response. The loss of RPE cells reduces the capability of the retina to control the immune system and may, therefore, lead to chronic inflammation. [59]

4.2.2.3 Drusen

Drusen contain many inflammation-related molecules such as the components of complement system, immunoglobulins, apolipoprotein E (APOE), amyloid-β, vitronectin and fibrinogen which suggests that the formation of drusen is caused by chronic inflammation. [73] Moreover, the contents of drusen can induce the activation of NLRP3 inflammasome and thus mediate inflammation [74]. For example, amyloid-β is an activator of the alternative pathway of the complement system. [59] Therefore, it is not clear whether inflammation is the cause or result of drusen formation.

4.2.2.4 Macrophage Malfunction

Macrophages are immune system cells that participate in innate immunity and maintain homeostasis by phagocytosing cellular debris and bacteria [18]. Retina has resident macrophages, microglia, that provide immune surveillance in the inner retina. In addition, the release of cytokines can recruit circulating monocytes from the bloodstream. [75] These monocytes can then differentiate into macrophages [18]. Macrophages are divided into M1 or M2 type cells. M1 macrophages are pro-inflammatory and produce inflammatory cytokines as well as toxic reactive oxygen species whereas M2 macrophages are anti-inflammatory and pro-angiogenic. [65]

Macrophages seem to have a role in AMD. They are present near AMD-induced lesions and cytokines that mediate macrophage recruitment are associated with AMD. [53] The mechanism how macrophages are related to AMD is not known. One hypothesis is that the development of AMD is related to the change in the relative amounts of pro-inflammatory M1 and anti-inflammatory M2 types. This hypothesis is based on the idea that that M1 type harms retina by inducing inflammation whereas M2 type serves a more protective role by producing anti-inflammatory factors. [53, 76] This macrophage polarization change may be caused by various insults such as genetic predisposition or oxidative stress [76]. Support to this idea has been provided by Cao et al. [76] who observed that the ratio of transcripts of M1 to M2 chemokines was increased in AMD patients compared to the non-AMD patients indicating a shift to M1 activity in AMD patients.

Additionally, M2 type cells can induce retinal damage by producing pro-angiogenic factors and promoting fibrosis and might thus be related to the development of CNV [53, 76]. It is also worth noting that the AMD-related activation of macrophages might not promote disease development but instead serves to protect the retina [53]. Nevertheless, the role of macrophages in the development of AMD is unclear.

4.3 Oxidative Stress

According to the current view, aging is caused by the accumulation of structural damage over the lifetime of the organism. A major part of this structural damage is caused by oxidative stress. [31] Oxidative stress occurs when there is an excessive amount of reactive oxygen species (ROS) due to their accelerated production or impairment of removal

mechanisms [66]. ROS are unstable and highly reactive oxygen-containing chemical species [57]. They include free radicals such as superoxide anion [31]. Free radicals are species that have an unpaired electron in their outermost molecular orbital. They readily give up their unpaired electron or take an electron from another molecule. [18] ROS also include powerful oxidizing agents such as hydrogen peroxide that readily remove electrons from other molecules [18, 31].

A certain amount of ROS is required for the normal metabolism of the cell. They function as signaling molecules in regulatory pathways related to cell proliferation, gene expression, and apoptosis. However, an excessive amount of ROS can have pathophysiological consequences because of their highly reactive nature. Exogenous factors producing ROS include smoking, alcohol consumption, and exercise. [31]

ROS induce damage to the molecules that they react with. In cells, this may include lipids, proteins, and nucleic acids. ROS cause lipid peroxidation which disturbs membrane integrity, fluidity and function. [31] Especially polyunsaturated fatty acids (PUFAs) are susceptible to lipid peroxidation because they contain many double bonds that are targeted by ROS [77]. The retina contains high amounts of PUFAs and is therefore prone to lipid peroxidation. For proteins, ROS cause oxidation which can alter the protein structure preventing their normal functioning. In addition, ROS generate DNA oxidation in nuclear and mitochondrial genomes resulting in strand breaks, base modification or DNA-protein cross-linkages. If the DNA damage is not repaired properly, it can lead to cell death or replication errors. [31]

4.3.1 Sources of Oxidative Stress in Retina

The retina is particularly prone to oxidative stress because it contains chromophores that produce ROS in response to light exposure. A chromophore is a part of a molecule where the energy difference between two molecular orbitals corresponds to the energy of a photon in the visible light spectrum. Light incoming to the eye excites electron of chromophore from its ground state to higher energy state. The resulting excitation state is highly unstable and may interact with other molecules to produce ROS. [78] Chromophores of the retina include photoreceptor cell photopigments and lipofuscin [31]. Lipofuscin is an aggregate that consists mostly of oxidatively damaged protein and lipids [22]. RPE cells are unable to degrade lipofuscin and therefore it accumulates to RPE cells with age increasing the production of ROS [31, 79].

Besides light exposure, ROS are generated as by-products in normal physiological processes including the functions of mitochondria and peroxisomes as well as enzymes such as nicotinamide adenine dinucleotide phosphate (NADPH) oxidase and phospholipase A_2. In retinal cells, mitochondria are the main source of ROS. [31] Mitochondria are particularly vulnerable to oxidative damage due to the close proximity of mitochondrial DNA (mtDNA) to the ROS-producing mitochondrial respiratory chain. In addition, mtDNA is more susceptible to oxidative damage than nuclear DNA (nDNA) because it is not associated with DNA-related proteins such as histones that would protect the genetic material from damage. Moreover, mtDNA has no introns that would decrease the probability of oxidative damage occurring in crucial location. Additionally, the DNA repair mechanisms of mtDNA are less effective than those of nDNA. [57] Mitochondrial damage can reduce the ability of the mitochondria to produce energy and thereby further increase their ROS production [57, 58].

4.3.2 Prevention and Repair of Oxidative Damage in Retina

Blue light is particularly harmful to the retina due to its high energy content and absorption to lipofuscin [80, 81]. The retina contains various pigments that protect it from blue light by absorbing it. These pigments include melanin and carotenoid pigments lutein, zeaxanthin and mesozeaxanthin. Together lutein, zeaxanthin, and mesozeaxanthin are referred to as macular pigment. [31]

Moreover, lutein, zeaxanthin and mesozeaxanthin act as antioxidants [82]. Antioxidants are substances that reduce oxidative stress by inactivating free radicals [18]. Enzymatic antioxidants such as superoxide dismutase, glutathione and catalase serve a key role in the prevention of oxidative damage [31]. Other antioxidants protecting the retina from oxidative damage include melanin and vitamins such as vitamin C and E [31, 81].

Oxidatively damaged proteins, lipids, and nucleic acids can cause further damage to the cell and need to be either repaired or degraded. Lipid peroxidation products are removed by phospholipase enzyme and peroxisomes. The oxidative damage of DNA is repaired by specific DNA repair mechanisms. [31] Repair of oxidatively damaged proteins is conducted by HSPs, which also prevent aggregation of damaged proteins. The degradation of misfolded proteins is carried out by the ubiquitin-proteasome system or lysosomal system and is discussed in more detail in Chapter 4.4. [29] However, these mechanisms are incapable of completely protecting the cells from oxidative damage that accumulates during aging and causes cell dysfunction and death. In many tissues, dead and

dysfunctioning cells are replaced from stem or progenitor cell populations. However, the vertebrate retina is not able to regenerate and therefore the accumulation of oxidative damage poses a threat to the aging retina. [31]

4.3.3 Oxidative Stress and AMD

The risk factors of AMD support the role of oxidative stress in the development of the disease. Most of the known risk factors of AMD such as cigarette smoking, exposure to sunlight and low dietary intake of antioxidants are related to the oxidative stress. The toxic compounds of cigarette smoke and exposure to intense light may both induce production of ROS. [57] Antioxidants, in turn, have an important role in the prevention of oxidative damage. Cigarette smoke can, however, decrease antioxidant capacity. [31, 57]

Figure 8 presents a mitochondria-based model proposed by Liang and Godley [57] that associates oxidative stress and the development of AMD. In this cyclic model, initial ROS produced by exogenous and endogenous factors leads to the production of an increasing amount of ROS. ROS induce damages to mtDNA and due to inefficient mtDNA repair, these damages accumulate to the mtDNA causing eventually mitochondrial dysfunction. Malfunctioning mitochondria, in turn, produce more ROS, which increases the amount of oxidative damage. Further mitochondrial damage induces a reduction of energy production which results in RPE dysfunction as well as apoptosis and ultimately leads to the development of AMD. [57]

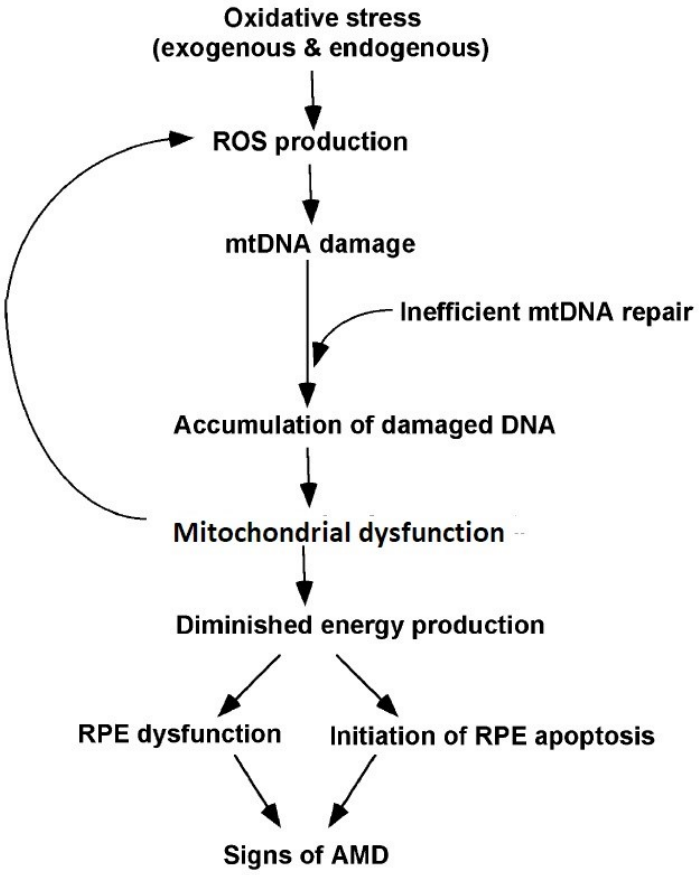

Figure 8. *Mitochondria-based model for the development of AMD. [57, modified]*

4.4 Dysfunction of Degradation of Misfolded Proteins

Proteins are polypeptides that have been folded in a specific way. During folding, non-covalent interactions form between amino acids and these interactions determine the final shape of the molecule. Folding proceeds spontaneously in the direction that is energetically most favorable and is assisted by molecular chaperones. The three-dimensional structure of a protein is important for its correct function. Therefore, damaged or misfolded proteins are normally unable to function properly and may form aggregates that are harmful to the cell. [43]

In cytoplasmic proteins, the hydrophobic residues of the polypeptide are located in the inner parts of the protein whereas the hydrophilic residues are left facing cytoplasm. Damaged and misfolded proteins are recognized by molecular chaperones such HSPs by their exposed hydrophobic region. [43] HSPs can repair misfolded or damaged proteins and prevent their aggregation [9]. If HSPs are unsuccessful in the repairment of the proteins, proteins are assigned to degradation [43]. Two major pathways of protein degradation are

the ubiquitin-proteasome system (UPS) and the lysosomal system. UPS is responsible for the degradation of most short-lived proteins as well as damaged and abnormal proteins whereas the lysosomal system is responsible for the degradation of most long-lived proteins, protein aggregates, and cellular organelles as well as extracellular material. [43] [83] Besides degrading damaged proteins, UPS and lysosomal system regulate many cellular processes by controlling the lifetime of proteins and by recycling amino acids. [83]

4.4.1 Ubiquitin-Proteasome System

In the ubiquitin-proteasome system, the proteins assigned for degradation are marked with ubiquitin. Marked proteins are then transferred to proteasome which degrades them. Proteasomes are barrel-shaped proteins that contain multiple subunits. Subunits are assembled into four stacked protein rings around the central cavity. Proteasomes contain many protease enzymes that are able to degrade proteins. The active sites of protease enzymes are directed towards the inner space of the proteasome. Ends of the barrel are associated with cap protein complexes through which the proteins designated for degradation are guided to the proteasome core. As they move through these cap proteins, ATP-driven reaction unfolds the target proteins. Unfolded proteins are then degraded by the protease enzymes. [43]

4.4.2 Lysosomal System

The lysosomal system degrades both intracellular and extracellular material. Degradation occurs in specialized, membrane-bound organelles, lysosomes. Lysosomes contain various hydrolytic enzymes that break down cellular molecules. These hydrolytic enzymes are active in the acidic environment of the interior of the lysosome but lose their activity if they are released to the approximately neutral cytoplasm. This mechanism protects the cells against leaking lysosomal contents. [43]

Lysosomes digest material via various pathways. Autophagy is a lysosomal degradation system that maintains cellular homeostasis by degrading various intracellular components such as proteins and organelles [79]. There are three different autophagic routes: macroautophagy, microautophagy, and chaperone-mediated autophagy. Macroautophagy is considered the major autophagic route. Macroautophagy starts by the enclosure of the debris by a double membrane which creates autophagosome. This autophagosome then fuses with lysosome forming autolysosome where the degradation is finalized. [84] Microautophagy, on the other hand, is uncommon in mammals [59]. In microautophagy,

cytosolic proteins and organelles are degraded by lysosomes without the formation of autophagic vacuole [79]. In chaperone-mediated autophagy, chaperone HSPA8 recognizes proteins with a specific amino acid motif and transports them to the lysosome. [59, 84] Because macroautophagy is the main autophagic route in mammals, it is hereafter referred to as autophagy.

Endocytosis is a process where the cell takes up extracellular components. There are two kinds of endocytosis: pinocytosis where cells ingest small extracellular solutes and fluid, and phagocytosis where cells ingest large extracellular particles. Phagocytosis is most efficient in phagocytes which are cells that have specialized to the digestion of large particles, micro-organisms, and dead cells. In phagocytosis, cell ingests the particles to large endocytic vesicles referred to as phagosomes. These phagosomes then fuse with lysosomes where the degradation of the particles occurs. [43] RPE cells allow the regeneration of photoreceptor outer segments by phagocytosing outer segment tips [29].

4.4.3 AMD and Dysfunction of Degradation of Misfolded Proteins

Aging decreases the function of both UPS and lysosomal system. The mechanisms how these declines occur is unknown. [83] Age-related changes include accumulation of ubiquitinated proteins in cells, increase in lysosomal volume, decrease in lysosomal stability and decrease in the activity of some lysosomal hydrolases [79, 83]. Aging also induces accumulation of indigestible materials such as lipofuscin into the lysosomes decreasing their ability to fuse with autophagosomes. The mechanism how lipofuscin induces this lysosomal inhibition is not known. However, A2-E fluorophore of lipofuscin has been shown to increase the lysosomal pH which leads to inhibition of lysosomal hydrolases and therefore prevention of lysosomal degradation. [79]

The decreased function of UPS and lysosomal system leads to the accumulation of toxic debris inside cells [83]. It is therefore hypothesized that decreased UPS activity and lysosomal function have a role in aging as well as in the development of many age-related diseases such as AMD [74]. Changes in UPS and lysosomal system have been associated with the development of multiple neurodegenerative diseases such as Parkinson’s disease and Alzheimer’s disease [83].

4.5 Multifactorial Nature of AMD

AMD is most likely a multifactorial disease. The possible mechanisms leading to AMD development discussed previously in this chapter are highly interrelated. Figure 9 presents one theory of how different mechanisms may act together to induce AMD pathogenesis. In this figure, RPE phagocytosis of photoreceptor outer segments causes accumulation of lipofuscin to the RPE cells. Lipofuscin both induces the generation of ROS when exposed to light and inhibits the lysosomal system. Oxidative stress then promotes mitochondrial damage, which leads to the generation of more ROS. This ROS together with ROS from other cellular sources cause protein misfolding. Misfolded proteins that are not degraded by UPS or lysosomal system form aggregates that activate NLRP3 inflammasomes and thus induce inflammation. Accumulated protein aggregates are removed from the cell by exocytosis and form drusen. [58]

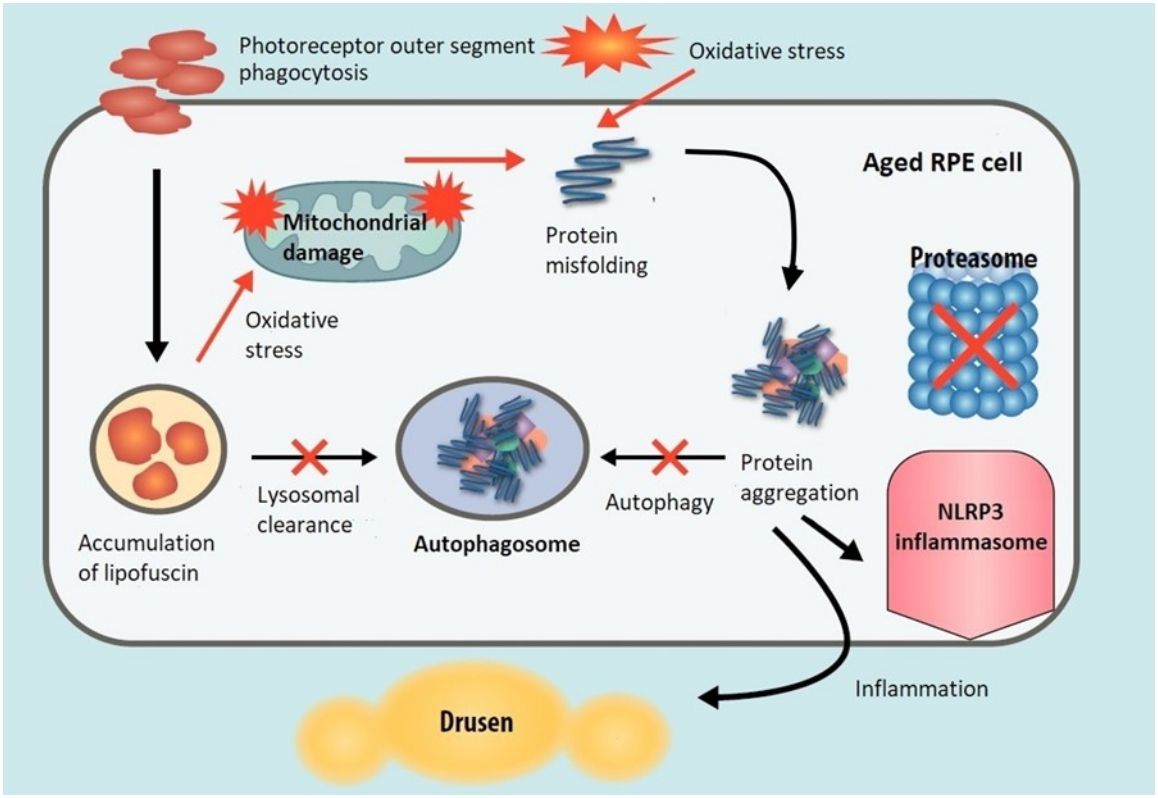

Figure 9. *Possible mechanism of AMD development [58, modified]*

In addition to this, also other mechanisms may take place. For example, inflammation can promote ROS production and oxidative stress can inactivate proteasomal function [85, 86]. Moreover, hypoxia increases ROS production and can lead to cell death that promotes inflammation. On the other hand, inflammation can generate hypoxia because of the

increased metabolic activity of the tissue. [87] Due to these multiple interactions between presented mechanisms it is difficult to determine what the initial cause of AMD is.

The reason why macula is more susceptible to degeneration is not known. One proposed reason is the high density of photoreceptor cells in macula, which exposes RPE cells to higher metabolic load. [88] Furthermore, Bruch's membrane structure is different at macula [89]. Chong et al. [89] showed that the elastic layer of Bruch's membrane is three to six times thinner and two to five times more porous in the macular region compared to the peripheral region. They hypothesize that this difference may contribute to the higher susceptibility of the macular retina to AMD. [89]

5. Current Treatment of AMD

Currently, there are no effective treatments for dry AMD. For wet AMD, there are treatments that are able to slow or halt the progress of the disease but no treatment exist that can cure or reverse the course of the disease. [8] Therefore, prevention of AMD is crucial. Lifestyle recommendations aiming to prevent the development of AMD are based on the known risk factors of the disease. It is recommended to quit smoking, reduce the dietary intake of saturated fats, transfats, and omega-6 fatty acids, maintain a healthy weight as well as blood pressure and diet that provides sufficient amount of antioxidants. [2, 8]

Due to the uncertainty of the pathological mechanism of AMD, the development of the treatment is challenging. This chapter discusses the main treatment methods of AMD.

5.1 Oxidative Stress-Related Methods

Antioxidants protect cells against oxidative stress and, therefore, it is hypothesized that they have an important role in the prevention of AMD [2]. Some antioxidants, such as carotenoids, cannot be produced by humans and are therefore acquired only from food [90]. In addition to antioxidants, adequate intake of minerals is important for the proper regulation of antioxidant system [81]. Therefore, antioxidant and mineral supplements are a common approach in the prevention of AMD.

The effects of lutein, zeaxanthin, zinc, copper as well as vitamins C, E and A on AMD have been extensively studied [91, 92]. Even though the results of these studies have been inconsistent, the majority of the studies support the protective nature of lutein and zeaxanthin [81, 91, 92]. Age-Related Eye Disease Study (AREDS), a clinical trial that enrolled 3640 participants, concluded that daily doses of vitamin C (500 mg), vitamin E (400 IU), β-carotene (15 mg), zinc (80 mg as zinc oxide), and copper (2 mg as cupric oxide) reduce the probability of developing advanced AMD in individuals with high-risk characteristics [93]. AREDS was continued with AREDS2 which concluded that the β-carotene should be substituted with lutein and zeaxanthin [94]. Nevertheless, unnecessary antioxidant supplementation should be avoided because antioxidants can also act as pro-oxidants at high concentrations or have other adverse effects [31, 91]. For example, vitamin E is related to increased prostate cancer risk and heart failures in patients with vascular disease or diabetes mellitus [91].

Oxidative stress damages mitochondria and thus reduces their energy production. Metformin increases cell energy production and therefore it has been proposed to aid retina to withstand oxidative stress. Metformin is thought to regulate metabolism by activating adenosine monophosphate-activated protein kinase (AMPK) signaling. When activated, AMPK increases cell energy production by increasing glycolysis and promoting mitochondrial biogenesis. Metformin is an FDA approved drug that is prescribed for control of serum glucose levels in type 2 diabetes. [95] Xu et al. [95] observed that metformin can delay or prevent the degeneration of photoreceptors and RPE in three different retinal degeneration mouse models by increasing mitochondrial biogenesis and reducing oxidative stress.

Additional approach has been the reduction of ROS production in retina. Since damaged mitochondria are major ROS producers in the retina, there have been attempts to enhance their degradation by autophagy. Tested stimulators of autophagy include rapamycin and lithium. [31] Wilkinson et al. [96] showed that rapamycin slows the aging of mice and Harrison et al. [97] reported that rapamycin extends the lifespan of mice. However, more results are needed of the effect of rapamycin in human retinal aging.

5.2 Macular Translocation Surgery and RPE Replacement Approaches

According to current understanding, RPE malfunction is central in the events leading to the development of AMD. Because RPE cells are not capable of self-renewal, the replacement of diseased RPE cells has gained attention. [98] One of the proposed methods is macular translocation surgery where photoreceptors of macular area are moved to the area of the retina where RPE is healthy. During macular translocation surgery, the retina is detached from RPE and the macula is rotated axially. This method has been observed to increase visual acuity. However, the method is not commonly used because it involves difficult surgical procedures and may cause severe complications such as strabismus. [99]

Additionally, visual improvement has been obtained by transplanting autologous peripheral RPE underneath the fovea. However, these methods remain experimental due to the limited sources of autologous RPE tissue as well as challenges related to the tissue collection. In addition, autologous RPE shares the same genetic defects than diseased RPE and therefore, other RPE tissue sources such as fetal and non-autologous adult RPE might prove more suitable. However, these sources are limited and their use poses major ethical and technical issues. Another potential source is RPE cells derived from pluripotent stem

cells. [98] Possible pluripotent cells include human embryonic stem cells (hESC) and human-induced pluripotent stem cells (iPSC) [100]. iPSCs are differentiated somatic cells that are altered to become pluripotent. Therefore, in contrast to hESCs, iPSCs derived RPE cells would be patient-specific and thus prevent any immune rejection related issues. [98]

Even though mammalian RPE cells are non-proliferative, RPE cells have been activated in vitro to a self-renewing retinal pigment epithelial stem cells (RPESCs). These cells are another potential cell source for RPE replacement therapy. [100, 101] Additional possible sources include stem cells isolated from the umbilical cord and neural progenitor cells [100].

In addition to finding a proper source of stem cells, the delivery method has to be established [98]. Investigations concentrate on two different therapeutic strategies for delivering the RPE cells: injection of cell suspension and surgical implantation of RPE monolayer with or without a supporting membrane. From these two options, the injection is less invasive but injected cells are more likely to form clusters and show limited phagocytosis of photoreceptor outer segments. Studies in animal models suggest that the implanted monolayers survive longer without evidence of tumor formation. [100] Further studies are needed to answer the questions about long-term survival, function and immune rejection of implanted cells as well as questions about the long-term safety of the procedure [98].

5.3 Intravitreal Anti-Angiogenic Therapy

Intravitreal anti-angiogenic therapy is the main therapy for wet AMD. In this method, antiangiogenic agents are injected to the vitreous. Injection allows the localization of the effect to the eye. However, injections can induce adverse effects such as retinal detachment, intraocular hemorrhage, increased intraocular pressure and anaphylaxis. [2] Most commonly used intravitreal anti-angiogenic agents are ranibizumab, bevacizumab, and aflibercept. Ranibizumab and aflibercept are approved by the FDA for the treatment of wet AMD. Bevacizumab is FDA approved for the treatment of several cancer types but it is used as an off-label drug for the treatment of wet AMD. [8]

Ranibizumab, bevacizumab, and aflibercept are able to prevent legal blindness in patients with wet AMD. However, to be effective, they need to be administered frequently. The frequency of injections varies. Treatment can be given in a fixed monthly interval or interval

can be decided depending on the disease state that is evaluated during monitor visits. Frequent injections and monitor visits are costly and inconvenient for the patient. Therefore, there is a need for treatments that have longer-lasting effects. [8] Additional concern is the possible leakage of the antiangiogenic agents to the bloodstream through AMD-induced damages in the blood-retina-barrier. Systemically administered antiangiogenic agents have been associated with serious adverse effects such as thromboembolic events and death. [2]

5.4 Anti-inflammatory Agents

One experimental approach to the treatment of AMD is the reduction of chronic inflammation by using anti-inflammatory agents. Studied anti-inflammatory agents include corticosteroids, nonsteroidal anti-inflammatory drugs (NSAIDs), immunosuppressive agents (such as methotrexate and rapamycin) and biologics (such as infliximab, daclizumab and complement inhibitors). [102]

In addition to their anti-inflammatory properties, corticosteroids have anti-angiogenic, anti-fibrotic and anti-permeability properties that may prove useful in the treatment of AMD. They can reduce the permeability of choroidal endothelial cells, inhibit the activation of MMPs, and reduce the expression of VEGF. For example, corticosteroid dexamethasone has been examined in the treatment of wet AMD as a combined treatment with verteprofin photodynamic therapy and anti-VEGF agents with promising results. [102] Adverse effects of corticosteroids include cataract formation and increase in intraocular pressure that can lead to the development of glaucoma. [102, 103]

NSAIDs have anti-inflammatory properties and they reduce pain as well as fever. In contrast to corticosteroids, NSAIDS do not induce an increase in intraocular pressure and may thus provide a safer treatment alternative. However, topical administration of NSAIDs has been observed to induce allergy and hypersensitivity related problems as well as corneal toxicity. [102] Aspirin is the most studied NSAID in the treatment of AMD. Yet, the results remain inconsistent. [104]

Because of its key role in innate immunity, various regulators of the complement system have been targeted in AMD treatment. [102] Studied complement system inhibitors include lampalizumab, ARC1905, TNX-234, eculizumab and POT-4 [8, 102]. Lampalizumab was considered as the most promising therapeutic agent for dry AMD [8]. However, in two

phase 3 clinical trials reported by Holz et al. [105] lampilizumab failed to reduce AMD-related geographic atrophy.

5.5 Photodynamic Therapy

Due to the clear optical pathway to the fundus, laser light can be used to activate drug molecules in the retina and RPE. In photodynamic therapy (PDT), light-sensitive dye verteprofin is administered intravenously where it concentrates in CNV-related blood vessels. When activated by 689-nm laser beam, verteprofin induces the formation of highly reactive singlet oxygen that damages the endothelial cells and causes occlusion of the new vessels. [22] The selectivity of verteprofin to the CNV allows directing the treatment to the lesion and prevents the damaging of surrounding tissues [8].

The beneficial effects of PDT have been demonstrated by the Treatment of Age-Related Macular Degeneration With Photodynamic Therapy (TAP) Study Group [106] and the Verteprofin in Photodynamic Therapy Study Group [107]. PDT does not improve vision but limits the wet AMD-related vision loss [106, 107]. However, the results of PDT are unpredictable and prone to AMD recurrence. Therefore, if PDT is used, it is often used in combination with another treatment method such as intravitreal antiangiogenic therapy. [8]

5.6 Laser Heating Treatment

The aim of retinal laser heating treatment is to induce positive changes in the retinal tissue by heating it with laser light. When laser light is shone to the eye, it is absorbed by ocular pigment molecules. [108] As the light is absorbed by tissue, its energy is transformed to heat. Heat is conducted from the heated area to the surrounding, cooler tissues. [109] The laser-induced retinal temperature increase is proportional to laser power and spot size, exposure duration, laser wavelength, fundus pigmentation, choroidal blood flow and transparency of ocular media [12, 13, 14].

The major ocular pigments are melanin, hemoglobin, and xanthophyll. Melanin is found in the RPE and choroid. It absorbs the majority of incoming light in the visible and near-infrared spectrum. Xanthophyll is found mostly in the macular area and absorbs blue light. [108] Hemoglobin is a protein found in red blood cells [18]. It has high absorbance for blue, green and yellow light but has poor red and infrared light absorption [108, 110].

Figure 10 shows temperature profiles in the fundus in response to different wavelengths of light. The data in Figure 10 is calculated by Vogel et al. [111]. In these calculations, the scattering of light before retina and reflection from sclera are not taken into consideration. [111] The absorbance of melanin, hemoglobin, and xanthophyll decreases with longer wavelengths [110, 111]. As shown in Figure 10, decreased absorbance tends to shift the temperature elevation towards deeper tissues. In addition, when using a longer wavelength of light, the higher laser intensity is needed to produce the same temperature increase. [111] Moreover, at longer infrared wavelengths, the absorbance of water increases preventing the penetration of light [112].

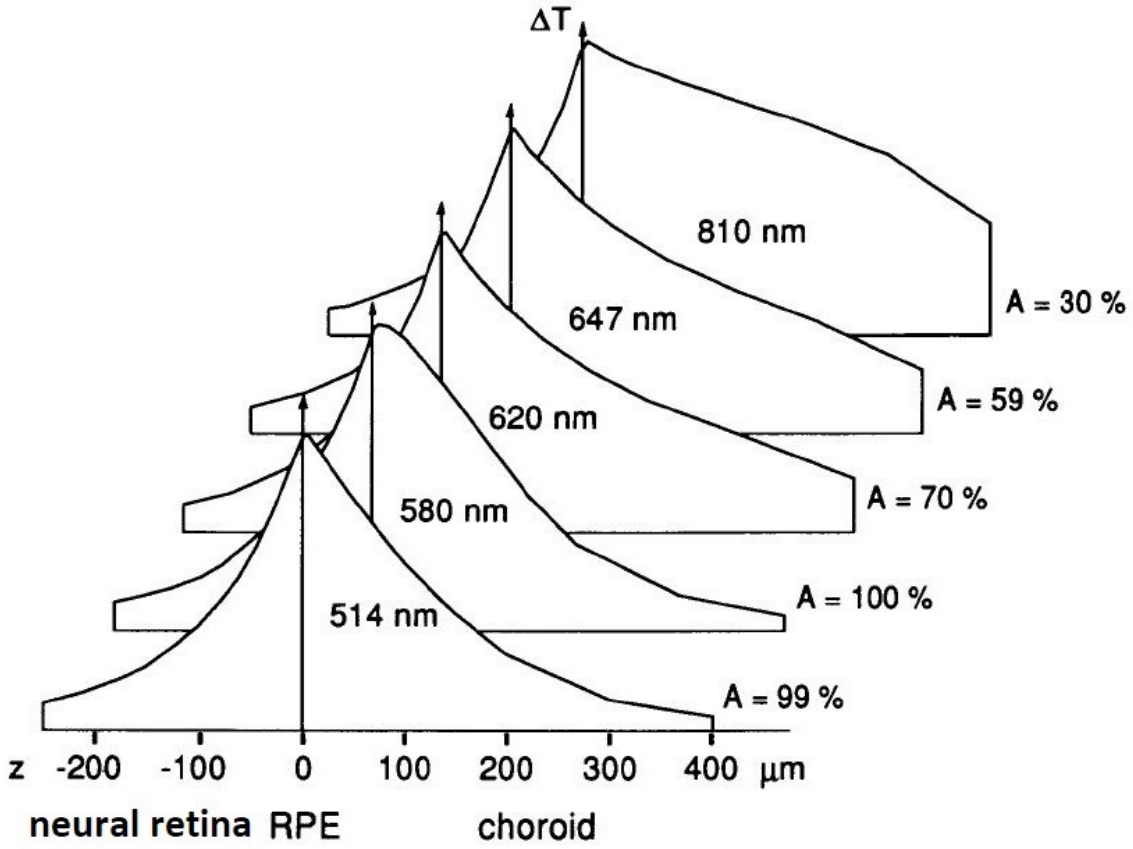

Figure 10. *Calculated temperature profiles during laser treatment. The diameter of the laser beam is 500 μm and heating duration is 100 ms. ΔT is the maximal temperature increase in each location z. Data is normalized to have the same temperature elevation at RPE for all wavelengths. A is the total percentage of light absorbed by RPE and choroid. [111]*

There are several different treatment modalities for retinal laser therapy. These modalities include methods designed to cause retinal cell death, methods that aim to limit cell death to RPE cells and methods that aim to avoid cell death completely.

5.6.1 Photocoagulation

Laser photocoagulation is the oldest laser treatment modality. The aim of this treatment is to induce visible burns to the retinal tissues. In photocoagulation, the retina is heated with a high-power laser. [113] This induces temperature elevation that causes proteins to lose their three-dimensional structure and form aggregates in a process referred to as coagulation [114]. The coagulation can be observed during treatment as a decrease in transparency of neural retina. [113]

Photocoagulation has been used to treat choroidal neovascularization in wet AMD [115]. However, the mechanism how photocoagulation could improve the retinal state is not known [108]. One hypothesis is that photocoagulation-induced heat damage in the capillaries causes the formation of clots that block the capillaries and prevent leakage of blood. Other idea is that photocoagulation reduces hypoxia in the retina. In the normal retina, oxygen diffuses from choriocapillaris to the retina and is mostly consumed by photoreceptors. Photocoagulation causes the death of photoreceptors allowing oxygen to diffuse deeper to the retina and thus increases retina's oxygen concentration. [108] Aiello et al. [116] observed that hypoxia increases VEGF expression in retinal cells. Therefore, the reduction of hypoxia could reduce VEGF expression and thus prevent neovascularization. [116] This idea is supported by an observation made by Lip et al. [117] that photocoagulation decreases VEGF production in patients suffering from retinal neovascularization related to either diabetes or ischemic vein occlusion. In addition, reduced hypoxia could reduce vasodilatation and endothelial stretching that promote neovascularization [118]. Elevated VEGF expression in response to stretching of retinal endothelial cells was observed by Suzuma et al. [119].

Nevertheless, photocoagulation is associated with several adverse effects including visual field defects, alterations in color vision and reduced contrast sensitivity [115]. Since photocoagulation induces permanent damage to the neural retina, it could only be used for a limited number of patients where the positive effects outweigh the adverse effects of the treatment. Moreover, photocoagulation treatment leads to a high prevalence of recurrences and, therefore, in the treatment of CNV, photocoagulation has nowadays been mostly replaced with intravitreal anti-angiogenic therapy [115, 120].

5.6.2 Neural Retina Sparing Methods

In order to overcome problems related to photocoagulation, new laser treatment methods that avoid damaging neural retina have been developed. These methods can be roughly divided into two groups: methods aiming to cause RPE cell death and to cell death avoiding subthreshold methods. RPE cell death-inducing methods include nanosecond laser therapy and selective retinal therapy (SRT) [56]. Promising results of nanosecond laser therapy was obtained by Guymer et al. [121] who observed slowing of AMD progression in a specific subgroup of AMD patients. In both nanosecond laser therapy and SRT, temperature elevation is concentrated in a small area by using a pulsed laser instead of continuous laser [56, 122]. Nanosecond laser therapy utilizes laser pulses in nanosecond range whereas SRT utilizes microsecond long laser pulses [113, 123]. Figure 11 shows how the laser pulse duration affects the resulting temperature profile during laser treatment. Laser pulses lasting 1 μs cause localized temperature elevation around light-absorbing melanosomes that are presented in Figure 11 as high-temperature peaks within RPE. [124] Localized temperature elevation causes vaporization of the cytoplasm that surrounds melanosomes resulting in the formation of microbubbles. Microbubbles disrupt the structure of RPE cells leading to cell death. [113, 125]

Subthreshold methods include transpupillary thermotherapy (TTT), thermal stimulation of the retina (TS-R) and subthreshold diode micropulse photocoagulation (SDM). These methods avoid causing retinal cell death. In TTT and TS-R, the retina is heated using a continuous laser. [56, 125] Used laser pulse durations are 60 s in TTT and 10 ms in TS-R [56, 123]. As shown by Figure 11, longer laser pulse duration allows heat conduction to a larger area [124]. Laser power in TTT and TS-R is low and the aim is to produce a smaller temperature increase than in photocoagulation. [56, 126] Aim in TTT is to produce less than 10°C temperature rise instead of the temperature increase ranging from 33-63°C used in photocoagulation. [127, 128] In SDM, the temperature increase is directed to RPE by using micropulsed laser [129]. However, to avoid cell death, lower power and longer pulse duration (0.1 – 0.3 ms) are used than in SRT, which results in milder temperature elevation and spread of heat to a larger area [123].

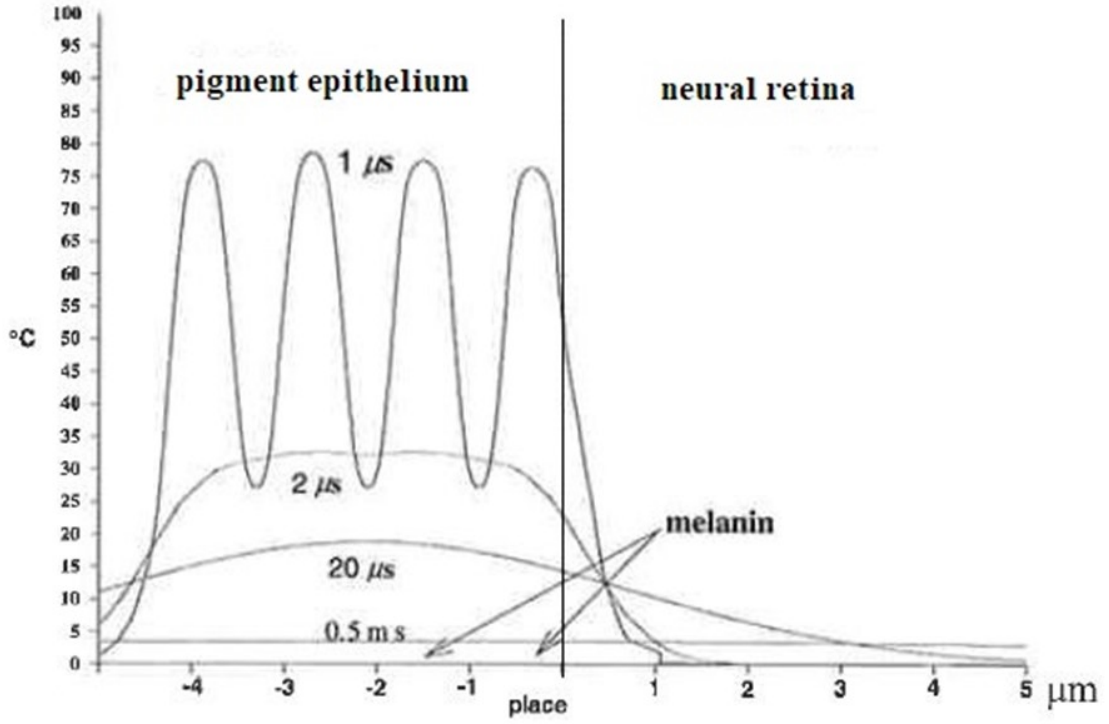

Figure 11. *The calculated temperature profile in the pigment epithelium and neural retina after laser treatment with laser wavelength 514 nm, laser diameter 110 µm and energy 2 µJ with varying heating pulse durations. [124, modified]*

5.6.2.1 Treatment Mechanisms

Heat shock response after retinal laser treatment is a well-known phenomenon. Increased HSPA expression after subthreshold laser treatment has been observed in rabbit choroid by Desmettre et al. [130, 131], in mouse retina by Sramek et al. [132], in rat optic nerve head by Kim et al. [133], in rat retina by She et al. [134], in rabbit RPE by Lavinsky et al. [123] as well as in cell culture of porcine RPE by Kern et al. [135], rabbit RPE by Wang et al. [136] and in immortal human RPE cell line (ARPE-19) by Inagaki et al. [137] .

As discussed in Chapter 2.1, HSPAs act as chaperones preventing protein aggregation and repairing misfolded proteins. It is hypothesized that these properties can prove useful in the treatment of AMD. Overexpression of HSPs can inhibit the accumulation of misfolded proteins as well as protein aggregates to the RPE cells and thus prevent the formation of drusen. Reduction of drusen formation may protect retinal function by preventing drusen-associated inflammation. Additionally, drusen reduction may prevent hypoxia and nutrient deprivation in RPE by limiting the drusen-induced increase of diffusion distance between

choroid and RPE. However, in their review Virgili et al. [138] concluded that even though photocoagulation results in a reduction of drusen, there is no evidence that the removal of drusen reduces the risk of developing CNV, geographic atrophy or visual acuity loss.

Besides its chaperone functions, HSPA is able to regulate several cellular processes. HSPA inhibits inflammatory response via prevention of activation of immune system regulator NFκB [10]. Moreover, HSPA prevents apoptotic cell death by blocking caspase activation and thus promotes RPE cell survival and the normal functioning of RPE [11].

Additionally, HSPA, with help from its co-chaperones, can aid the functioning of UPS. HSPA maintains misfolded proteins in the non-aggregated form to allow their degradation in the proteasome. In addition, HSPA helps ubiquitylation system to recognize misfolded proteins. After ubiquitylation, HSPA assists in the delivery of ubiquitinated protein to the proteasome. It is unknown what determines whether HSPA repairs the misfolded protein or promotes its degradation. [139]

Besides mechanisms related to increased HSPA, other possible treatment mechanisms exist. These mechanisms include RPE regeneration, reduced angiogenesis, enhancement of cell defense systems against oxidative stress and prevention of Bruch's membrane thickening. Laser treatment may have a regenerative effect on RPE. Vessey et al. [122], Zhang et al. [140], Jobling et al. [141] and Richert et al. [142] have observed that after RPE cell death-inducing laser treatment, new RPE cells are formed that repair the laser-induced lesion. They hypothesize that in response to laser treatment otherwise non-mitotic RPE cells regain their ability to divide and repair the laser-induced lesions with new cells. This would imply that RPE damaging laser treatment can replace the old and diseased RPE cells with new, younger cells and therefore, nanosecond laser therapy and SRT treatment are sometimes referred to as rejuvenating therapies. [113, 122]

In addition, laser treatment can affect angiogenesis of the retina. Retinal reduction of proangiogenic VEGF and increase of antiangiogenic PEDF was observed after SRT in porcine choroid explants by Richert et al. [142] and after SDM in cultivated mouse RPE cells by Li et al. [143]. Li et al. [143] also observed that after SDM, proangiogenic factors transforming growth factor (TGF-β) and basic fibroblast growth factor (bFGF) were downregulated in cultivated mouse RPE cells. These results indicate that laser treatment reduces angiogenesis and may thus prevent the formation of CNV. [143] Nevertheless, in studies

conducted by Cordeiro et al. [144] and Faby et al. [145] VEGF expression of ARPE-19 cells and isolated human RPE cells increased when they are exposed to elevated temperatures.

Sublethal hyperthermia has been observed to enhance the cell defense system against oxidative stress. The ratio of reduced glutathione (GHS) to oxidized glutathione (GSSG) is often used as an indicator of oxidative stress. GHS is important antioxidant and its reaction with ROS generates GSSG. Cells recycle GSSG back to GHS. During oxidative stress, the ratio of GHS to GSSG decreases since a larger portion of GHS have reacted with ROS to produce GSSG. Iwami et al. [146] observed that hyperthermia-induced increase in GSH/GSSG ratio in cultivated porcine RPE cells. In addition, after H_2O_2 exposure, the hyperthermia preconditioned RPE cells showed less ROS induced toxic 4-hydroxynonenal (4-HNE) adducts which indicates that hyperthermia protected RPE cells against oxidative stress. [146] Increased GHS levels were observed also by Cillà et al. [147] in mice after laser treatment. Additionally, they observed increased levels of the antioxidant enzyme superoxide dismutase 1 (SOD1) and lowered levels of ROS induced lipid peroxidation end product malondialdehyde (MDA).

Laser treatment may contribute to the prevention of Bruch's membrane thickening by increasing the activity of Bruch's membrane degrading MMPs. Changes in the amounts of activated MMPs have been observed after retinal laser treatment. Increase in active MMP after nanosecond laser treatment was observed in human RPE-choroid explants by Zhang et al. [140] and in AMD model mouse $ApoE^{-/-}$ by Jobling et al. [141] as well as after SRT in porcine RPE-choroid explants by Richert et al. [142] and Treumer et al. [148]. Bruch's membrane thinning was observed after nanosecond laser treatment in $ApoE^{-/-}$ mice by Jobling et al. [141] as well as after SR-T in the AMD model mice $ApoE^{-/-}$ and $NRF2^{-/-}$ by Tode et al. [56]. It is not clear whether the MMP increase requires RPE cell death or not. Results of Treumer et al. [148] suggest that the MMP increase can only be triggered by RPE cell death or removal. However, Tode et al. [56] observed Bruch's membrane thinning after TS-R in $ApoE^{-/-}$ and $NRF2^{-/-}$ mice without significant changes in RPE cell structure.

Bruch's membrane thinning after laser treatment may also be related to increased HSPA expression. Sims et al. [149] observed that in breast cancer cell culture, depletion or inhibition of HSPA decreases MMP family member MMP-2 activation. Therefore, it is likely that HSPA has an important role in the activation of MMP-2. [149]

5.6.2.2 Retinal Temperature During Laser Treatment

Elevated temperature damages retinal cells and can even lead to cell death. The extent of heat-induced cellular damage depends on the magnitude of the heat elevation as well as the duration of the temperature increase. [135] Therefore, the central goal in heat shock-inducing retinal laser treatment is finding a combination of duration and magnitude of temperature increase that induces heat shock response expression but not cell death.

Several studies have aimed to find out this therapeutic window: Kern et al. [135], Sramek et al. [132], Desmettre et al. [130, 131], Kim et al. [133], Lavinsky et al. [123] and Wang et al. [136, 150]. However, these studies lack a method to determine retinal temperature during laser treatment and have instead estimated temperature using mathematical models or compared the end-results of treatments conducted with different laser powers. This approach may prove problematic since temperature elevation during laser treatment is affected by various factors such as the amount of pigmentation, the distribution of pigmentation, the transparency of ocular media and blood flow [13, 14, 150]. Therefore, it is likely that heating with the same laser power does not yield the same retinal temperature in different patients and between different locations within the patient's retina.

One method for the estimation of thermal damage and HSPA expression is Arrhenius damage integral. Arrhenius damage integral assumes that the rate of protein denaturation caused by hyperthermia can be represented as a temperature-dependent chemical reaction. The value of Arrhenius integral is calculated as follows

$$\Omega(\tau) = A\int_0^{\tau} e^{-\frac{E^*}{RT(t)}}\,dt \tag{1}$$

where A is rate coefficient, E^* is activation energy, T is temperature and R is the gas constant. Arrhenius damage integral describes the amount of denaturation caused by temperature $T(t)$ in time τ . The arrhenius damage integral model assumes that cell death occurs at a certain level of denaturation. [150] Sramek et al [151] found in rabbit RPE that the activation energy is $E^* = 340\,{}^{kJ}\!/_{mol}$ and that the rate coefficient is $A = 1.6\cdot 10^{55}\ s^{-1}$ when the Arrhenius integral is normalized to $\Omega = 1$ at the cell damage threshold. Sramek et al. [152] observed that in mouse the threshold of HSPA expression is Ω = 0.11. Therefore, non-damaging hyperthermia corresponds to Arrhenius integral values between 1 and 0.11. [152] Arrhenius damage integral model simplifies the thermal denaturation process in cells to a single reaction rate with one activation energy and assumes that there is no cellular

repair during hyperthermia [123, 150]. Despite this, the model can be used to determine damage and HSPA expression thresholds during short heating times. However, already with the pulse duration of 200 ms, the model becomes unreliable. [150] Therefore, other temperature estimation methods are required for longer heating durations.

This Master's thesis utilizes the ERG-based temperature determination method developed by Pitkänen et al. [15] to investigate the therapeutic window of subthreshold laser treatment. This method allows the assessment of retinal temperature during continuous laser heating treatments. The method is based on temperature-induced changes in the ERG signal and is described in more detail in [15].

The heating duration in this Master's thesis was 10 minutes. HSPA expression in response to similar heating duration was studied by Barbe et al. [153]. They observed that raising the body temperature of rats to 41°C for 15 minutes induced HSPA expression in the rat retina. Lower temperatures with longer exposure times up to 60 minutes did not result in increased HSPA expression. [153] Based on their results, it seems that 41°C for 15 minutes corresponds to the lower limit of HSPA expression in the rat retina. In addition, HSPA expression was observed in the rat retina after 15 minutes of whole-body hyperthermia to 41 - 42°C by Tytell et al. [154]. Besides retina, the temperature of 42 - 42.2°C for 15 to 20 minutes has been used to induce increase HSPA expression in adult rat cardiomonocytes, rat heart and cortical cultures by Kawana et al. [155], Gowda et al. [156] and Rodolf et al. [157].

Rylander et al. [158] studied HSPA expression in cultured bovine aortic endothelial cells. They searched for optimal heating protocol by testing several temperatures and heating durations. They observed that highest HSPA expressions were achieved with 44°C, 46°C, 48°C and 50°C for 24 min, 12 min, 6 min, and 3 min, respectively. However, these treatments induced cell death. [158] Similar results were obtained by Kern et al. [135], who observed that in primary porcine RPE cultures the highest HSPA expression is achieved with heating that induces cell death. They calculated that cell death threshold is 50°C and the threshold for occurrence of apoptotic changes is 47°C when heating porcine RPE cell culture for 10 s. [135]

The kinetics of HSPA expression were studied in rat optic nerve head after TTT by Kim et al. [133], in rat retina after the whole body hyperthermia by Tytell et al. [154] and in cultured choroid-retinal endothelial cells after laser irradiation by Du et al. [159]. Based on their

results, it seems that the peak of HSPA expression occurs around 18 hours after heating treatment and decreases thereafter. After 24 hours, the HSPA amount has moderately decreased but is still significantly higher compared to control. [133, 135, 159] After 48 hours, Du et al. [159] observed HSPA levels similar to control. However, HSPA amounts above baseline level were observed after 48 hours by Kern et al. [135], after 50 hours by Tytel et al. [154] and after 72 hours by Kim et al. [133].

6. Methods

The purpose of this Master's thesis was to study how laser heating treatment affects the retinal function in mice and to probe the therapeutic window of heat shock response in the laser heating treatment of RPE. During the experiments, retinas were subjected to different temperature elevations and we examined the effect of these temperature elevations on the retina. In order to reach the desired treatment temperature, ERG-based temperature assessment method was used during the heating treatment. We studied the effect of heating treatment to RPE using immunohistochemistry. RPE damage was assessed from the phalloidin staining of actin filaments that shows the cellular structure and increased amount of HSPA was used as an indicator for the heat shock response. This chapter describes the used methods. The chapter begins by introducing the theory of ERG-based temperature estimation and staining methods and continues with the detailed description of used methods.

6.1 Electroretinography-Based Retinal Temperature Estimation

Electroretinography (ERG) records changes in the electrical activity of the retina that are caused by light stimulation. It can be used to evaluate the retinal function and to diagnose various retinal disorders such as retinitis pigmentosa, congenital stationary night blindness, central retinal vein occlusion, central retinal artery occlusion, and retinal detachment. [160] ERG can be recorded from a living animal (*in vivo* ERG). Additionally, ERG can be recorded from an isolated retina or eyecup (*ex vivo* ERG). [17, 161]

During darkness, retinal cells maintain extracellular ion currents, such as photoreceptor dark current. As stated by Ohm's law, ion currents moving in resistive extracellular space create extracellular potential differences between the two sides of the retina. Combination of these potential differences created by different retinal cells constitutes the ERG signal. [17] Voltage during darkness is defined as a reference level in ERG recordings [162]. Light exposure changes extracellular ion currents and thus results in alterations in extracellular voltage [161]. For example, as described in Chapter 1.2.1, photoreceptor dark current reduces in response to light because of the closure of cGMP gated channels [19]. Due to the parallel organization of retinal cells, the radial currents sum up. However, the lateral arrangement of the retina is symmetrical and therefore lateral currents in retina mainly cancel each other. [161]

ERG signal is often divided into three components: P-I, P-II, P-III. These components are shown in Figure 12. P-I component is caused by pigment epithelium and P-II component by ON bipolar cells [163]. P-III component can be divided into fast P-III and slow P-III. Fast P-III component is caused by the activity of photoreceptor cells and slow P-III component by Muller cells. [161] Figure 13 shows ERG signal waveforms that are typically seen in the *in vivo* ERG signal of dark-adapted retina in response to light stimulus. The response starts with a negative a-wave. A-wave consists of fast P-III component and is partially overlapped by positive b-wave that is a summation of P-II and P-III components. B-wave is followed by c-wave that is mainly a summation of P-I and P-III components. [161]

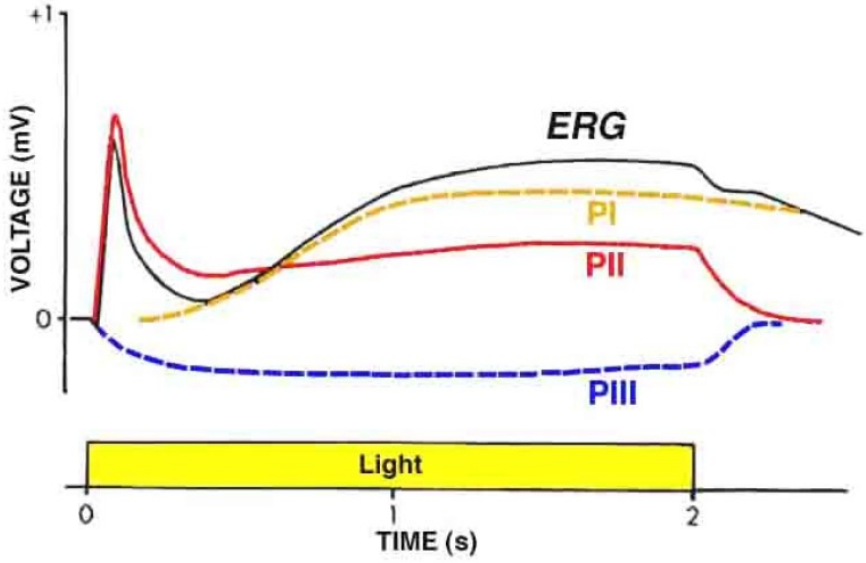

Figure 12. *ERG signal recorded from cat eye in response to 2 s stimulus. P-I, P-II, and P-III components have been recorded by deepening the anesthesia. [161]*

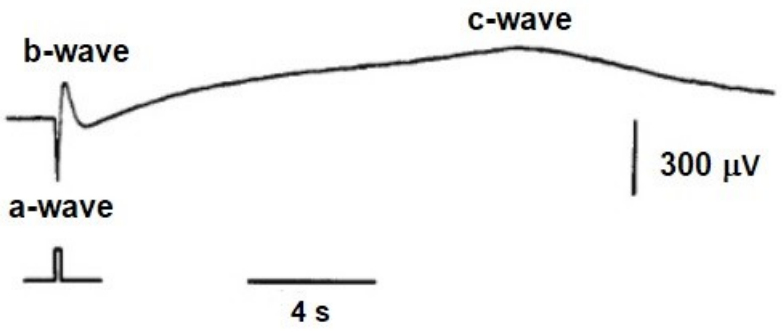

Figure 13. *ERG signal recorded from dark-adapted skate eye cup in response to stimulus lasting 0.2 s. Signal contains a-, b- and c-wave that are typically seen in in vivo ERG signal. [164, modified]*

In this Master's thesis, RPE heating was achieved by laser irradiation. Suitable laser power was selected using the ERG signal based temperature estimation method developed by Pitkänen et al. [15, 165]. They observed that temperature-dependent changes in ERG photoresponse kinetics and amplitudes can be used to estimate retinal temperature [15, 165].

From heated RPE, heat spreads mainly by conduction to the rest of the retina. Ibarra et al. [13] found no significant difference between the temperatures of the inner limiting membrane and subretinal space in a rabbit during one-minute heating laser exposure. Therefore, temperature-induced changes in the ERG signal can be used to estimate RPE temperature during long heating treatments where the heat has a sufficient amount of time to dissipate from RPE to the rest of the retina.

In this Master's thesis, the temperature of the retina was estimated based on temperature dependent changes in the time from stimulus light pulse to ERG signal b-wave peak (referred in this Master's thesis as time-to-maximum, TTM). Pitkänen et al. [15] showed that near mouse body temperature TTM decreases linearly with increasing temperature. They observed that the change of TTM compared to the body temperature is 3.6% per 1°C for a mouse *in vivo* [15]. Temperature differences compared to body temperature ΔT were calculated using the equation

$$\Delta T = \frac{TTM_r - TTM_{ref}}{TTM_{ref}} \cdot B \tag{2}$$

where TTM_{ref} is the mean of reference TTM values measured in the body temperature, TTM_r is the recorded TTM and B is a coefficient that describes the temperature dependence of TTM. For mouse *in vivo*, the coefficient B is -27.8 [15].

6.2 Immunohistochemistry

Immunohistochemistry allows detection and localization of target molecules. The method is based on the interaction between antibody and antigen. [19] Antibodies or immunoglobulins are glycoproteins that are produced by the vertebrate immune system cells in response to a foreign substance. This foreign substance is referred to as antigen [166]. Antibodies have the ability to recognize and bind to the antigen as well as to the specialized cells and proteins of the immune system [167].

Figure 14 shows a schematic presentation of the antibody structure. Antibodies have Y-shape and they consist of four polypeptide chains: 2 heavy chains and 2 light chains. Antibodies are divided into five classes based on the structure of heavy chains. In mammals, types of heavy polypeptides are named alphabetically as α, δ, ε, γ and μ, and give rise to five classes of antibodies IgA, IgD, IgE, IgG, and IgM, respectively. The arms of Y are referred to as Fab domains and they contain a site that can bind to the specific part of antigen. This part of the antigen is referred to as an epitope or immunodeterminant region. The binding occurs via reversible, noncovalent interactions and therefore the antibody-antigen complex is in equilibrium with its free components. Antibodies are usually highly specific to one antigen. The base of the Y is referred to as the Fc domain and is important for the function and regulation of the immune system. [167]

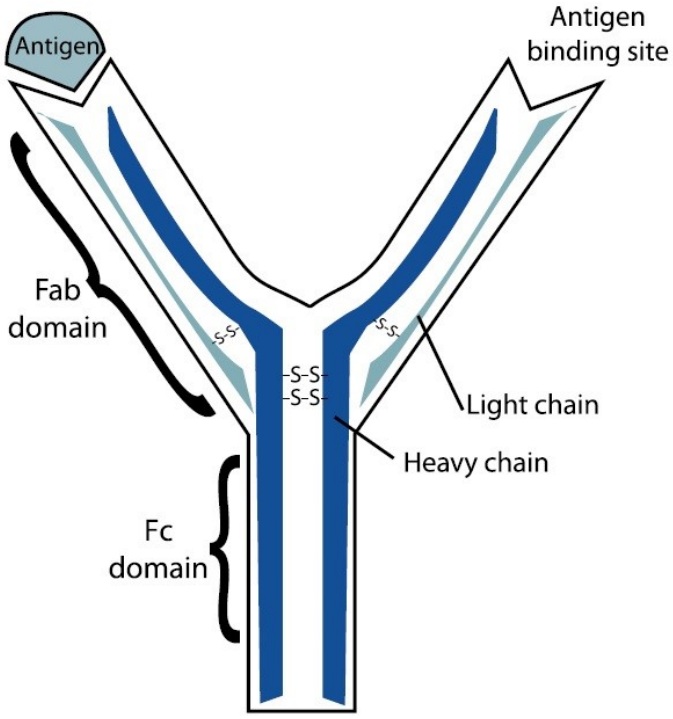

Figure 14. *Schematic presentation of the antibody structure. [167]*

The specificity of an antibody refers to its ability to recognize certain antigen when other antigens are present. Affinity describes the binding strength of the antibody to antigen. Antibodies with higher affinity are preferable in immunochemical assays because they bind larger amounts of antigen with higher stability in a shorter time. [166]

Antibodies used in immunohistochemistry are produced in live animals by injecting a purified target molecule under the skin or into the bloodstream of the animal. The injected molecule initiates an immune response in the animal which causes the generation of antibodies. [19] Most antigens are highly complex and therefore, the immune system may produce several different antibodies that recognize different epitopes of the same antigen. Polyclonal antibodies are isolated from the serum of the animal and thus contain various antibody molecules that can bind to the same antigen. Production of monoclonal antibodies begins by isolating antibody-producing immune cells from the animal. Then, immune cells that produce the desired antigen are cultured and finally, the antigen is harvested from the culture. Monoclonal antibodies, therefore, bind to the same epitope. Polyclonal antibodies are more often used in the immunohistochemistry because they are not as sensitive to small changes in the antigen structure caused by polymorphism or denaturation. Polyclonal antibodies can also be produced more rapidly, at less expense and with less technical skill than monoclonal antibodies. [166] On the other hand, monoclonal antibodies have more homogenous specificities and affinities [167].

Antibodies are attached to a label molecule that allows the detection of the bound antigen. Fluorophores are commonly used as label molecules in immunohistochemistry. Fluorophores are molecules that emit light when excited by light. [166] When the fluorophore molecule absorbs a photon, it receives energy and enters excited state. The excited state is short-lived and the fluorphore returns to its ground state by losing the excess energy. The excess energy can be lost as heat or by emitting photon. The wavelength of emitted light differs from the exciting wavelength when part of the energy has been lost as heat. This difference is referred to as the Stokes shift. Fluorophores can be detected with a fluorescence microscope. Fluorescence microscope illuminates the specimen with excitation wavelength light and separates emission light using filters. The emission light is then focused on the detector. [168]

Figure 15 illustrates a direct and indirect method for antigen detection. In the direct method, the primary antibody attached to the marker molecule binds to the antigen. Similarly, in the indirect method, the primary antibody binds to the antigen but the marker molecule is attached to a secondary antibody that binds to the primary antibody. The indirect method allows amplification of the signal since multiple secondary antibodies can bind to the same primary antibody. [167]

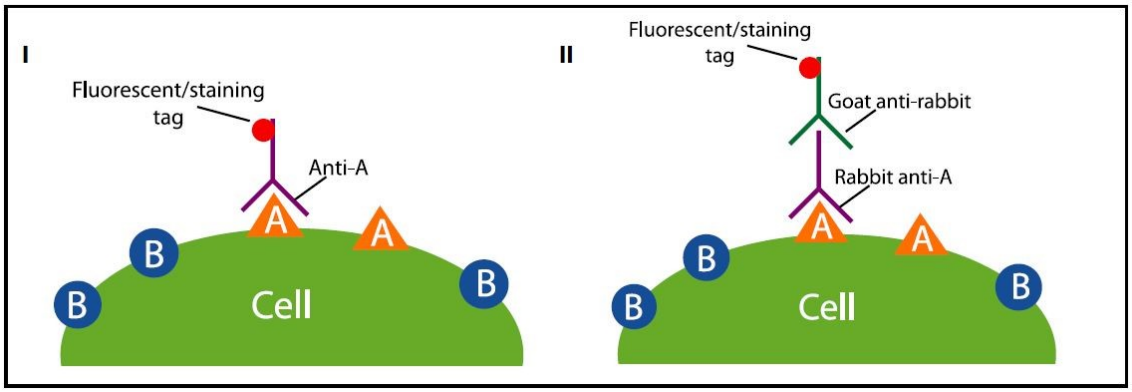

Figure 15. *Direct (left) and indirect (right) antigen detection [167]*

Immunohistochemistry staining protocols vary according to application. However, commonly used steps include tissue fixation, antigen retrieval, blocking, incubation with antibody, counterstaining and mounting. Prior to staining, the tissue is fixed to preserve its structure [169]. Formaldehyde is one of the most commonly used fixatives [170]. However, formaldehyde fixation may alter the structure of proteins reducing their detectability by immunohistochemistry. [171] One of these alterations is cross-linking of proteins by methylene bridges that mask the antibody binding sites [172]. The aim of antigen retrieval is to reverse these fixation-induced modifications in order to allow better detectability of the antigen. [171] Antigen retrieval can be achieved by using either protease digestion or heating. These methods are referred to as protease induced epitope retrieval (PIER) or heat-induced epitope retrieval (HIER).

Blocking is done before the addition of primary antibody. The purpose of blocking is to prevent antibody binding to other proteins than the desired antigen. In blocking, a solution containing proteins, such as serum, is added to the tissue sample. These protein molecules bind to the sites that would otherwise potentially bind to the antibody thereby preventing or “blocking” antibody binding to other locations than the desired epitope. [170] Counterstaining can be used to make surrounding tissue morphology visible which aids in the localization of antigen [169]. After the staining is completed, the specimen is mounted between a slide and a cover-slip with mounting medium. The purpose of mounting medium is to physically protect the specimen by binding the specimen, slide, and coverslip together. [173] The stained specimen can then be imaged using a fluorescence microscope.

6.3 Retinal Heating Experiments

The recording protocol and the equipment were developed in the Department of Neuroscience and Biomedical Engineering (NBE) of Aalto University. The used equipment is described in more detail in the Master's thesis by Kaikkonen [174]. The used retinal temperature estimation method is developed by Pitkänen et al. [15].

6.3.1 Animals and Preparation

The use and handling of the animals were in accordance with the Finnish Act on Animal Experimentation 2006 and the guidelines of the Animal Experiment Board in Finland. The project plan has been approved by the Finnish Animal Experiment Board (project license number: ESAVI/6345/04.10.07/2015).

Female mice of age 4-5.5 months of strain C57BL/6JRccHsd were used in the experiments. This age group was selected because the mice of this age are mature but not yet affected by senescence [175]. The mice were kept in a 12:12 light/dark rhythm and dark-adapted overnight before the experiment day. The mouse was placed in an induction chamber and anesthetized using inhalation of isoflurane (Animalcare Ltd. York, UK). The induction concentration of isoflurane was approximately 4.5 % and maintenance 1.1 % in 100 % oxygen. Righting reflex was tested by tipping the induction chamber over. After losing righting reflex, the animal was placed on a custom-made polycarbonate bed equipped with anesthetic supply. All handlings were done under dim red light.

In order to prevent the movement of the eye during heating, 0.5 mg/kg of medetomidine (Orion Corporation Orion Pharma, Espoo, Finland) diluted in 9 mg/ml NaCl solution (B.Braun, Melsungen, Germany) was injected subcutaneously. During anesthesia, respiration was monitored using piezo electrode (Pico Movement Sensor, MFi BV, Heerlen, The Netherlands) that was placed underneath the mouse slightly behind the thoracic diaphragm. Isoflurane concentration was adjusted during the experiment to maintain respiration rate 2-2.5 Hz. The body temperature was measured by a rectal thermistor (Betatherm 30K6A309I, Oy Farnell Finland Ab, Helsinki, Finland). Appropriate body temperature was maintained by adjusting the temperature of the water circulation inside a polycarbonate bed, underneath the mouse.

The pupil of the right eye was dilated using 10 mg/ml atropine sulfate eyedrop (Bausch + Lomb UK Ltd., London, UK) and 100 mg/ml phenylephrine HCl eyedrop (Bausch + Lomb UK Ltd., London, UK). The corneas of both eyes were anesthetized using 4 mg/ml oxybuprocaine HCl eye drops (Santen Ltd., Tampere, Finland). Eyes where moisturized using 6 mg/ml methylcellulose (Yliopiston Apteekki, Helsinki, Finland) in 9 mg/ml NaCl solution (B.Braun, Melsungen, Germany)

Figure 16 presents the restraining of the mouse and the position of the electrodes. The position of the mouse was fixed using ear holders and a rubber band that was placed over the mouse's forehead. Whiskers of the mouse were cut to prevent them from disturbing the contact between electrodes and eyes. The electrodes were Ag-AgCl pellet electrodes (ground and recording electrodes: EP1, reference electrode: EP2, World Precision Instruments Ltd., Hitchin, UK). The reference electrode was placed inside a holder made of 1 ml syringe. The syringe was filled with the methylcellulose solution to provide contact between the eye and electrode and the tip was placed around the left eye. The ground electrode was moisturized with the methylcellulose solution and placed in the rectum of the mouse.

Figure 17 presents the placement of the recording electrode and the fundus lens. The measurement electrode was placed in a custom made holder filled with the methylcellulose solution. The electrode holder has a glass capillary tip that allows electrical contact between the electrode and the eye. This tip was placed next to the fundus lens of the heating device and the fundus lens was brought in contact with the methylcellulose solution on the right eye of the mouse. The fundus lens was placed using monochrome video camera imaging through the fundus lens. During the placement of the fundus lens, the mouse eye was illuminated by infrared light and by heating laser light with low power setting. After lens placement, a small amount of methylcellulose solution was added to the eye through the glass capillary tip to ensure proper moisturization of the eye and electrical contact between the eye and measurement electrode. The heating laser spot was placed approximately in the center of the dilated pupil.

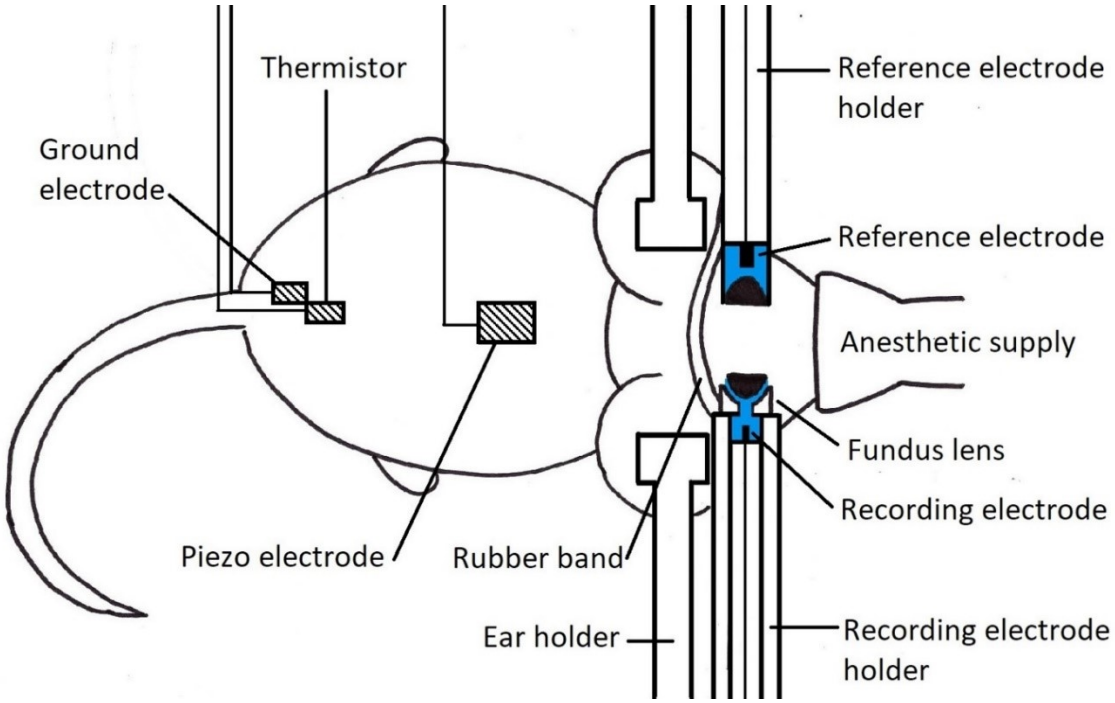

Figure 16. *Restraining of the mouse and the position of electrodes.*

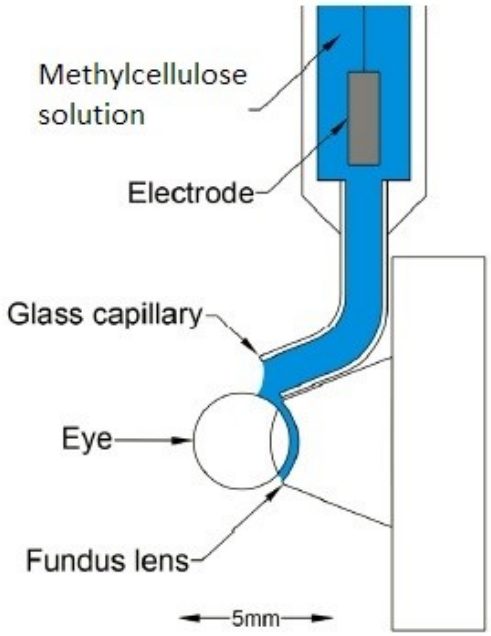

Figure 17. *Placement of recording electrode and fundus lens. [174, modified]*

6.3.2 Heating Treatment

In this Master's thesis, the temperature-dependent changes in ERG-signal were used to estimate mouse retinal temperature during laser-induced retinal heating. The potential difference was recorded between the electrode placed in contact with the eye and the grounding electrode placed to the rectum of the mouse. The potential difference was recorded simultaneously from both of the eyes. The right eye was stimulated with short light pulses and heated with infrared light whereas the left eye acted as a reference. Studied ERG signal was obtained by subtracting the potential difference measured from the left eye from potential difference measured from the right eye. The difference of potential differences during darkness was defined as a baseline level and set to zero.

Light stimuli were generated using two diode lasers with wavelengths 515 nm (LD-520-120MG, 120 mW, Roithner Lasertechnik GmbH, Vienna, Austria) and 785 nm (RLT780-1000G, 1W, Roithner Lasertechnik GmbH, Vienna, Austria) referred in this Master's thesis as green and near-infrared laser. The intensity of stimuli was not changed during the experiment. Instead, stimulus strength was adjusted by changing the stimulus duration, maximum stimulus duration being 2 ms. These stimuli lengths are short enough to be perceived as impulse-like stimuli by the rod cells [176]. The DC-ERG signals were amplified 1000-fold, low-pass filtered with eight-pole Bessel filter (cutoff frequency 1 kHz) and digitized at 5 kHz with 30 nV resolution.

Heating was conducted using a diode laser (RLCO-1064-2000-TO3, 2 W, Roithner Lasertechnik GmbH, Vienna, Austria) with a wavelength of 1064 nm. This wavelength of light does not induce significant light adaptation of mouse rod cells in the laser power used in these experiments [174]. Figure 18 presents the power density profile of the heating laser beam. The approximate diameter of the heating laser spot on the retina was 0.8 mm and the diameter of stimulus laser spot was 0.5 mm [174].

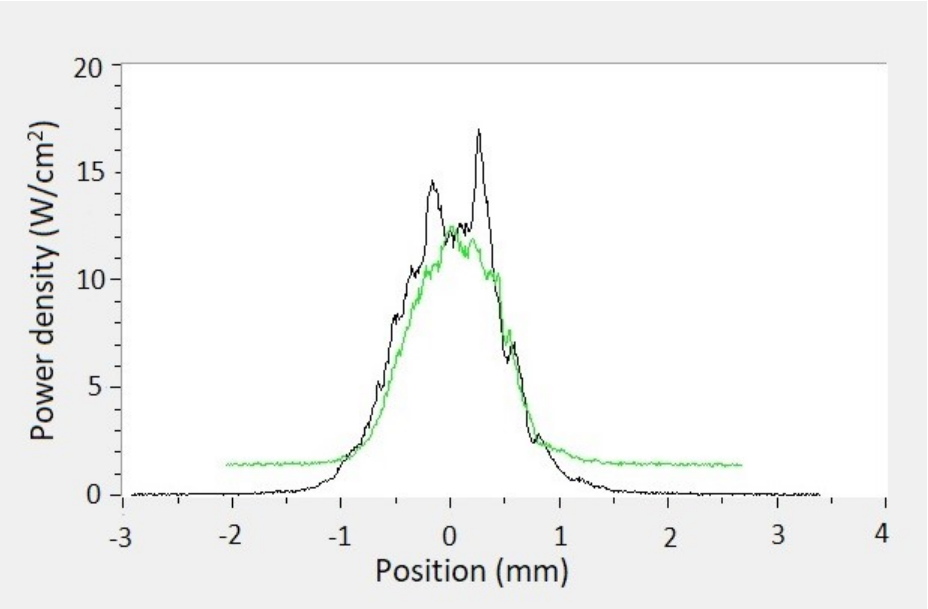

Figure 18. *Heating laser beam power density profile. The black and green line represent power density in the direction of x-axis and y-axis, respectively. The center of the heating laser beam is at zero position.*

ERG stimulus strengths were selected for each mouse based on their individual ERG-responsiveness. For each mouse, a stimulus strength was found that yielded an ERG signal with an a-wave amplitude of ~ 30-50 μV. From this signal, the difference between the b-wave peak and the a-wave peak was calculated. In this Master's thesis, this value is referred to as peak-to-peak amplitude.

The peak-to-peak amplitude was utilized to determine stimulus strengths used during the experiment. ERG-signals were recorded in response to near-infrared as well as green laser stimuli to allow study the of long-wavelength relative sensitivity described by Pitkänen et al. [165] (analysis not included in this Master's thesis). Stimulus strengths were selected to result in the b-wave amplitude of 40 % of the peak-to-peak amplitude separately for the light sources. Additionally, a small number of responses to stronger stimuli were recorded. These stimuli are referred to in this Master's thesis as strong stimuli in contrast to shorter lasting dim stimuli. Strong stimuli were only recorded using the green laser. Strong stimulus duration was equal to 400 times the duration of a dim green stimulus. In this Master's thesis, only ERG responses recorded in response to dim stimuli were analyzed.

During the experiment, dim flash responses were recorded repetitively. Green and near-infrared dim flashes alternated. In addition, strong flash responses were recorded

sporadically. The interval between dim flashes was 3.5 s and after strong flash, no additional flashes were given for 20 s to allow photoreceptor cells to return to their dark-adapted state [15].

After the placement of the lens, the mouse was let to dark-adapt for 12 minutes without exposure to the dim red light that was used during the preparations. Suitable light stimuli strengths were searched during the dark-adaptation period. Heating treatment started after the dark-adaptation. In this Master's thesis, the retinal temperature was determined from the change in the b-wave time-to-maximum (TTM) compared to the TTM values recorded in the body temperature. After dark-adaptation, ERG signals that were used as a reference in the temperature estimation were recorded at the body temperature. During the experiment, 20 or more ERG responses were recorded for the reference. From reference ERG responses, an average of TTM was calculated and set as a reference level to which later determined TTM values were compared in order to estimate retinal temperature changes. After the recording of reference, the representativeness of this reference was confirmed by recording further ERG responses in the body temperature and comparing the temperature estimate based on these responses to the temperature recorded from the rectum of the mouse. Mouse body temperature during the recording of reference was 37.1 - 37.5 °C.

After finding an acceptable reference, heating was initiated. Heating consisted of two parts referred in this Master's thesis as pre-heating and treatment heating. In pre-heating, the retina was heated to 41 $\pm$ 0.3 °C. The heating laser power needed to arrive at the pre-heating temperature was searched by testing different power settings starting from the small power values. The duration of this search varied from 2 minutes to 5 minutes. When a suitable heating power was found, the treatment heating phase was initiated by multiplying the power needed to reach the pre-heating temperature with a predefined factor. Three factors were used in this Master's thesis: 2, 2.5 and 3. This two-phase method was used because the temperature estimation method was calibrated by Pitkänen et al. [15] up to 42.5°C and the method's capability of estimating temperature above this point was unknown. The retina was heated with the treatment power for 10 minutes. After this, the heating laser was turned off and ERG responses were recorded for a couple of minutes. Figure 19 providing an example of the heating laser power and estimated retinal temperature during the different stages of the experiment is presented in Chapter 7.1.

During the experiment, the room air temperature was elevated so that the difference in the temperatures of air around the mouse and the water circulating beneath the mouse

was no more than 4 °C. Therefore, it was assumed that the temperature measured by rectal thermistor matches the temperature of the retina when the retina is not heated. The temperature of the water circulation underneath the mouse and air around the mouse were not adjusted during the heating.

6.3.3 Animal Recovery

After the heating treatment, electrodes were detached, the rectal thermistor was removed and the mouse was released from the ear holders and rubber band. 0.25 mg/kg of medetomidine reversal atipamezole (Orion Corporation Orion Pharma, Espoo, Finland) was injected subcutaneously. Isoflurane administration was terminated and the mouse was placed in a clean and empty cage with a pre-heated bottom. The mouse was moved to a quieter room to recover. Electric heating pad (Beurer GmbH. Ulm, Germany) was placed underneath the cage and the temperature of the pad was adjusted to maintain appropriate body temperature. Moisturized, soft food was available for the mouse. Approximately one hour after the end of isoflurane administration, bedding, nest material, and solid food were added to the cage. The mouse was transferred to the animal room for the night and the cage was partially placed on a heating pad (Braintree Scientific, Inc. Braintree, Massachusetts, United States) in order to help the mouse to maintain appropriate body temperature.

6.4 Histological analysis

Immunostaining protocol developed by André et al. [177] was modified by Mooud Amirkavei to be applicable to this study. Staining and imaging were performed by Mooud Amirkavei.

Mice were euthanized 24 hours after heating treatment by inhalation of CO_2 and cervical dislocation. The eyes were removed and eyecups isolated. Posterior eyecups containing RPE, choroid, and sclera were dissected from the surrounding tissues.

Tissue samples were fixed for 10 minutes at room temperature in 4% formaldehyde solution (FA; Solveco, Rosersberg, Sweden) in phosphate-buffered saline (PBS) (Gibco, Paisley, UK). Tissue fixation was followed by washing of the sample with PBS. Antigen retrieval was accomplished by microwave heating for 3 minutes in Diva Decloaker (Biocare Medical, Concord, CA, USA) diluted to 1:10. After antigen retrieval, samples were incubated

for 1 hour at room temperature in blocking solution that consisted of 10% normal goat serum (Invitrogen, Camarillo, MD, USA) in PBS containing 0.1% Triton X-100 (Sigma-Aldrich Corp., St. Louis, MO, USA). After blocking, the sample was incubated in primary antibody overnight at 4°C. The used primary antibody was HSP70/HSP72 monoclonal antibody (Santa Cruz Biotechnology, Paso Robles, CA, USA) diluted to 1:50. The secondary antibody was anti-rabbit A594 (Invitrogen, Camarillo, MD, USA) that was diluted to 1:500. For counter-staining, Hoechst 33258 (5 g/L in PBS; Sigma-Aldrich Corp.) diluted to 1:2000 and Phalloidin A488 (Invitrogen, Camarillo, MD, USA) diluted to 1:2000 were added to the secondary antibody. The secondary antibody was incubated for one hour at room temperature. Antibody dilutions were performed in blocking solution. After each antibody step, the tissue sample was washed with PBS. Tissue was post-fixed for 10 minutes at room temperature in 4% formaldehyde solution in PBS after which the sample was flat-mounted with fluorescent mounting medium (Dako, Carpinteria, CA, USA). Images were acquired with Axioimage fluorescence microscope with the Zen software (Zeiss, Gottingen, Germany).

6.5 Data Analysis

The analysis of ERG responses was performed in Matlab 2018b and 2014b (MathWorks) and in Microsoft Excel 2013. Periodical artifacts, such as artifacts caused by the mouse's breathing, were removed from the signal using an autoregressive model of order 2500 [15]. This model predicted the baseline behavior after the stimulus based on the baseline behavior before the stimulus. The predicted baseline behavior was subtracted from the recorded signal to yield the final ERG signal.

The peak of b-wave was located from the dim responses by fitting quadratic polynomial around the global maximum. Correction of the fitting was obtained by repeating the fitting around the peak obtained from the first fit. TTM was defined as the maximum of the second fit.

Analyzed ERG responses were assigned to a category depending on which phase of the experiment they were recorded. The reference category contained the ERG responses used as a reference during the experiment and the responses that were used during the experiment to confirm the representativeness of selected reference. The pre-heating category contained ten last ERG responses before the multiplication of the heating laser power with the selected treatment factor. The treatment heating category contained all the ERG responses where treatment heating laser power was used except for ten first

responses. The after category contained responses recorded after the heating laser power was switched off at the end of the experiment excluding 20 first responses.

The autoregressive model was unable to remove artifacts with unfixed interval. Incomplete artifact removal and random response noise resulted in variation in TTM. Within each category, inter-quartile range method (IQR-method) was used to find potential outliers of TTM values. The inter-quartile range is defined as an interval between the 25th percentile and 75th percentile of the data. The method defines recorded TTM values outside the range -1.5 * IQR and 1.5 * IQR are defined as possible outliers and values outside the range -3 * IQR and 3 * IQR as probable outliers. [178] The outliers were confirmed by visual inspection before excluding them from the analysis. The temperature of the retina was estimated based on temperature dependent changes in the TTM values using a method that was described in Chapter 6.1.

Analysis of the fluorescence microscope images was done using Zeiss Zen Lite Blue 2.6. The mean HSPA intensity values were calculated from the whole flat-mounted tissue area of the control eye and heated eye by approximately selecting the tissue area from the images and calculating mean of pixel brightness values of that area. Lesion diameter was measured by approximately fitting circle to the lesion images. Statistical analysis was conducted using Microsoft Excel 2013 and figures were drawn by Microsoft Excel 2013 and Matlab 2014b (MathWorks).

7. Results

7.1 Stages of the Experiment

Figure 19 demonstrates the different stages of heating treatment experiments. Figure 19 A illustrates the laser power during the treatment and Figure 19 B the subsequent temperature elevation in the retina estimated based on the temperature dependent changes in ERG time-to-maximum (see Chapter 6.1). The experiment starts with the recording of reference responses at body temperature without heating laser exposure and the temperature estimation begins after collecting the first reference set. The representativeness of the reference is confirmed by recording an additional set of reference responses at body temperature and comparing estimated retinal temperature to the body temperature measured by a rectal thermistor. In the experiment presented by Figure 19 B, the estimated temperature increase compared to the body temperature before heating laser onset is approximately zero indicating that the selected reference was representative. The reference collection is followed by the pre-heating phase where heating laser power is adjusted to induce retinal heating to 41°C. This corresponds to the temperature increase of approximately 4°C in Figure 19 B. When 41°C is reached, the used heating laser power is multiplied with the selected treatment factor to induce the treatment heating. After 10 minutes of treatment heating, the laser is turned off and retinal temperature returns approximately to the initial level as demonstrated in Figure 19 B. Additionally, Figure 19 B presents a small, gradual decrease in the estimated retinal temperature during treatment heating that was observed in some of the experiments.

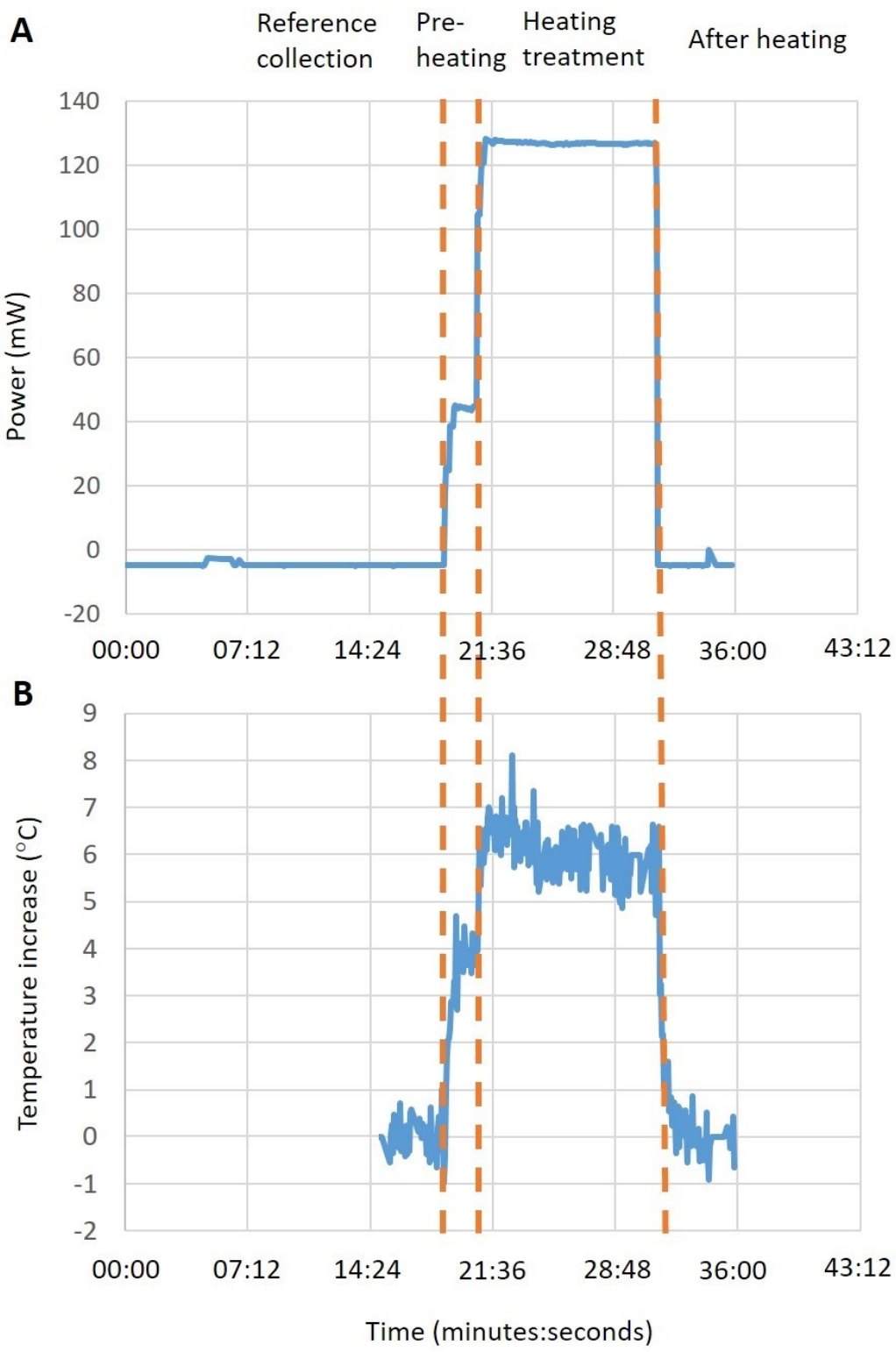

Figure 19. *The different stages of heating treatment experiment with treatment factor of 3.* ***A.*** *Heating laser power during experiment* ***B.*** *Estimated retinal temperature increase compared to body temperature during the experiment. Data in figures A and B are recorded from one mouse during one heat treatment. In the beginning and end of the experiment, the heating laser power deviates from zero due to calibration error.*

Figure 20 shows ERG responses to a dim green stimulus at the different stages of the experiment. The presented responses are non-averaged green stimulus responses and are filtered with a low pass FIR filter (Hamming window, n = 400, f_c = 30 Hz). Figure 20 demonstrates how the kinetics of ERG response accelerate as the retinal temperature increases and that the response kinetics return approximately to the initial level after the heating laser is turned off. Additionally, Figure 20 shows a time-dependent amplitude decrease that we usually observed during the experiments.

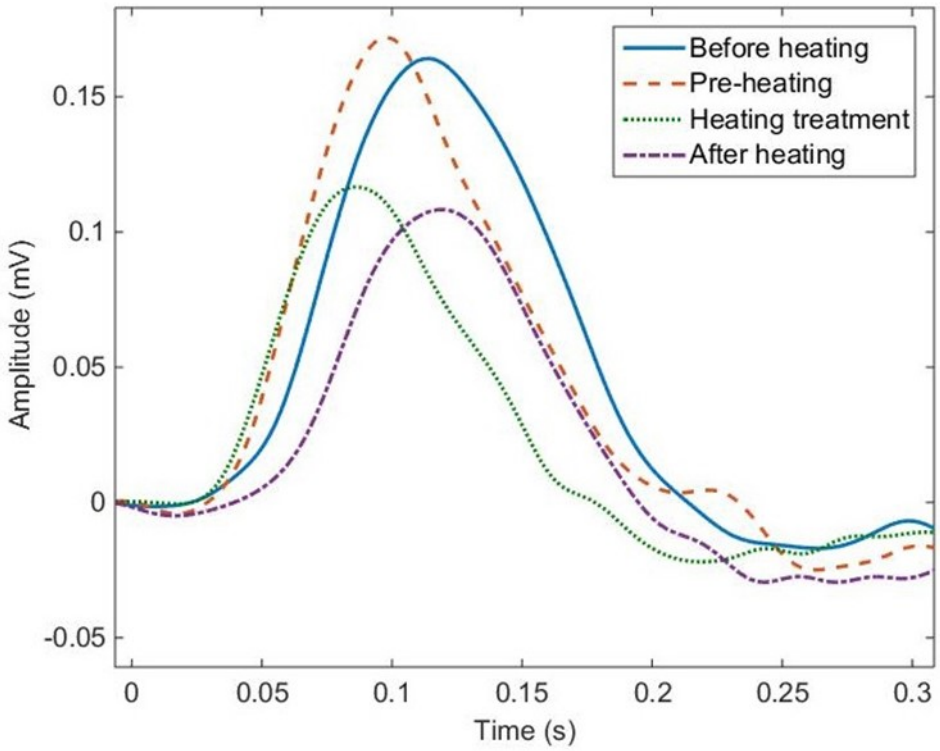

Figure 20. *ERG responses from different experiment stages. Responses are single responses recorded using a dim flash response and filtered with a low pass FIR filter (Hamming window, n = 400, fc = 30 Hz).*

7.2 Power in the Pre-Heating Phase

We investigated the relationship between the heating laser power and the estimated retinal temperature in different mice at the pre-heating phase where the retina was heated to 41 ± 0.3 °C. Suitable heating laser power was searched by testing different power settings starting from low power values. Figure 21 shows the estimated retinal temperature increase in the pre-heating phase as a function of the heating device power.

Figure 21 demonstrates that the power needed to reach the target temperature varied substantially between experiments. Two experiments shown in Figure 21 were rejected from the analysis due to excessively high temperature during the pre-heating phase and unreliableness of the temperature estimation caused by a large artifact superimposed to the ERG signal from mouse breathing. Without these experiments, the mean temperature increase during the pre-heating phase was 3.8 ± 0.2 °C and heating laser power was 48.1 ± 10.3 mW (presented as mean ± standard deviation (STD)).

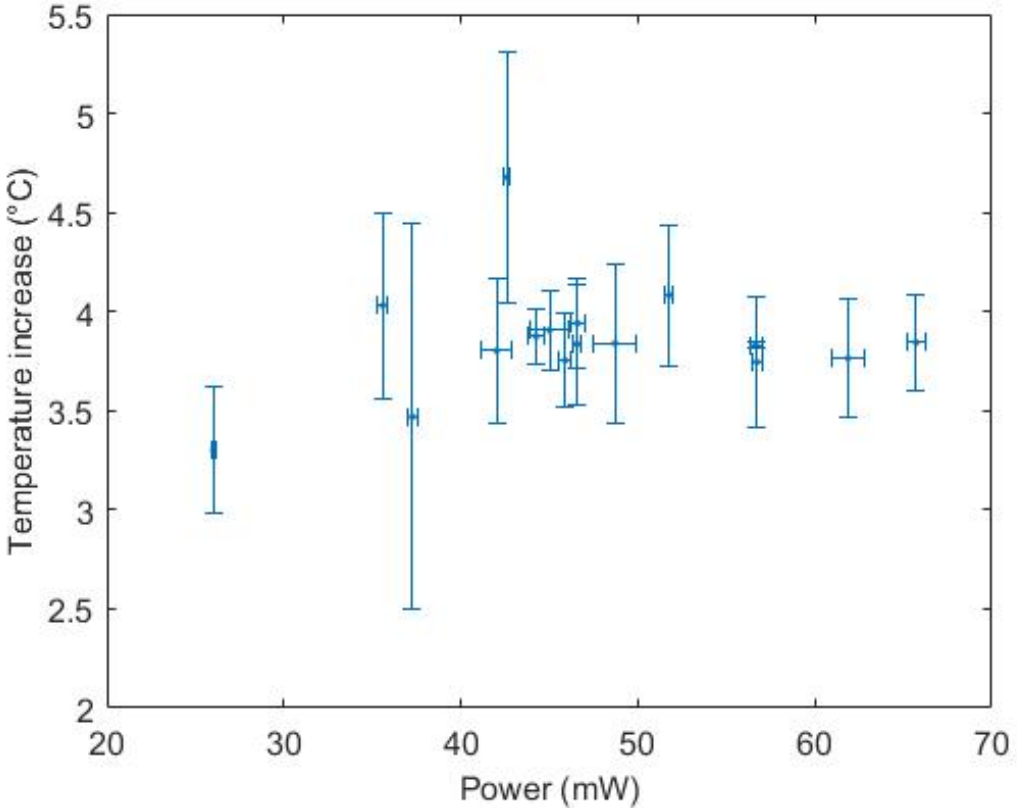

Figure 21. *The temperature increase in the pre-heating phase compared to body temperature as a function of heating laser power in 16 mice. Each data point represents the mean of estimated temperature increase determined from ten last ERG responses in the pre-heating phase in one mouse when the temperature had stabilized. Only minor adjustments to the heating laser power were done during this time. Error bars present standard deviation.*

7.3 Temperature Estimate During Heating Treatment

The aim of this Master's thesis was to study the effect of three different treatment temperatures on retinal HSPA expression and RPE cell structure. These temperatures were achieved by multiplying the heating laser power of the pre-heating phase with three different treatment factors (2, 2.5 or 3). However, we observed using one-way analysis of variance that this method did not result in a statistically significant difference in used heating laser power (p-value 0.33) or estimated temperatures (p-value: 0.08) during heating treatment. In addition to the experiments rejected in the analysis of the pre-heating phase, one experiment was rejected from the analysis because of unreliableness of temperature estimation at the heating phase that was caused by a large artifact superimposed to the ERG signal from mouse breathing.

Figure 22 A presents boxplots of the heating laser power during the treatment heating in each treatment group. Figure 22 B illustrates the estimated treatment heating temperatures in each treatment group. It is noteworthy that the estimated median temperature elevation compared to the body temperature in a group treated with treatment factor 2.5 was lower than in a group with treatment factor 2 (Figure 22 B), even though the median heating laser power was higher (Figure 22 A). Figure 23 shows the estimated temperature increase in the pre-heating phase and in the treatment heating phase as a function of heating laser power. The relation of the temperature increase and the heating laser power was non-linear.

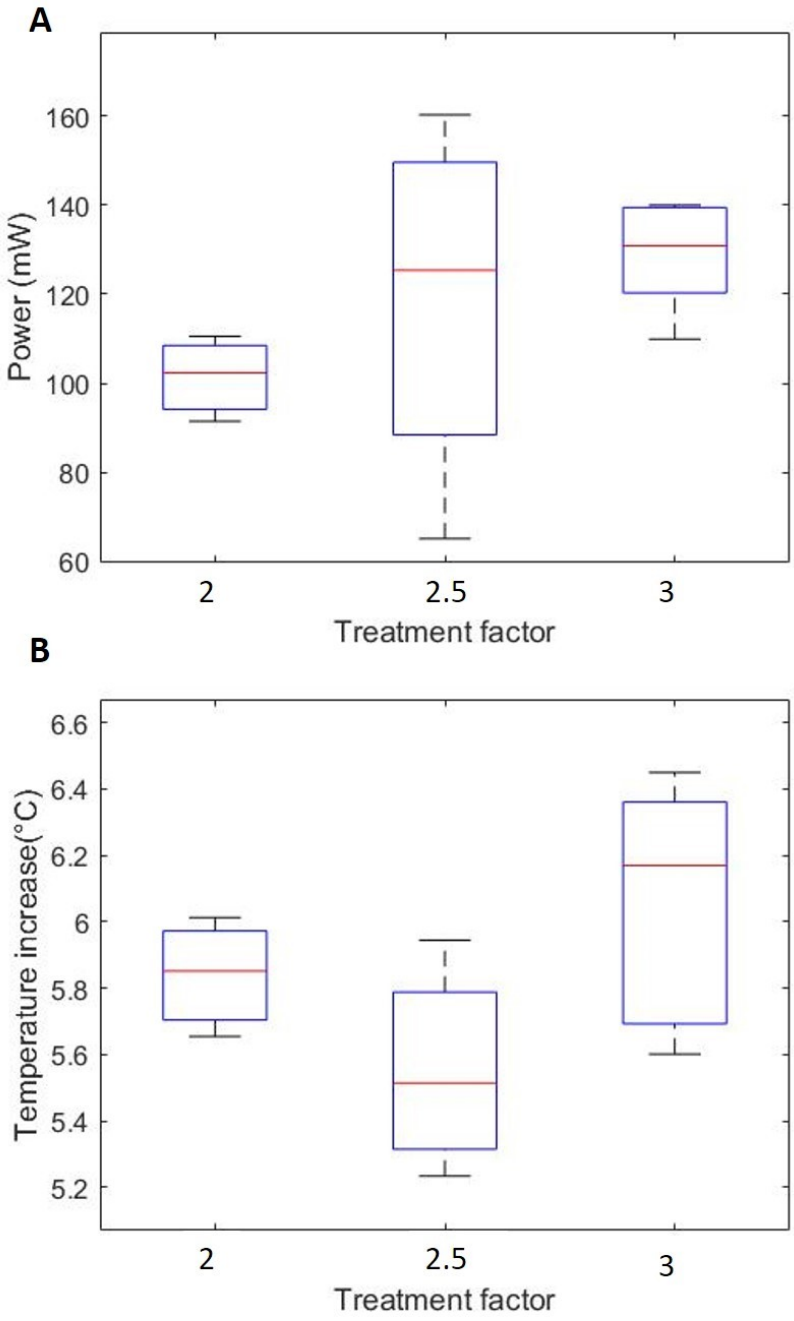

Figure 22. *Boxplots of (A) heating laser power and (B) estimated retinal temperature increase compared to the body temperature during heating treatment phase when using three different heating treatment factors. The number of experiments for factor 2 is 3, for factor 2.5 is 4 and for factor 3 is 6.*

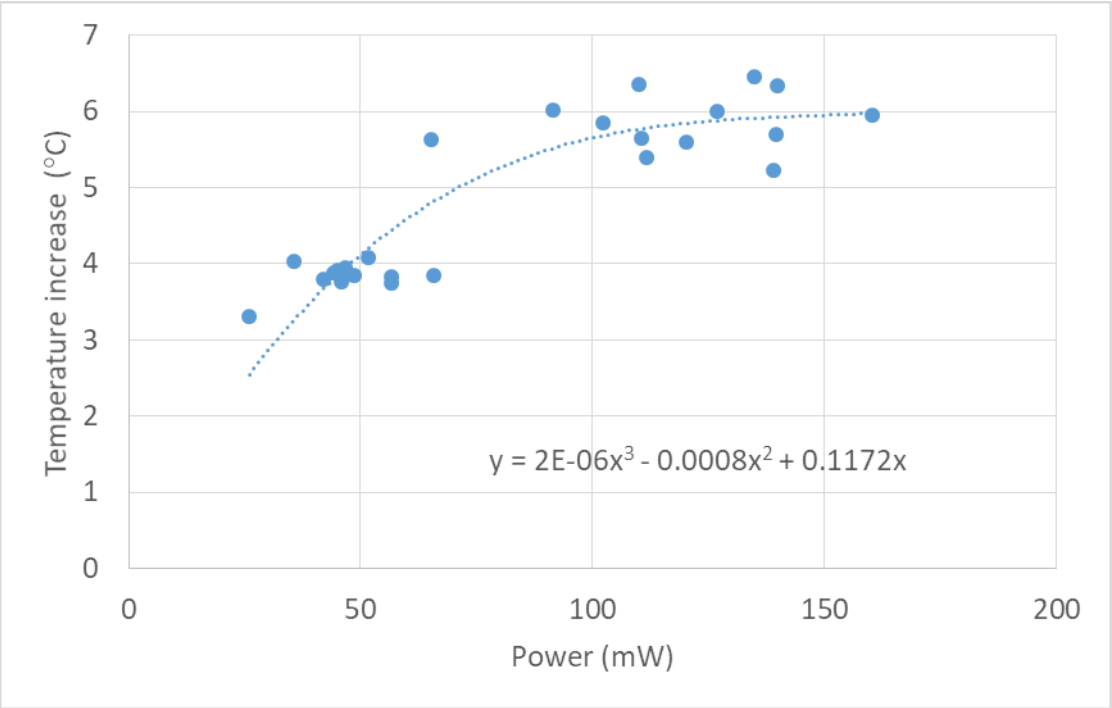

Figure 23. *The estimated temperature increase in the pre-heating phase and in the treatment heating phase compared to the body temperature as a function of the heating laser power. The figure presents data of 13 mice. From each mouse, two data points were obtained: one from the pre-heating phase (temperature increase approximately 4 ℃) and one from treatment heating phase (temperature increase approximately 5-6.5 ℃). The fitted curve is determined using the least-squares method. Since, at zero heating power, the retinal temperature is assumed to correspond to the body temperature, the fitted curve is forced through the origin.*

7.4 HSPA Expression and Cell Structure

Figures 24, 25 and 26 show example fluorescence microscope images of the flat-mounted RPEs of the control eye (A) and treated eye (B) obtained using treatment factors 2, 2.5 and 3, respectively. In these figures, the arrow indicates the location of the optic disk. The right eye of the mouse was always treated and the left eye acted as a control. HSPA is constantly expressed in cells and is therefore present also in the control eye. Larger versions of Figures 24, 25 and 26 are presented in the Appendix.

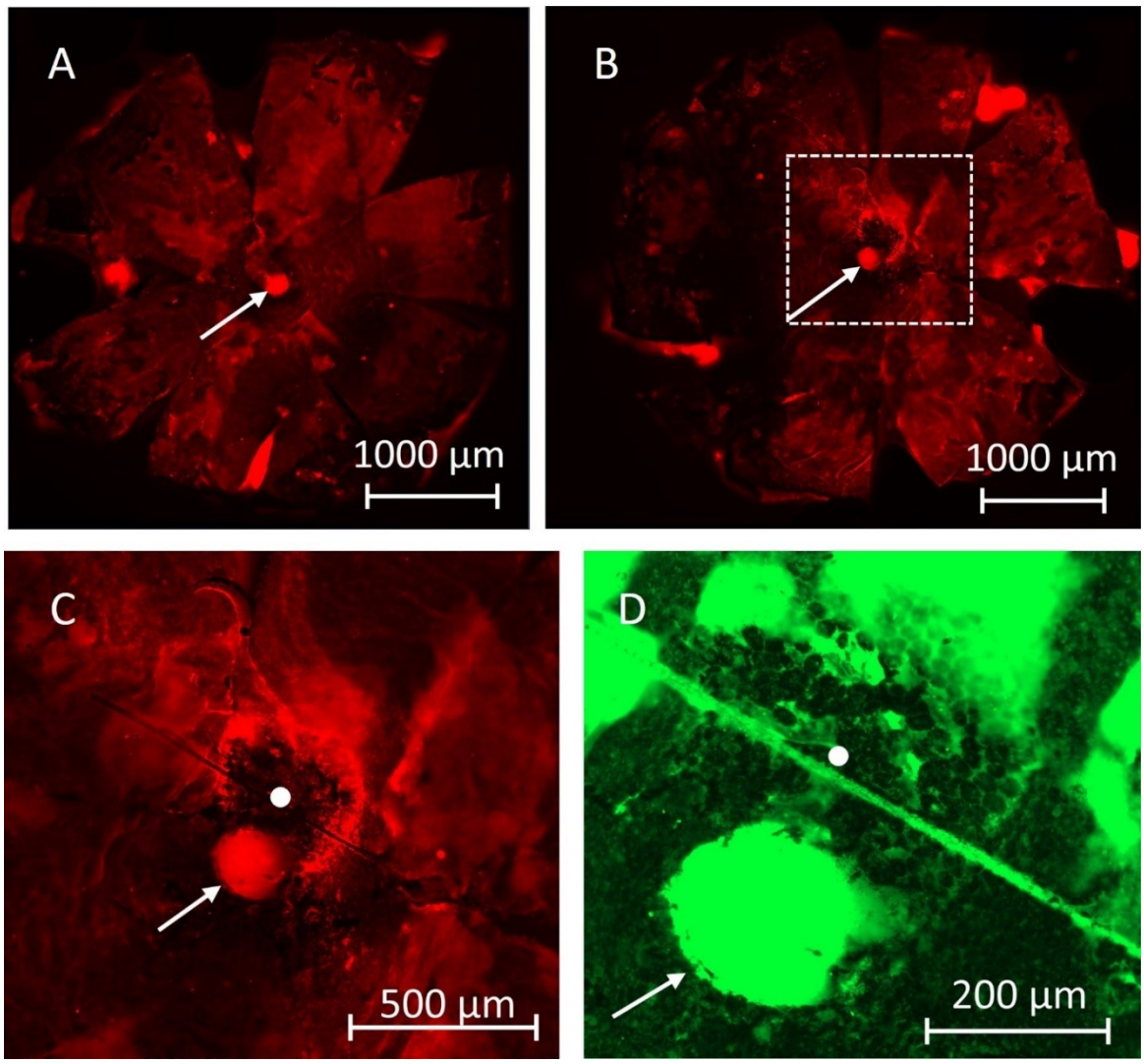

Figure 24. *Images of stained and flat-mounted RPEs after heating with treatment factor 2. Arrow indicates the location of the optic disk.* ***A.*** *HSPA staining of the control eye.* ***B.*** *HSPA staining of the treated eye.* ***C.*** *Close-up image of the heated area. Image borders are indicated with a dashed rectangle in Figure 24 B.* ***D.*** *Phalloidin staining of the center of the heated area. The location of the white dot is the same in Figures 24 C. and 24 D.*

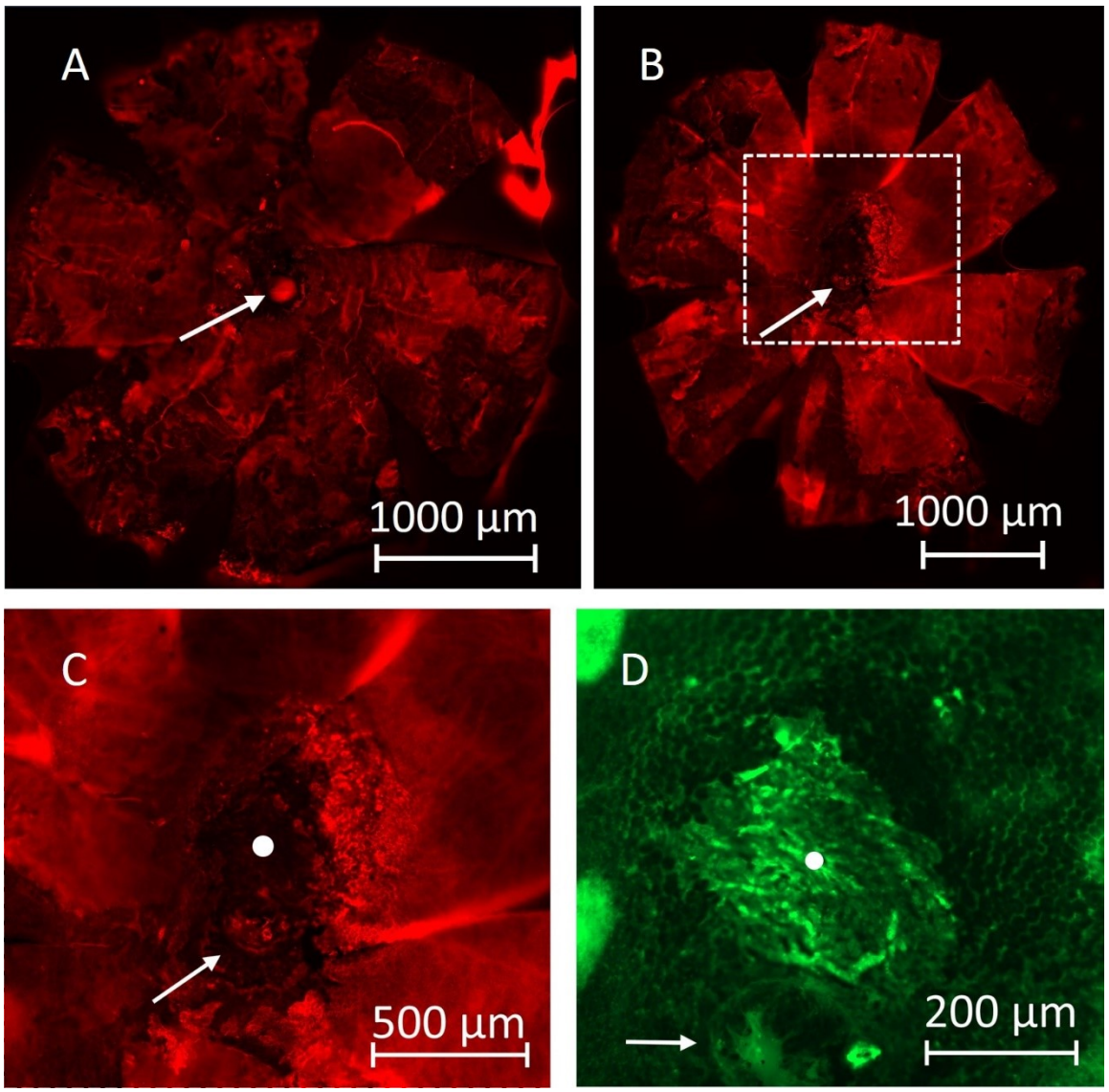

Figure 25. *Images of stained and flat-mounted RPEs after heating with treatment factor 2.5. Arrow indicates the location of the optic disk.* ***A.*** *HSPA staining of the control eye.* ***B.*** *HSPA staining of the treated eye.* ***C.*** *Close-up image of the heated area. Image borders are indicated with a dashed rectangle in Figure 25 B.* ***D.*** *Phalloidin staining of the center of the heated area. The brighter area at the center of the figure is probably neural retina that was not properly removed during dissection. The location of the white dot is the same in Figures 25 C. and 25 D.*

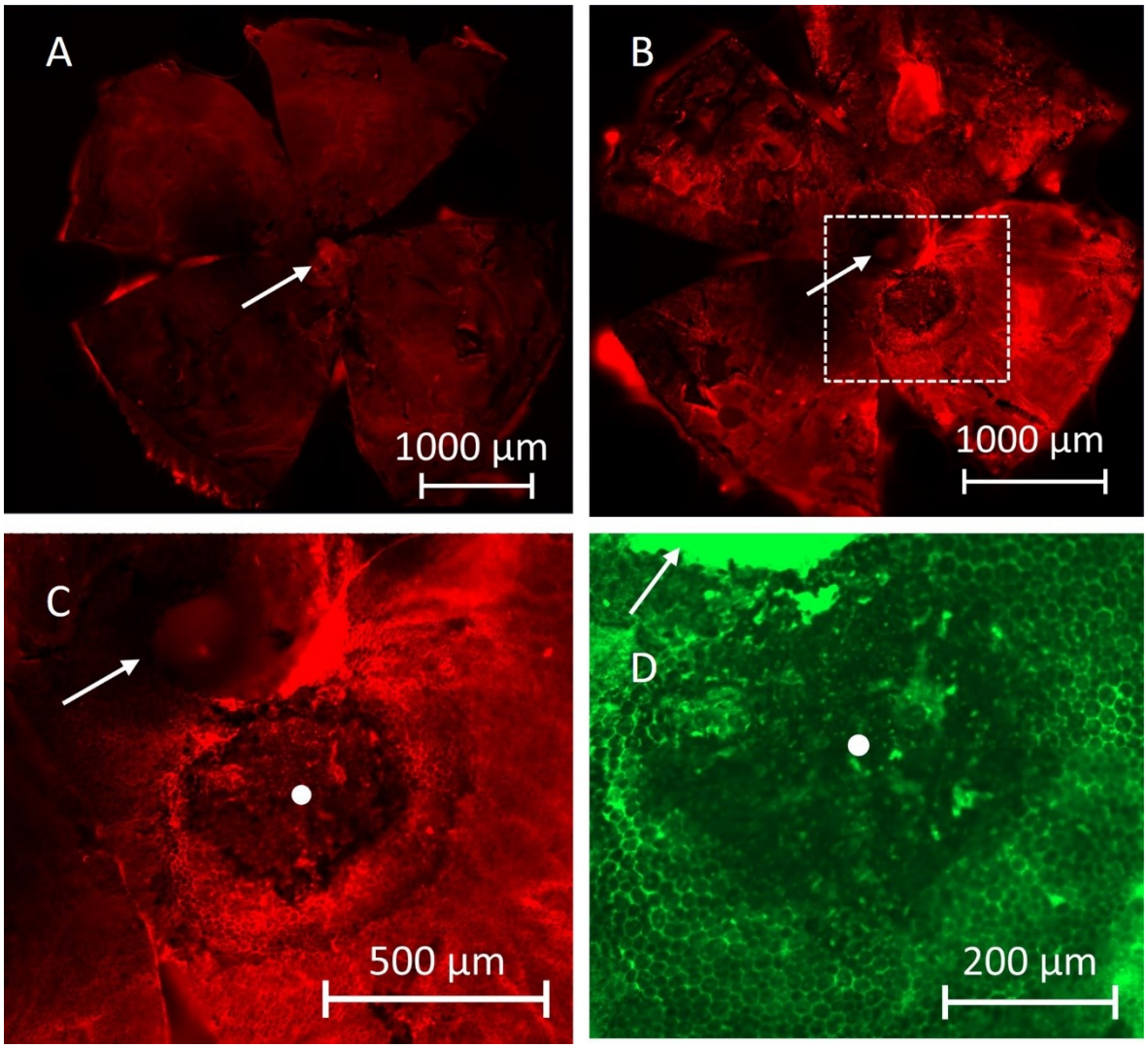

Figure 26. *Images of stained and flat-mounted RPEs after heating with treatment factor 3. Arrow indicates the location of the optic disk.* ***A.*** *HSPA staining of the control eye.* ***B.*** *HSPA staining of the treated eye.* ***C.*** *Close-up image of the heated area. Image borders are indicated with a dashed rectangle in Figure 26 B.* ***D.*** *Phalloidin staining of the center of the heated area. The location of the white dot is the same in Figures 26 C. and 26 D.*

In order to find out whether the heating treatment increased the overall HSPA expression in the treated retina compared to the non-treated control retina, we calculated the mean HSPA intensity values from the whole flat-mounted tissue area. Table 2 presents the descriptive statistics of the collected data. The number of imaged tissue samples was smaller than the number of heating treatments due to unsuccessful staining or recovery from anesthesia. Additionally, one experiment with factor 2.5 was excluded from the intensity analysis due to inappropriate staining. We used a one-tailed paired t-test to assess whether there is a statistically significant difference in HSPA intensity values between

control and treated eye. We found a statistically significant increase in the HSPA intensity compared to the control eye when using treatment factor 3 (p-value: 0.003).

Table 2. *Descriptive statistics of mean HSPA intensity values measured from the flat-mounts of the control eye and heated eye and expressed as average ± standard error of the mean (SEM). P-values of the one-tailed paired t-test are marked with * when the result is statistically significant using significance level 0.05.*

Treatment factor	Control	Heated	P-value	N
3	3 267 ± 1 130	7 396 ± 1 637	0.003 **	4
2.5	7 633 ± 1 862	13 335 ± 5 061	0.163	2
2	6 809 ± 2 068	8 327 ± 3 719	0.256	3

Additionally, we studied the mean flat-mount HSPA intensity of the treated eye relative to the control eye between the different treatment factors. Figure 27 shows a boxplot of the relative HSPA intensity in different treatment factors. We identified with one-way analysis of variance that there is a statistically significant difference between relative HSPA intensity (p-value: 0.035). Post hoc analysis using one-tailed two-sample t-test revealed statistically significant differences between treatment factor 3 compared to treatment factor 2 (p-value: 0.009). We found no statistically significant difference between treatment factors 3 and 2.5 (p-value: 0.051) and between treatment factors 2.5 and 2 (p-value: 0.106).

Figure 28 presents the relative HSPA flat-mount intensity between control and treated the eye as a function of heating laser power. We found a strong correlation between the relative HSPA intensity and the heating laser power (Pearson correlation coefficient: 0.85). Additionally, we found a strong correlation between the relative HSPA intensity and the treatment factor (Pearson correlation coefficient: 0.81). Using the statistical test described by Steiger [179] we determined that the difference of these correlation coefficients is not statistically significant (p-value: 0.826).

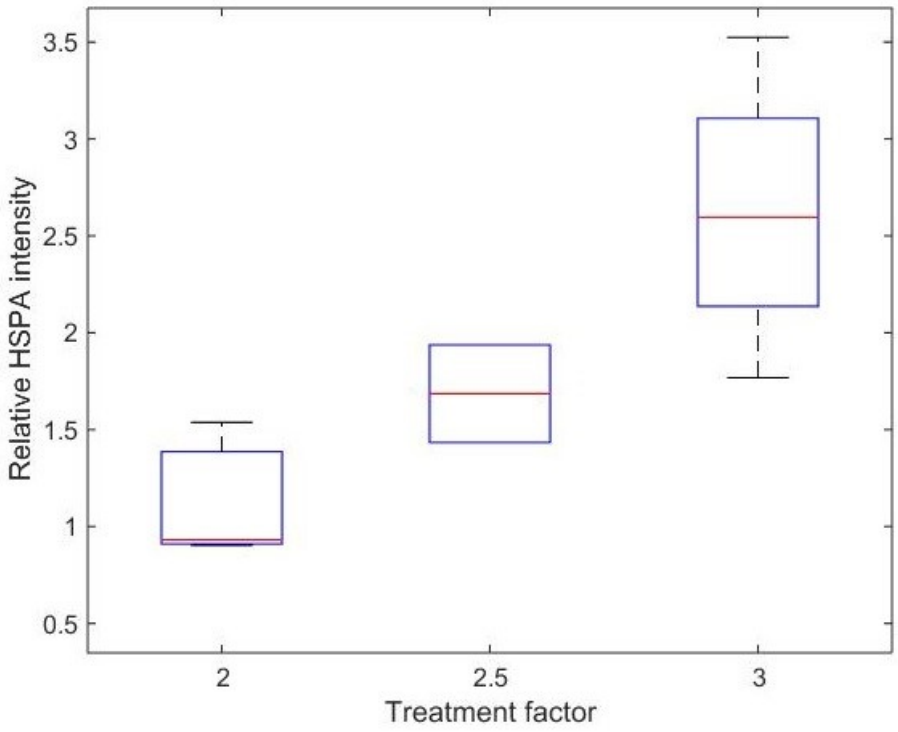

Figure 27. *Boxplot of the relative HSPA intensity in the treated eye recorded after heating with treatment factors 2, 2.5 and 3.*

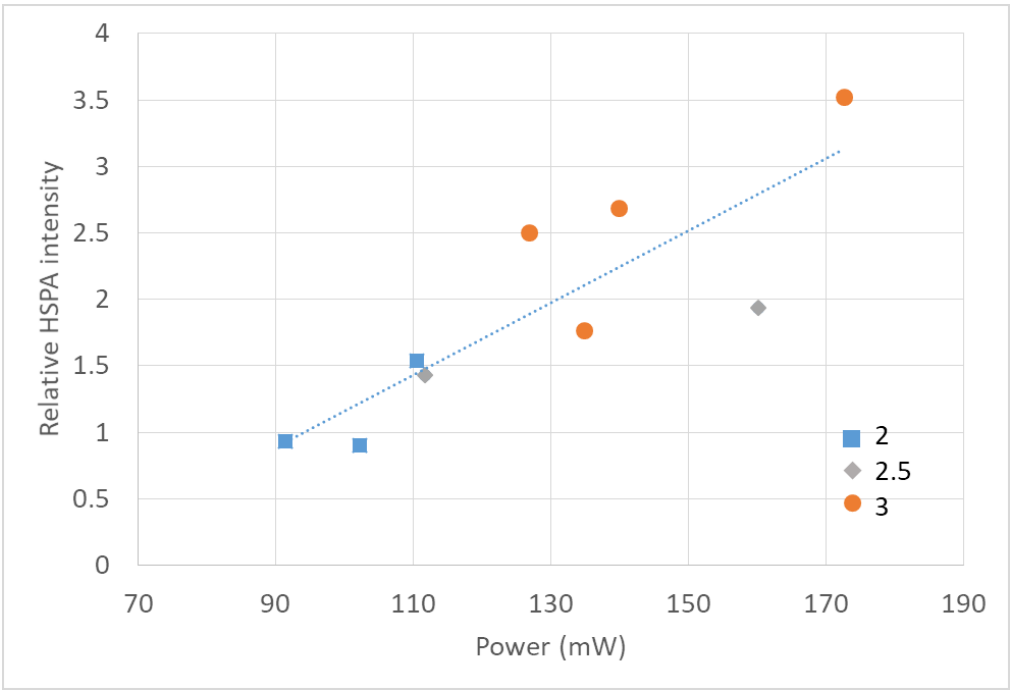

Figure 28. *The relative HSPA flat-mount intensity of the treated eye as a function of heating laser power. The trend line is determined using the least-squares method. Treatment factors were 2 (blue square), 2.5 (grey diamond) and 3 (red circle).*

Figures 24 B, 25 B and 26 B show a distinct, approximately a circular area near the optic disk where HSPA intensity is low. Furthermore, this low HSPA intensity area is surrounded by a ring of brighter HSPA intensity. This HSPA expression pattern is assumed to be located within the heated area since it can be identified in the majority of treated eyes and a similar area is not visible in the control eyes. Figures 24 C, 25 C and 26 C show close-up images of this area with different treatment factors.

We studied the effect of treatment factor on the diameter of the low HSPA expression area. The diameter was determined as the diameter of a circle that was fitted to the edges of the low HSPA expression area in the fluorescence microscope images of HSPA staining. The analysis was conducted for the tissue samples from which we were able to determine the low HSPA expression area diameter. Treatment factor 2 was not included in this analysis due to difficulties in determination of the diameter. The low HSPA expression area diameter in tissues treated with factor 3 was 472 ± 31 and in tissues treated with factor 2.5 was 505 ± 153 (expressed as average $\pm$ standard error of the mean (SEM)). We performed a one-tailed two-sample t-test to analyze the statistical significance of the treatment factors 3 and 2.5 on the diameter of the low HSPA expression area. According to this t-test, there was no statistically significant difference in lesion size between treatment factors 3 (N = 3) and 2.5 (N = 3) (p-value: 0.424). The overall average lesion diameter in these treatments was 488 ± 70 μm (presented as average $\pm$ SEM) corresponding to roughly 60 % of the approximated diameter of the heated area.

Figures 24 D, 25 D, and 26 D illustrate phalloidin staining of the heated area where the location of the white dot is the same as in Figure 24 C, 25 C, and 26 C, respectively, and where the arrow indicates the location of the optic disk. The edges of the concerned area show a normal, hexagonal RPE cell structure where the cells are presumably intact. However, we observed abnormal RPE cell structure in the center of the heated area indicating cell death. The abnormal RPE cell structure in the middle of the heated area appeared in the majority of tissue samples independent of the treatment factor.

8. Discussion

The purpose of this Master's thesis was to study how laser heating treatment affects the retinal function in mice. The aim was to collect information for ongoing research developing a subthreshold heating treatment protocol that induces heat shock without causing cell death in the retina. The heating treatment protocol was evaluated by studying the effect of treatment on the HSPA expression and cell structure of RPE cells. In addition, the necessity of usage of temperature determination method during heating treatment and the suitability of ERG based temperature estimation method were assessed by studying the relationships between the estimated retinal temperature increase, the heating laser power, and the observed effect in the immunostaining of the RPE. This chapter discusses the results obtained in this Master's thesis.

8.1 Variation in Heating Laser Power

It was found that in different mice, different heating laser power was needed to reach the same retinal temperature elevation. Possible reasons for this variation include both interindividual and intraindividual differences in fundus pigmentation, choroidal blood flow, and cataract formation during the experiment.

Contribution of topographical and interindividual pigmentation differences on the needed laser power is supported by previous research. Topographical differences in RPE melanosome content have been observed in mice by Williams et al. [180] and in rats by Howell et al. [181]. They both conclude that melanosome content is lower in the superior RPE compared to the inferior RPE. Additionally, Howell et al. [181] found that melanosome content was lower in the central RPE compared to the peripheral RPE. In addition to rodents, topographical differences have been found in humans. Gabel et al. [182] observed that in humans absorption of light by RPE and choroid depends on the location of the retina and varies up to a factor of 4 between individuals. Also, Schmidt et al. [26] found topographical alterations in the melanin concentration of human retina. They observed that in humans melanin concentration is the lowest in the area around the macula, higher in mid-periphery and the highest in the far periphery. [26] In addition, Schmidt et al. [26] and Sarna et al. [183] observed that in human RPE the melanin concentration decreases with age. However, this decrease does not include the macular area [26]. Furthermore, additional variation to the fundus pigmentation is induced by choroidal blood vessels that cause a local decrease in choroidal pigmentation [184]. Therefore, it seems plausible that variation in pigmentation is an important factor causing interindividual and intraindividual

differences in laser power needed to reach a specific retinal temperature during laser treatment. This needs to be taken into consideration when developing laser heating treatment methods.

Besides pigmentation, variation in perfusion and choroidal vasculature may contribute to the observed variation. Herrmann et al. [12] observed in a rabbit that when heating lasts several seconds or more, choroidal perfusion has a considerable cooling effect on retinal temperature. Mathematical model by Kandulla et al. [14] indicates that perfusion lowers the temperature increase within heating laser spot but steepens the temperature gradient at the border of the heating laser spot. Therefore, interindividual differences in choroidal perfusion and vasculature may induce variations in the resulting retinal temperature and temperature profile during heating treatment. In addition, spatial variation in perfusion within the retina can cause differences in the resulting temperatures. During the treatment, areas of high-temperature increases might occur in locations where choroidal perfusion is low. However, also too small temperature increases may occur in areas above main vessels where perfusion is high. In addition to the vasculature, the perfusion rate depends on the intraocular pressure [12]. Herrmann et al. [12] were able to increase the temperature elevation of laser irradiated retina by increasing intraocular pressure. This could explain some of the observed variation since, in some of the experiments during the laser treatment, the fundus lens may have pressed against the eye increasing the intraocular pressure.

Additionally, the transparency of ocular media affects the laser-induced temperature increase of the retina [150]. The transparency can be reduced by conditions such as cataract. Cataract formation is frequently observed in rodents during anesthesia. Rodent cataract formation during anesthesia is hypothesized to be caused by drying of the corneal surface, lowered body temperature, hypertonic osmolarity, and anesthetics. [185] Cataract formation was observed in all of the experiments of this Master's thesis and the amount of cataract increased gradually during each experiment.

Due to multiple reasons affecting the laser-induced retinal temperature elevation during the heating treatment, it is not reasonable to treat all mice and all parts of the retina with the same heating laser power. This is also supported by our finding that the laser power needed to reach the temperature of 41 ± 0.3 °C varies substantially between the mice. Furthermore, the observed variance in heating laser power needed to reach the pre-heating temperature may be more prominent in human patients compared to inbred C57BL/6JRccHsd mice that have a practically identical genome. Therefore, in order to

facilitate sub-threshold heating treatment, a reliable real-time temperature determination method needs to be used during the treatment.

8.2 Doughnut Shaped HSPA Pattern

In the immunohistological analysis, we observed a doughnut-shaped HSPA pattern where HSPA intensity was the highest in a circular area surrounding an area with low HSPA expression. Similar HSPA pattern has been observed in porcine cell cultures by Kern et al. [135], in rabbit by Lavinsky et al. [123] and in rabbit by Wang et al. [136]. Consistent with our results, all these groups observed RPE tissue damage in the dark middle area. In addition, they observed that with lower heating power, the dark area was missing and heating induced a disc of elevated HSPA expression. [123, 135, 136]

In this Master's thesis, we used a roughly top hat-shaped heating laser beam. For heating treatments lasting less than 1 ms, top hat-shaped heating laser beam induces nearly uniform radial temperature distribution within the laser spot [186]. However, when heating laser pulse lasts longer, as was in the experiments of this Master's thesis, the temperature profile resembles a bell curve where the temperature in the middle of the beam is higher than at the edges [14, 187]. This may explain the observed doughnut pattern. Figure 29 A illustrates a hypothesis on how the bell curve-shaped temperature profile could induce a doughnut-shaped HSPA expression. Near the center of the laser, spot cells are subjected to lethal temperatures. Dead cells do not produce HSP and consequently, the center of the spot is seen as a dark area in fluorescent microscope images. Further away from the center of the heating spot, the induced temperature is not lethal but is high enough to induce HSPA expression that is observed in the staining images as a bright ring around the dark center of the laser spot. Near the edges of the laser beam, the temperature is close to body temperature and is not sufficient to induce an increase in HSPA expression.

The preferred result of sub-threshold heating treatment is a large disc-shaped area of elevated HSPA expression. According to the hypothesis presented in Figure 29, disc-shaped HSP expression pattern could be achieved by lowering heating laser power as shown in Figure 29 B. However, due to the shape of the temperature profile, resulting area of elevated HSP expression is smaller than the heating laser spot [188]. The size of the heating laser spot is restricted by the size of the pupil. Therefore, in order to increase the area of HSPA expression without increasing the laser spot size, the retinal temperature profile should be top hat-shaped. This can be achieved by using a heating laser with an intensity that increases with distance from the beam center [188].

We did not observe a statistically significant difference in the lesion size between treatment factors 3 and 2.5. This may imply that the theory presented in Figure 29 is incorrect. However, it is also possible that the statistically significant difference was not observed due to the small temperature difference between the treatments, difficulties in determination of the lesion size or small sample size.

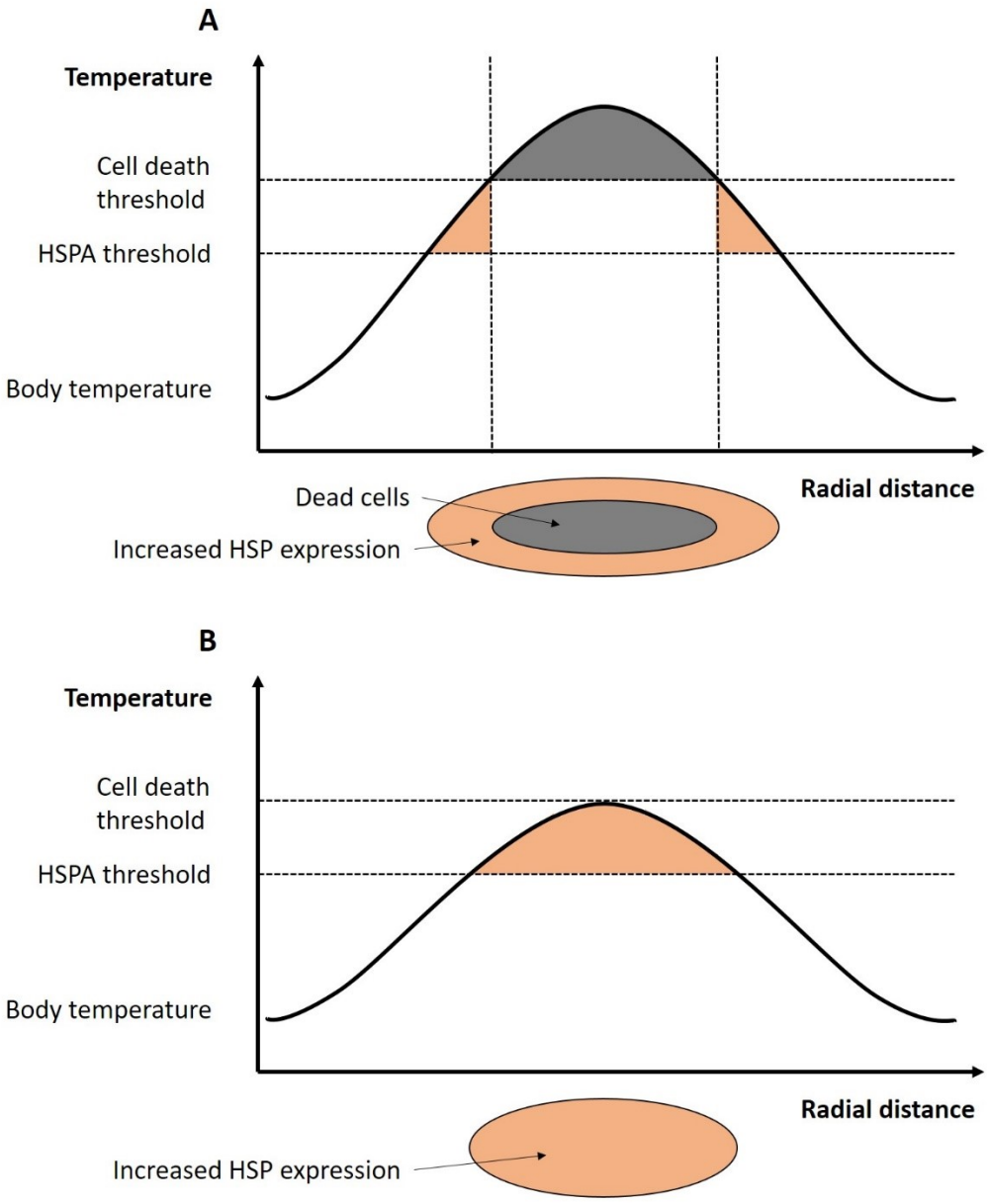

Figure 29. *Hypothetical presentation on how bell curve-shaped lateral retinal temperature profile yields (**A**) doughnut-shaped and (**B**) disc-shaped HSPA expression patterns.*

8.3 Non-Linear Relationship Between Retinal Temperature Estimate and Power

The ERG based temperature estimation method has been calibrated *in vivo* up to 42.5°C and *ex vivo* up to 44°C by Pitkänen et al. [15, 165]. They found linear behavior between b-wave TTM and temperature up to these temperatures [15, 165]. The reliability of temperature estimation method in temperatures above 42.5°C in *in vivo* is hence uncertain. However, based on the literature review (see Chapter 5.6.2.2) and preliminary testing of the method (unpublished data) it was estimated that higher temperatures than 42.5°C is needed for significant HSPA induction in response to 10 minutes heating. In order to allow usage of higher treatment temperatures, the method with a pre-heating step was used in this Master's thesis.

We observed that with high treatment heating powers the relationship between retinal temperature estimate and the heating laser power was non-linear (see Fig. 23). However, studies conducted by Baade et al. [187], Ibarra et al. [13], Hermann et al. [12] and Cain et al. [189] in rabbit as well as by Priebe et al. [190] in rhesus macaque indicate that retinal temperature during laser heating treatment increases linearly with increasing heating laser power. Therefore, it seems that the temperature estimation method used in this Master's thesis is not capable to correctly determine the retinal temperature with the used treatment powers. Possible reasons for observed non-linearity include reaching of limit in the acceleration of b-wave TTM, the variation of temperature within the recorded retinal area, photoreceptor damaging, heating on top of the optic disk and cataract formation during experiment or combination of these effects.

The used temperature estimation method is based on the acceleration of photoresponse kinetics in elevated temperatures that results in an observed linear decrease of b-wave TTM. The b-wave TTM, however, cannot decrease indefinitely. Dependence of the rate of biochemical processes on temperature is described by thermal performance curves (TPCs). Figure 30 illustrates the general shape of the TPC. Rate of the biological reactions typically increases as temperature increases until they reach a maximum point (T_{opt}) after which the rates rapidly decrease. Even though TPCs tend to take the same general shape, the height, position in the x-axis, width and shape of rising and descending slopes can vary depending on the process in question. The shape of TPC is a result of the kinetics of biochemical reactions. The rising phase is typically exponential and is caused by an increase in the number and energy of thermal collisions between molecules. The descending phase of the curve, however, is attributed to enzyme deactivation caused by protein denaturation. [191] Additionally, the shape of TPC is affected by the temperature dependence of the probability of an enzyme being in its active state. Normally, this probability is lower in low

and high temperatures and arrives at the maximum at an intermediate temperature. TPCs are not only limited to biochemical reactions but also explain most biological rate processes at the whole organism level such as the growth and development of ectotherms. [192]

The shape of TPC may explain the observed non-linear dependence of temperature on heating laser power. It is likely that b-wave TTM follows its own TPC. Therefore, when the temperature reaches T_{opt} of b-wave TTM, the TTM does not increase anymore even though the temperature increases. We observed non-linearity already at the lowest treatment temperature and found no statistically significant difference in retinal temperature estimates. Therefore, in order to explain observed temperature estimate values, b-wave TTM TPC should have a plateau that covers all the tested temperatures.

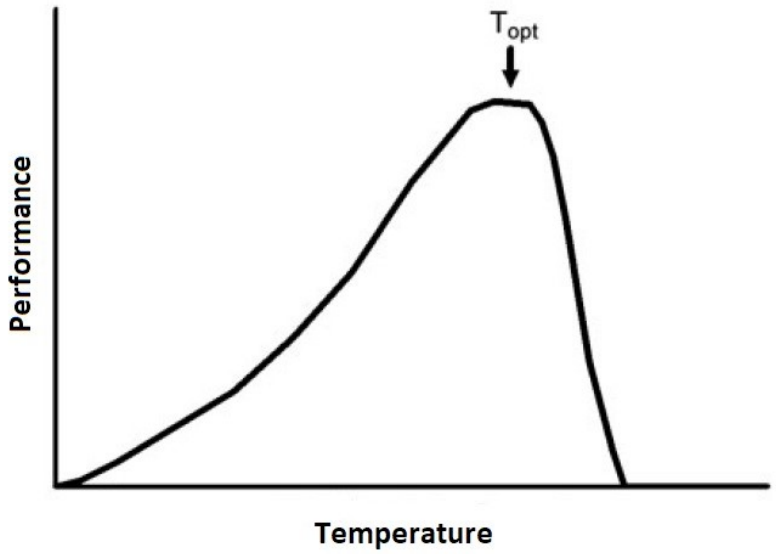

Figure 30. *Hypothetical thermal performance curve (TPC) describing the relationship between the performance of a biological process and temperature. T_{opt} is the temperature value at which performance is maximized. [191, modified]*

Another possible reason for the observed non-linearity is the variance in temperature within the heated retinal area. As discussed in Chapter 8.2, the middle area of the heating spot has a higher temperature than the distal areas. The temperature estimation is based on the recorded ERG signal that is a summation of photoreceptor and bipolar cell responses over the ERG stimulus spot. Pitkänen et al. [165] observed that in addition to the b-wave TTM, the b-wave amplitude decreases linearly with increasing temperature. They observed that the change of b-wave amplitude compared to the body temperature is 3.6% per 1°C

for mouse *ex vivo.* [165] Therefore, the ERG signal arising from the hotter middle of the beam has smaller amplitude and TTM and thus participates less in the TTM determined from the recorded ERG signal compared to the cooler distal areas of the heating spot. This may result in temperature estimate values resembling the temperature of the distal areas of the heating spot. However, we tried to reduce this effect by using a smaller stimulus laser spot compared to the heating laser spot.

Similarly, if the temperature at the center of the heating laser spot increases sufficiently to prevent the normal functioning of photoreceptor cells, these cells do not contribute any more to the recorded ERG signal and the retinal temperature estimate originates from surrounding cells with lower temperature. RPE cell damage was observed after heating in the middle of the heated area and therefore, it is possible that also the photoreceptor cells were damaged at the center of the heating spot. Furthermore, when heating close to the optic disk, no ERG signal is received from the areas that lack photoreceptor cells. This may have affected the retinal temperature estimate values in experiments where heating spot located close to the optic disk.

An additional factor that may have contributed to the non-linearity of temperature is cataract formation during the experiment. It is possible that cataract formation during the course of the experiment prevented light passage to the retina and thus halted the retinal temperature increase. Cataract unlikely explains entirely the observed non-linearity since, in order to greatly affect retinal temperature during treatment heating, the cataract development should have occurred in a narrow time interval between the determination of power needed to reach 41°C and the beginning of heating treatment which was not seen during the experiments. However, cataract formation may explain the small, gradual decrease of estimated retinal temperature during heating treatment observed in some of the experiments (see Figure 19 B).

8.4 HSPA intensity

We observed a statistically significant increase in the HSPA intensity of the whole flat-mount of the treated eye compared to the control eye in tissues treated with treatment factor 3. In addition, we observed a strong correlation between flat-mount HSPA intensity and heating laser power as well as between flat-mount HSPA intensity and treatment factor. These results, however, need to be carefully interpreted due to several aspects affecting the staining intensity. These aspects include variation in dissection successfulness, staining process, light exposure, RPE melanin pigment content and small sample size.

Immunofluorescence images can be affected by tissue damage that has occurred during dissection or staining. Additionally, in some parts of the fluorescence images, a leftover of the neural retina was observed on top of the RPE. Lavinsky et al. [123] and Wang et al. [136] observed that at high temperatures, photoreceptor outer segments fuse to the RPE. This may result in a higher likelihood of leftover neural retina being in the heated area compared to the non-heated surrounding areas. We often observed remnants of the neural retina on top of the RPE cell layer in the middle of the heated area (see Figure 25 D). Therefore, the tendency of the neural retina to fuse with RPE in the heated area may have affected our results.

Staining protocol is highly delicate and any alterations in the staining process may have induced variation in staining results. In addition, the fluorophores are sensitive to light. Light exposure reduces their fluorescence property due to irreversible light-induced damage. Therefore, the differences in the amount of light exposure either during staining, storing or imaging of tissue samples may induce intensity differences between tissues. In this Master's thesis, the effect of these aspects was minimized by the following means. Firstly, the staining of all tissues was conducted by the same person. Secondly, heated and control tissues were stained and stored together. Thirdly, heated and control tissues were imaged together using the same microscope and imaging settings. Additionally, the alterations in the staining process or light exposure occur sporadically and do not cause systematic bias. Therefore, they cannot fully explain the obtained results.

Additional difficulties in the analysis of HSPA staining intensity may arise from the high melanin content of RPE cells. RPE contains high amounts of melanin pigment which attenuates light that is passing through the RPE layer. Therefore, when imaging from the apical side of RPE, it is not possible to see stained HSPA proteins located in the basolateral side of the RPE cells. The depth to which HSPA can be detected depends on the pigment content of the cells. In addition, the damaging of cells during dissection or staining may reveal areas of the cell that are otherwise not visible by immunofluorescence microscopy. [193]

Despite these factors that affect the staining intensity, we have clearly demonstrated that the laser heating treatment induces elevated HSPA expression in RPE cells. Similar results have been previously obtained by Kern et al. [135], by Lavinsky et al. [123] and by Wang et al. [136]. This promising result provides a solid base for further research on HSPA's role in the laser heating treatment of AMD.

8.5 Future Perspectives

The experiments of this Master's thesis gave valuable insight on retinal heating treatment using the ERG based temperature estimation method. Even though HSPA-inducing non-damaging treatment protocol was not achieved in this thesis, the obtained information can be used in the future to further develop the heating treatment protocol.

In the future experiments, shorter heating duration or lower treatment factor should be used in order to prevent retinal damage. Shorter treatment duration would also reduce cataract formation. Additionally, shorter treatment duration reduces mouse anesthesia duration and is more applicable to the clinical setting. Besides the reduction of treatment factor or duration of the treatment, improvements related to the heating treatment protocol and the assessment of treatment outcome could be made.

8.5.1 Heating Treatment

The intensity profile of heating laser used in these experiments was not entirely homogenous (see Figure 18) and may have caused higher temperature areas within the heated area referred here as hotspots. At hotspot, the temperature increase can be significantly higher compared to the rest of the heated retina and result in choroidal vessel damage. The damaging of vessels may lead to even higher temperatures by preventing the cooling of tissue by blood flow. Therefore, hotspots can hypothetically cause severe burns to the retina during otherwise subthreshold heating. In order to reduce unwanted cellular damage during heating, a light source that produces more homogenous heating spot should be used in future experiments.

In the majority of experiments, the heated area located near the optic disk. Optic disk, however, has different structure compared to the rest of the retina. It lacks photoreceptors and RPE and contains large retinal vessels [19]. Therefore, no temperature estimate values can be obtained from the optic disk. Additionally, structural differences may result in deviant temperature profile and response to temperature elevation compared to the rest of the retina. In future experiments, the heating of the optic disk should be avoided. The current heating laser spot is approximately the same size as the mouse pupil. The laser spot covers the majority of the visible part of the fundus and there is only limited possibility to select the heated area within the visible fundus. In order to allow a more precise selection of the heating area within the visible area, a smaller spot should be used. Alternatively, the

angle between the eye and the fundus lens can be adjusted in a way that the optic disk is outside of the visible area of fundus.

In this Master's thesis, the heated location of the retina was unknown. It was assumed that the observed doughnut-shaped HSPA expression patter located in the center of the heating laser spot. In order to gain more definitive information about the location of the heating, methods to mark the heating laser spot location should be investigated. One possibility is to induce small, intense marker burns outside the heating laser spot to mark the location. Additionally, the retinal imaging capabilities of the heating device could be improved in order to better visualize the heated area.

8.5.2 Assessment of Treatment Outcome by Immunohistochemistry

Immunohistochemical staining is best suited for the localization of target proteins and gives only limited information about the amount of target protein. In this Master's thesis, the HSPA staining intensity was assumed to have a direct relationship with the amount of retinal HSPA. However, due to reasons discussed in Chapter 8.4, this assumption might be somewhat misleading. More reliable quantitative information about HSPA can be achieved by Western blot method. However, disadvantages of the Western plot include the need for many RPE samples for single analysis and lack of ability to determine the localization of detected target proteins in the tissue.

Based on cell structure changes observed in phalloidin staining, it was hypothesized that the observed dark area inside circular high-intensity HSPA staining is caused by the death of cells that were exposed to lethal temperature increases. However, this hypothesis needs to be confirmed by staining of apoptosis and necrosis markers. Additionally, the timing of staining may need to be adjusted. In this Master's thesis, the staining was conducted 24 hours after the heating treatment. This time-point was selected based on literature to yield high HSPA amounts in RPE (see literature review in Chapter 5.6.2.2). However, it has been observed by Kern et al. [135] that apoptotic cell death may occur between 24 and 48 hours after laser heating. They also hypothesize that some of the cells strongly expressing HSPA at 24 hours are under apoptosis [135]. If their hypothesis is correct, it would be beneficial to conduct the staining later in order to gain more accurate information about the extent of cell death.

In addition to measuring HSPA expression after treatment, treatment's effect on other biomolecules should be investigated. Even though the expression of HSPA after hyperthermia is a well-known phenomenon, it may not contribute to the prevention of AMD development or other more essential mechanisms may exist. Other potential treatment mechanisms that were discussed in Chapter 5.6.2.1 include RPE regeneration, reduction of angiogenesis, enhancement of mechanism protecting RPE cells against oxidative stress and thinning of Bruch's membrane. All these mechanisms could be studied. Yet, additional potential treatment mechanisms may exist. All in all, more information about the pathogenesis of AMD is needed to better understand which cellular mechanisms could be utilized to prevent the progression of this disease.

9. Conclusions

The purpose of this Master's thesis was to study how laser heating treatment affects the retinal function in mice. In addition, this Master's thesis reviewed the function and regulation of HSPA as well as the pathogenesis of AMD and its current treatment modalities. The study was conducted as a part of ongoing research in the Department of Neuroscience and Biomedical Engineering (NBE) of Aalto University aiming to develop a novel heating treatment for AMD.

In this Master's thesis, we observed substantial variation in the power needed to reach the same temperature increase in different mice. This finding supports the usage of temperature estimation method during non-damaging retinal heating treatment. Additionally, we found that the dependence of estimated retinal temperature on heating laser power is non-linear. However, the reason for non-linearity was not revealed and requires further research.

We observed a statistically significant increase in HSPA intensity in tissues treated with the highest treatment factor compared to control tissue. Additionally, we found that HSPA intensity correlates with heating laser power and treatment factor. We observed similar HSPA expression pattern in all the used treatment factors. This pattern consisted of an area with low HSPA intensity surrounded with circular high HSPA intensity area. The central area showed signs of cellular damage in phalloidin staining and was associated with cell death. Based on our results, in future experiments, one should use a lower treatment factor or shorter treatment duration in order to reduce the amount of heat-induced retinal damage.

In general, more information about the pathogenesis of AMD is required to better understand which cellular mechanisms could be utilized in the treatment of the disease. In addition, the capability of heating treatment to regulate these mechanisms needs to be investigated. The ERG based retinal temperature estimation method offers a novel way to personalize heating laser power during retinal heating treatment and can be used in the future to uncover how retinal tissue responds to heat. Our results can be used as the foundation for further research on the subject.

References

[1] Happonen, P. Holopainen, M. Sariola, H. Sotkas, P. Tenhunen, A. Tihtarinen-Ulmanen, M. Venäläinen, J. Bios 4: Ihmisen biologia. 5th ed. Helsinki: WSOYpro OY, 2011. S.110-111. ISBN: 978-951-0-27632-7

[2] Rama, D. William, M. Miller, J. Age-Related Macular Degeneration. The New England Journal of Medicine, 2008. Vol 358:24. pp. 2606-2617. ISSN: 1533-4406

[3] Brody, B. Gamst, A. Williams, R. Smith, R. Lau, P. Dolnak, D. Rapaport, M. Kaplan, R. Brown, S. Depression, visual acuity, comorbidity, and disability associated with age-related macular degeneration. Ophthalmology, 2001. Vol. 108:10. pp. 1893-1900. ISSN: 0161-6420

[4] Wood, J. Lacherez, P. Black, A. Cole, M. Boon, M. Kerr, G. Risk of falls, injurious falls, and other injuries resulting from visual impairment among older adults with age-related macular degeneration. Investigative Ophthalmology & Visual Science, 2011. Vol. 52. pp. 5088-5092. ISSN: 1552-5783

[5] Hassell, J. Lamoureux, E. Keeffe, J. Impact of Age Related Macular Degeneration on Quality of Life. British Journal of Ophthalmology, 2006. Vol. 90:5. pp. 593-596. ISSN: 1468-2079

[6] Zarbin, M. Current Concepts in the Pathogenesis of Age-Related Macular Degeneration. JAMA Ophthalmology, 2004. Vol. 122:4. pp. 598-614. ISSN: 2168-6173

[7] Bhutto, I. Lutty, G. Understanding age-related macular degeneration (AMD): Relationships between the photoreceptor/retinal pigment epithelium/Bruch's membrane/choriocapillaris complex. Molecular Aspects of Medicine, 2012. Vol. 33:4. pp. 295-317. ISSN: 0098-2997

[8] Al-Zamil, W. Yassin, S. Recent developments in age-related macular degeneration: a review. Clinical Interventions in Aging, 2017. Vol. 12. pp. 1313-1330. ISSN: 1178-1998

[9] Mayer, M. Bukau, B. Hsp70 chaperones: Cellular functions and molecular mechanism. Cellular and Molecular Life Sciences, 2005. Vol. 62. pp. 670-684. ISSN: 1420-9071

[10] Yenari, M. Liu, J. Zheng, Z. Vexler, Z. Lee, J. Giffard, R. Antiapoptotic and Anti-inflammatory Mechanisms of Heat-Shock Protein Protection. Annals New York Academy of Sciences, 2005. Vol. 1053:1. pp. 74-83. ISSN: 1749-6632

[11] Lanneau, D. Brunet, M. Frisan, E. Solary, E. Fontenay, M. Garrido, C. Heat shock proteins: essential proteins for apoptosis regulation. Journal of Cellular and Molecular Medicine, 2008. Vol. 12:3. pp. 743-761. ISSN: 1582-4934

[12] Herrmann, K. Flöhr, C. Stalljohann, J. Apiou-Sbirlea, G. Jochen, K. Birngruber, R. Brinkmann, R. Influence of choroidal perfusion on retinal temperature increase during

retinal laser treatments. SPIE-OSA Biomedical Optics, 2007. Vol. 6632. ISBN: 9780819467768

[13] Ibarra, M. Miraz, N. Wu, I. Ying, G. Mainster, M. Tolentino, M. Retinal Temperature Increase during Transpupillary Thermotherapy: Effects of Pigmentation, Subretinal Blood, and Choroidal Blood Flow. Investigative Ophthalmology & Visual Science, 2004. Vol. 45. pp. 3678-3682. ISSN: 1552-5783

[14] Kandulla, J. Elsner, H. Birngruber, R. Brinkmann, R. Noninvasive optoacoustic online retinal temperature determination during continuous-wave laser irradiation. Journal of Biomedical Optics, 2006. Vol. 11:4. ISSN: 1560-2281

[15] Pitkänen, M. Kaikkonen, O. Koskelainen, A. In vivo monitoring of mouse retinal temperature by ERG photoresponses. Experimental Eye Research, 2019. In Press.

[16] Tzekov, R. Arden, G. The Electroretinogram in Diabetic Retinopathy. Survey of Ophthalmology, 1999. Vol 44:1, pp. 53-60. ISSN: 0039-6257

[17] Karwoski, C. Xu, X. Yu, H. Current-source density analysis of the electroretinogram of the frog: methodological issue and origin components. Journal of the Optical Society of America A, 1996. Vol. 13:3. pp. 549-556. ISSN: 1084-7529

[18] Tortora, G. Derrickson, B. Principles of Anatomy & Physiology. 13th ed. Asia: John Wiley & Sons, 2011. pp. 33, 87, 130, 642-656, 735, 886-898. ISBN 978-0-470-64608-3

[19] Bear, M. Connors, B. Paradiso, M. Neuroscience – Exploring the brain. 4th ed. China: Wolters Kluwer, 2016. pp. 294-329. ISBN 978-1-4511-0954-2

[20] Iuvone, P. Neurotransmitters and Receptors: Dopamine. Printed in Encyclopedia of the Eye, 2010. Elsevier Ltd. ISBN: 978-0-12-374203-2

[21] Rodieck, R. The First Steps in Seeing. Sinauer Associates, Inc., 1998. ISBN: 0-87893-757-9

[22] Nowak, J. Age-related macular degeneration (AMD): pathogenesis and therapy. Pharmacological Reports, 2006. Vol. 58. pp. 353-363. ISSN: 1734-1140

[23] Nickla, D. Wallman, J. The multifunctional choroid. Progress in Retinal and Eye Research, 2010. Vol. 29:2. pp. 144-168. ISSN: 1350-9462

[24] Molday, R. Kaupp, U. Ion Channels of Vertebrate Photoreceptors. Printed in Handbook of Biological Physics, 2000. Vol. 3. pp. 143-181. ISBN: 978-0-444-50102-8

[25] Lamb, T. Pugh, E. Phototransduction, Dark Adaptation, and Rhodopsin Regeneration. Investigative Ophthalmology & Visual Science, 2006. Vol. 47. pp. 5138-5152. ISSN: 1552-5783

[26] Schmidt, S. Peisch, R. Melanin Concentration in Normal Human Retinal Pigment Epithelium - Regional Variation and Age-Related Reduction. Investigative Ophthalmology & Visual Science, 1986. Vol. 27. pp 1063-1067. ISSN: 1552-5783

[27] Burke, J. Hjelmeland, L. Mosaicism of the Retinal Pigment Epithelium. Molecular Interventions, 2005. Vol. 5:4. pp. 241-249. ISSN: 1543-2548

[28] de Jong, P. Age-Related Macular Degeneration. The New England Journal of Medicine, 2006. Vol 355:14. pp. 1474-1485. ISSN: 1533-4406

[29] Kinnunen, K. Petrovski, G. Moe, M. Berta, A. Kaarniranta, K. Molecular mechanisms of retinal pigment epithelium damage and development of age-related macular degeneration. Acta Ophthalmologica, 2012. Vol 90:4. pp. 299-309. ISSN: 1755-3768

[30] Ishikawa, M. Sawada, Y. Yoshitomi, T. Structure and function of the interphotoreceptor matrix surrounding retinal photoreceptor cells. Experimental Eye Research, 2015. Vol. 133. pp. 3-18. ISSN: 0014-4835

[31] Jarrett, S. Boulton, M. Consequences of Oxidative Stress in Age-Related Macular Degeneration. Molecular Aspects of Medicine, 2012. Vol. 33:4. pp. 399-417. ISSN: 0098-2997

[32] Veleri, S. Lazar, C. Chang, B. Sieving, P. Banin, E. Swaroop, A. Biology and therapy of inherited retinal degenerative disease: insights from mouse models. Disease Models & Mechanisms, 2015. Vol. 8. pp. 109-129. ISSN: 1754-8411

[33] Volland, S. Esteve-Rudd, J. Hoo, J. Yee, C. Williams, D. A Comparison of Some Organizational Characteristics of the Mouse Central Retina and the Human Macula. Plos One, 2015. Vol. 10:4. ISSN: 1932-6203

[34] Fu, Y. Yau, K. Phototransduction in mouse rods and cones. Pflügers Archiv - European Journal of Physiology, 2007. Vol. 454. pp. 805-819. ISSN: 1432-2013

[35] Richter, K. Haslbeck, M. Buchner, J. The Heat Shock Response: Life on the Verge of Death. Molecular Cell, 2010. Vol. 40:2. pp. 253-266. ISSN: 1097-2765

[36] Radons, J. The human HSP70 family of chaperones: where do we stand? Cell Stress and Chaperones, 2016. Vol. 21:3. pp. 379-404. ISSN: 1466-1268

[37] Kianga, J. Tsokos, G. Heat Shock Protein 70 kDa: Molecular Biology, Biochemistry, and Physiology. Pharmacology & Therapeutics, 1998. Vol. 80:2. pp. 182-201. ISSN: 0163-7258

[38] Kennedy, D. Jäger, R. Mosser, D. Samali, A. Regulation of Apoptosis by Heat Shock Proteins. IUBMB Life, 2014. Vol. 66:5. pp. 327-338. ISSN: 1521-6551

[39] Kampinga, H. Hageman, J. Vos, M. Kubota, H. Tanguay, R. Bruford, E. Cheetham, M. Chen, B. Hightower, L. Guidelines for the nomenclature of the human heat shock proteins. Cell Stress and Chaperones, 2009. Vol. 14:1. pp. 105-11. ISSN: 1466-1268

[40] Stetler, A. Gan, Y. Zhang, W. Liou, A. Gao, Y. Cao, G. Chen, J. Heat shock proteins: Cellular and molecular mechanisms in the central nervous system. Progress in Neurobiology, 2010. Vol. 92:2. pp. 184-211. ISSN: 0301-0082

[41] Daugaard, M. Rhode, M. Jäättelä, M. The heat shock protein 70 family: Highly homologous proteins with overlapping and distinct functions. FEBS Letters, 2007. Vol. 581:19. pp. 3702-3710. ISSN: 1873-3468

[42] Javid, B. MacAry, P. Lehner, P. Structure and Function: Heat Shock Proteins and Adaptive Immunity. The Journal of Immunology, 2007. Vol. 179:4. pp. 2035-2040. ISSN: 1550-6606

[43] Alberts, B. Johnson, A. Lewis, J. Raff, M. Roberts, K. Walter, P. Molecular Biology of the Cell. 5th ed. New York: Garland Science, 2008. pp. 115-118, 387-395, 493, 779-787, 952-953, 1115. ISBN: 978-0-8153-4106-2

[44] Åkerfelt, M. Morimoto, R. Sistonen, L. Heat shock factors: integrators of cell stress, development and lifespan. Nature Reviews Molecular Cell Biology, 2010. Vol. 11. pp. 545-55. ISSN: 1471-0080

[45] Naidu, S. Dinkova-Kostova, A. Regulation of the mammalian heat shock factor 1. The FEBS Journal, 2017. Vol. 284. pp. 1606-1627. ISSN: 1742-4658

[46] Neef, D. Jaeger, A. Thiele, D. Heat shock transcription factor 1 as a therapeutic target in neurodegenerative diseases. Nature Reviews Drug Discovery, 2011. Vol. 10. pp. 930-944. ISSN: 1474-1784

[47] Morimoto, R. The Heat Shock Response: Systems Biology of Proteotoxic Stress in Aging and Disease. Cold Spring Harbor Symposia on Quantitative Biology, 2011. Vol. LXXVI. pp. 91-99. ISSN: 1943-4456

[48] Sõti, C. Nagy, E. Giricz, Z. Vígh, L. Csermely, P. Ferdinandy, P. Heat shock proteins as emerging therapeutic targets. British Journal of Pharmacology, 2009. Vol. 146:6. pp. 769 - 780. ISSN: 1476-5381

[49] Qu, B. Jia, Y. Liu, Y. Wang, H. Ren, G. Wang, H. The detection and role of heat shock protein 70 in various nondisease conditions and disease conditions: a literature review. Cell Stress and Chaperones, 2015. Vol. 20: 6. pp. 885-892. ISSN: 1466-1268

[50] Murshid, A. Eguchi, T. Calderwood, S. Stress proteins in aging and life span. International Journal of Hyperthermia, 2013. Vol. 29:5. pp. 442-447. ISSN: 0265-6736

[51] Brown, I. Heat Shock Proteins and Protection of the Nervous System. Annals of the New York Academy of Sciences, 2007. Vol. 1113:1. pp. 147-158. ISSN: 1749-6632

[52] Piri, N. Kwong, J. Gu, L. Caprioli, Heat shock proteins in the retina: Focus on HSP70 and alpha crystallins in ganglion cell survival. Progress in Retinal and Eye Research, 2016. Vol. 52. pp. 22-46. ISSN: 1350-9462

[53] Patel, M. Chan, C. Immunopathological aspects of age-related macular degeneration. Seminars in Immunopathology, 2008. Vol. 30:2. pp. 97.110. ISSN: 1863-2300

[54] Wong, W. Su, X. Li, X. Cheung, C. Klein, R. Cheng, C. Wong, T. Global prevalence of age-related macular degeneration and disease burden projection for 2020 and 2040: a systematic review and meta-analysis. The Lancet, 2014. Vol. 2:2. pp. e106-e116. ISSN: 2214-109X

[55] The Writing Committee for the OPTOS PEripheral RetinA (OPERA) study (Ancillary Study of Age-Related Eye Disease Study 2). Peripheral Retinal Changes Associated with Age-Related Macular Degeneration in the Age-Related Eye Disease Study 2: Age-Related Eye Disease Study 2 Report Number 12 by the Age-Related Eye Disease Study 2 Optos PEripheral RetinA (OPERA) Study Research Group. Ophthalmology, 2017. Vol. 124:4. pp. 479-487. ISSN: 0161-6420

[56] Tode, J. Richert, E. Koizner, S. Klettner, A. von de Burchard, C. Brinkmann, R. Lucius, R. Roider, J. Thermal Stimulation of the Retina Reduces Bruch's Membrane Thickness in Age Related Macular Degeneration Mouse Models. Translational Vision Science & Technology, 2018. Vol. 7:3. ISSN: 2164-2591

[57] Liang, F. Godley, B. Oxidative stress-induced mitochondrial DNA damage in human retinal pigment epithelial cells: a possible mechanism for RPE aging and age-related macular degeneration. Experimental Eye Research, 2003. Vol. 76:4. pp. 397-403. ISSN: 0014-4835

[58] Kivinen, N. Koskela, A. Kauppinen, A. Kaarniranta, K. Silmänpohjan ikärappeuman patogeneesi – autofagian ja inflammasomien vuoropuhelua. Duodecim, 2017. Vol. 133:7. pp. 641-646. ISSN: 0012-7183

[59] Buschini, E. Piras, A. Nuzzi, R. Vercelli, A. Age related macular degeneration and drusen: Neuroinflammation in the retina. Progress in Neurobiology, 2011. Vol. 95:1. ISSN: 0301-0082

[60] Anderson, D. Mullins, R. Hageman, G. Johnson, L. A Role for Local Inflammation in the Formation of Drusen in the Aging Eye. American Journal of Ophthalmology, 2002. Vol. 134:3. pp. 411-431. ISSN: 0002-9394

[61] Kaarniranta, K. Salminen, A. Haapasalo, A. Soininen, H. Hiltunen, M. Age-Related Macular Degeneration (AMD): Alzheimer's Disease in the Eye? Journal of Alzheimer's Disease, 2011. Vol. 24:4. pp. 615-631. ISSN: 1875-8908

[62] Nebbioso, M. Barbato, A. Pescosolido, N. Scotopic Microperimetry in the Early Diagnosis of Age-Related Macular Degeneration: Preliminary Study. BioMed Research International, 2014. Vol. 2014. Article ID 671529. ISSN: 2314-6141

[63] Sun, Y. Smith, L. Retinal vasculature in development and diseases. Annual review of vision science, 2018. Vol. 4. pp. 101-122. ISSN: 2374-4650

[64] Stefánsson, E. Geirsdóttir, Á. Sirgurdsson, H. Metabolic physiology in age related macular degeneration. Progress in Retinal and Eye Research, 2011. Vol. 30:1. pp. 72-80. ISSN: 1350-9462

[65] Ardeljan, C. Ardeljan, D. Abu-Asab, M. Chan, C. Inflammation and Cell Death in Age-Related Macular Degeneration: An Immunopathological and Ultrastructural Model. Journal of Clinical Medicine, 2014. Vol. 3:4. pp. 1542-1560. ISSN: 2077-0383

[66] Xu, H. Chen, M. Forrester, J. Para-inflammation in the aging retina. Progress in Retinal and Eye Research, 2009. Vol. 28:5. pp. 348-368. ISSN: 1350-9462

[67] Abderrazak, A. Syrovets, T. Couchie, D. Hadir, K. Friguet, B. Simmet, T. Rouis, M. NLRP3 inflammasome: From a danger signal sensor to a regulatory node of oxidative stress and inflammatory diseases. Redox Biology, 2015. Vol. 4. pp. 296-307. ISSN: 2213-2317

[68] Freeman, S. Quillin, K. Allison, L. Biological Science. 5th ed. Essex: Pearson Education Limited, 2014. pp 1230. ISBN: 978-1-292-02639-8

[69] Takeuchi, O. Akira, S. Pattern Recognition Receptors and Inflammation. Cell, 2010. Vol. 140. pp. 805-820. ISSN: 0092-8674

[70] Steuer, H. Jaworski, A. Elger, B. Kaussmann, M. Keldenich, J. Schneider, H. Stoll, D. Schlosshauer, B. Functional Characterization and Comparison of the Outer Blood–Retina Barrier and the Blood–Brain Barrier. Investigative Ophthalmology & Visual Science, 2005. Vol. 46. pp. 1047-1053. ISSN: 1552-5783

[71] Zhou, R. Caspi, R. Ocular immune privilege. F1000 Biology Reports, 2010. Vol. 2:3. ISSN: 1740-4118

[72] Chen, M. Xu, H. Parainflammation, chronic inflammation, and age-related macular degeneration. Journal of Leukocyte Biology, 2015. Vol. 98. pp. 713-725. ISSN: 1938-3673

[73] Kauppinen, A. Paterno, J. Blasiak, J. Salminen, A. Kaarniranta, K. Inflammation and its role in age-related macular degeneration. Cellular and Molecular Life Sciences, 2016. Vol. 73:9. pp. 1765–1786. ISSN: 1420-9071

[74] Kaarniranta, K. Sinha, D. Blasiak, J. Kauppinen, A. Veréb, Z. Salminen, A. Boulton, M. Petrovski, G. Autophagy and heterophagy dysregulation leads to retinal pigment epithelium dysfunction and development of age-related macular degeneration. Autophagy, 2013. Vol. 9:7. pp. 973-984. ISSN: 1554-8635

[75] Cruz-Guilloty, F. Saeed, A. Echegaray, J. Duffort, S. Ballmick, A. Tan, Y. Betancourt, M. Viteri, E. Ramkhellawan, G. Ewald, E. Feuer, W. Huang, D. Wen, R. Hong, L. Wang, H. Laird, J. Sene, A. Apte, R. Salomon, R. Hollyfield, J. Perez, V. Infiltration of proinflammatory m1 macrophages into the outer retina precedes damage in a mouse model of age-related macular degeneration. International Journal of Inflammation, 2013. Article ID 503725. ISSN: 2042-0099

[76] Cao, W. Shen, D. Patel, M. Tuo, J. Johnson, M. Olsen, T. Chan, C. Macrophage polarization in the maculae of age-related macular degeneration: A pilot study. Pathology International, 2011. Vol. 61:9. pp. 528-535. ISSN: 1440-1827

[77] Nowak, J. Oxidative stress, polyunsaturated fatty acidsderived oxidation products and bisretinoids as potential inducers of CNS diseases: focus on age-related macular degeneration. Pharmacological Reports, 2013. Vol. 65:2. pp. 288-304. ISSN: 1734-1140

[78] Yossef, PN. Sheibani, N. Albert, DM. Retinal light toxicity. Eye, 2011. Vol. 25. pp. 1-14. ISSN: 1476-5454

[79] Martinez-Vicente, M. Sovak, G. Cuervo, A. Protein degradation and aging. Experimental Gerontology, 2005. Vol. 40:8-9. pp. 622-633. ISSN: 0531-5565

[80] Roberts, R. Green, J. Lewis, B. Lutein and zeaxanthin in eye and skin health. Clinics in Dermatology, 2009. Vol. 27:2. pp. 195–201. ISSN: 0738-081X

[81] Tokarz, P. Kaarniranta, K. Blasiak, J. Role of antioxidant enzymes and small molecular weight antioxidants in the pathogenesis of age-related macular degeneration (AMD). Biogerontology, 2013. Vol. 4:15. pp. 461-482. ISSN: 1573-6768

[82] Lima, V. Rosen, R. Farah, M. Macular pigment in retinal health and disease. International Journal of Retina and Vitreous, 2016. Vol. 2:19. ISSN: 2056-9920

[83] Lillenbaum, A. Relationship between the proteasomal system and autophagy. International Journal of Biochemistry and Molecular Biology, 2013. Vol. 4:1. pp. 1-26. ISSN: 2152-4114

[84] Kaarniranta, K. Tokarz, P. Koskela, A. Paterno, J. Blasiak, J. Autophagy regulates death of retinal pigment epithelium cells in age-related macular degeneration. Cell Biology and Toxicology, 2016. Vol. 33:2. pp. 113-128. ISSN: 1573-6822

[85] Khansari, N. Shakiba, Y. Mahmoudi, M. Chronic Inflammation and Oxidative Stress as a Major Cause of Age- Related Diseases and Cancer. Recent Patents on Inflammation & Allergy Drug Discovery, 2009. Vol. 3. pp. 73-80. ISSN: 2212-2710

[86] Kaarniranta, K. Hyttinen, J. Ryhanen, T. Viiri, J. Paimela, T. Toropainen, E. Sorri, I. Salminen, A. Mechanisms of protein aggregation in the retinal pigment epithelial cells. Frontiers in Bioscience, 2010. pp. 1374-1384 ISSN: 1945-0524

[87] Blasiak, J. Petrovski, G. Zoltan, V. Facskó, A. Kaarniranta, K. Oxidative Stress, Hypoxia, and Autophagy in the Neovascular Processes of Age-Related Macular Degeneration. BioMed Research International, 2014. Article ID 768026. ISSN: 2314-6141

[88] Volland, S. Esteve-Rudd, J. Hoo, J. Yee, C. Williams, D. A Comparison of Some Organizational Characteristics of the Mouse Central Retina and the Human Macula. Plos One, 2015. Vol. 10:4. ISSN: 1932-6203

[89] Chong, V. Keonin, J. Luthert, P. Frennesson, C. Weingeist, D. Wolf, R. Mullins, R. Hageman, G. Decreased Thickness and Integrity of the Macular Elastic Layer of Bruch's Membrane Correspond to the Distribution of Lesions Associated with Age-Related Macular Degeneration. The American Journal of Pathology, 2005. Vol. 166:1. pp. 241-251. ISSN: 0002-9440

[90] Loskutova, E. Nolan, J. Howard, A. Beatty, S. Macular Pigment and Its Contribution to Vision. Nutrients, 2013. Vol. 5:6 pp. 1962-1969. ISSN: 2072-6643

[91] Datta, S. Canon, M. Ebrahimi, K. Wang, L. Handa, J. The impact of oxidative stress and inflammation on RPE degeneration in non-neovascular AMD. Progress in Retinal and Eye Research, 2017. Vol. 60. pp. 201-218. ISSN: 1350-9462

[92] Beatty, S. Koh, H. Henson, D. Boulton, M. The Role of Oxidative Stress in the Pathogenesis of Age-Related Macular Degeneration. Survey of Ophthalmology, 2000. Vol. 45:2. pp. 115-134. ISSN: 0039-6257

[93] Age-Related Eye Disease Study Group. A Randomized, Placebo-Controlled, Clinical Trial of High-Dose Supplementation With Vitamins C and E, Beta Carotene, and Zinc for Age-Related Macular Degeneration and Vision Loss: AREDS Report No. 8. Arch Ophthalmol, 2006. Vol. 119:10. pp. 1417-1436. ISSN: 2168-6173

[94] The Age-Related Eye Disease Study 2 (AREDS2) Research Group. Lutein + Zeaxanthin and Omega-3 Fatty Acids for Age-Related Macular DegenerationThe Age-Related Eye Disease Study 2 (AREDS2) Randomized Clinical Trial. JAMA, 2013. Vol. 309:19. pp. 2005-2015. ISSN: 1538-3598

[95] Xu, L. Kong, L. Wang, J. Ash, J. Stimulation of AMPK prevents degeneration of photoreceptors and the retinal pigment epithelium. Proceedings of the National Academy of Sciences of the United States of America, 2018. Vol. 115:41. pp. 10475-10480. ISSN: 1091-6490

[96] Wilkinson, J. Burmeister, L. Brooks, S. Chan, C. Sabrina, F. Harrison, D. Hejtmanic, J. Nadon, N. Strong, R. Wood, L. Woodward, M. Rapamycin slows aging in mice. Aging Cell, 2012. Vol. 11. pp. 675-682. ISSN: 1474-9726

[97] Harrison, D. Strong, D. Sharp, Z. Nelson, J. Astle, C. Flurkey, K. Nadon, N. Wilkinson, E. Frenkel, K. Carter, C. Pahor, M. Javors, M. Fernandez, E. Miller, R. Rapamycin fed late in life

extends lifespan in genetically heterogeneous mice. Nature, 2009. Vol. 460. pp. 392-395. ISSN: 1476-4687

[98] Nazari, H. Zhang, L. Zhu, D. Chader, G. Falabella, P. Stefanini, F. Rowland, T. Clegg, D. Kashani, A. Hinton, D. Humayun, M. Stem cell based therapies for age-related macular degeneration: The promises and the challenges. Progress in Retinal and Eye Research, 2015. Vol. 48. pp. 1-39. ISSN: 1350-9462

[99] Takeuchi, K. Kachi, S. Iwata, E. Ishikawa, K. Terasaki, H. Visual function 5 years or more after macular translocation surgery for myopic choroidal neovascularisation and age-related macular degeneration. Eye, 2011. Vol. 26. pp. 51-60. ISSN: 1476-5454

[100] Forest, D. Johnson, L. Clegg, D. Cellular models and therapies for age-related macular degeneration. Disease Models & Mechanisms, 2015. Vol. 9. pp. 421-427. ISSN: 1754-8411

[101] Salero, E. Blenkinsop. T. Corneo, B. Harris, A. Rabin, D. Stern, J. Temple, S. Adult Human RPE Can Be Activated into a Multipotent Stem Cell that Produces Mesenchymal Derivatives. Cell Stem Cell, 2012. Vol. 10:1. pp. 88-95. ISSN: 1934-5909

[102] Wang, Y. Wang, Y M. Chan C. The role of anti-inflammatory agents in age-related macular degeneration (AMD) treatment. Eye, 2011. Vol 25. pp. 127-139. ISSN: 1476-5454

[103] Relief, J. Douglas, R. Corticosteroid-induced ocular hypertension and glaucoma: a brief review and update of the literature. Current Opinion in Ophthalmology, 2006. Vol. 17:2. pp. 163-167. ISSN: 1040-8738

[104] Modjtahedi, B. Fong, D. Jorgenson, E. Van Den Eeden, S. Quinn, V. Slezak, J. The Relationship Between Nonsteroidal Anti-inflammatory Drug Use and Age-related Macular Degeneration. American Journal of Ophthalmolgy, 2018, Vol. 188. pp. 111-122. ISSN: 0002-9394

[105] Holz, F. Sadda, S. Busbee, B. Chew, E. Mitchell, P. Tufail, A. Brittain, C. Ferrara, D. Gray, S. Honigberg, L. Martin, J. Tong, B. Ehrlich, J. Bressler, M. Efficacy and Safety of Lampalizumab for Geographic Atrophy Due to Age-Related Macular Degeneration Chroma and Spectri Phase 3 Randomized Clinical Trials. JAMA Ophthalmology, 2018. Vol. 136:6. pp. 666-677. ISSN: 2168-6173

[106] Treatment of Age-Related Macular Degeneration With Photodynamic Therapy(TAP) Study Group. Photodynamic Therapy of Subfoveal Choroidal Neovascularization in Age-Related Macular Degeneration With Verteporfin: Two-Year Results of 2 Randomized Clinical Trials-Tap Report 2. Archives of Ophthalmology, 2001. Vol. 119:2. pp. 198-207. ISSN: 0003-9950

[107] Verteprofin In Photodynamic Therapy Study Group. Verteporfin Therapy of Subfoveal Choroidal Neovascularization in Age-related Macular Degeneration: Two-year Results of a Randomized Clinical Trial Including Lesions With Occult With No Classic Choroidal

Neovascularization—Verteporfin In Photodynamic Therapy Report 2. American Journal of Ophthalmology, 2001. Vol. 131:5. pp. 541-560. ISSN: 0002-9394

[108] Lock, J. Fong, K. An update on retinal laser therapy. Clinical and Experimental Optometry, 2011. Vol. 94:1. pp.43 - 51. ISSN: 1444-0938

[109] Mainster, M. Reichel, E. Transpupillary Thermotherapy for Age-Related Macular Degeneration: Long-Pulse Photocoagulation, Apoptosis and Heat Shock Proteins. Ophthalmic Surgery and Lasers, 2000. Vol. 31:5. pp. 359 -373. ISSN: 1082-3069

[110] Prahl, S. Optical Absorption of Hemoglobin. [25.4.2019]. Available at: omlc.org/spectra/hemoglobin/

[111] Vogel, A. Birngruber, R. Temperature profiles in human retina and choroid during laser coagulation with different wavelengths ranging from 514 to 810 nm. Lasers and Light in Ophthalmology, 1992. Vol. 5:1. pp. 9-16. ISSN:0922-5307

[112] Hale, G. Querry, M. Optical Constants of Water in the 200-nm to 200-µm Wavelength Region. Applied Optics, 1973. Vol. 12:3. pp. 555-563. ISSN: 2155-3165

[113] Chhablani, J. Roh, Y. Jobling, A. Fletcher, E. Lek, J. Bansal, P. Guymer, R. Luttrull, J. Restorative retinal laser therapy: Present state and future directions. Survey of Ophthalmology, 2018. Vol. 63:3. pp. 307-328. ISSN: 0039-6257

[114] Fennema, O. Food Chemistry, 2nd ed. New York: Marcel Dekker Inc., 1985. S. 291 ISBN: 0-8247-7449-3

[115] Kallitsis, A. Moschos, M. Ladas, I. Photodynamic Therapy Versus Thermal Laser Photocoagulation for the Treatment of Recurrent Choroidal Neovascularization due to AMD. In Vivo, 2007. Vol. 21:6. pp. 1049 - 1052. ISSN: 0258-851X

[116] Aiello, L. Northrup, J. Keyt, B. Hypoxic Regulation of Vascular Endothelial Growth Factor in Retinal Cells. JAMA Ophthalmology, 1995. Vol. 113:12. pp. 1538-1544. ISSN: 2168-6173

[117] Lip, P. Belgore, F. Blann, A. Hope-Ross, M. Gibson, J. Lip, G. Plasma VEGF and Soluble VEGF Receptor FLT-1 in Proliferative Retinopathy: Relationship to Endothelial Dysfunction and Laser Treatment. Investigative Ophthalmology & Visual Science, 2000. Vol. 41. pp. 2115-2119. ISSN: 1552-5783

[118] Stefánsson, E. The therapeutic effects of retinal laser treatment and vitrectomy. A theory based on oxygen and vascular physiology. Acta Ophthalmologica Scandinavica, 2001. Vol. 79:5, pp. 435 - 440. ISSN: 1755-3768

[119] Suzuma, I. Hata, Y. Clermont, A. Pokras, F. Rook, S. Suzuma, K. Feener, E. Aiello, L. Cyclic Stretch and Hypertension Induce Retinal Expression of Vascular Endothelial Growth

Factor and Vascular Endothelial Growth Factor Receptor—2. Diabetes, 2001. Vol. 50. ISSN: 1939-327X

[120] Mitchell, P. Liew, G. Gopinath, B. Wong, T. Age-related macular degeneration. The Lancet, 2018. Vol. 392:10153. pp. 1147-1159. ISSN: 0140-6736

[121] Guymer, R. Wu, Z. Hodgson, L. Caruso, E. Brassington, K. Tindill, N. Zaw, K. McGuinness, M. Flecher, E. Chen, F. Chakravarthy, U. Arnold, J. Heriot, W. Durkin, S. Lek, J. Harper, C. Wickremasinghe, S. Subthreshold Nanosecond Laser Interventionin Age-Related Macular Degeneration. Ophthalmology, 2019. Vol. 126:6. pp. 829-838. ISSN: 0161-6420

[122] Vessey, K. Ho, T. Jobling, A. Mills, S. Tran, M. Brandli, A. Lam, J. Guymer, R. Fletcher, E. Nanosecond Laser Treatment for Age-Related Macular Degeneration Does Not Induce Focal Vision Loss or New Vessel Growth in the Retina. Investigative Ophthalmology & Visual Science, 2018. Vol. 59:2. pp. 731-745. ISSN: 1552-5783

[123] Lavinsky, D. Wang, J. Huie, P. Dalal, R. Lee, S. Lee, D. Palanker, D. Nondamaging Retinal Laser Therapy: Rationale and Applications to the Macula. Investigative Ophthalmology & Visual Science, 2016. Vol. 57:6. pp. 2488-2500. ISSN: 1552-5783

[124] Roider, J. Brinkmann, R. Birngruber, R. Selective retinal pigment epithelium laser treatment. Published in: Fankhauser, F. Kwasiewska, S. Lasers in Ophthalmology – Basic, Diagnostic and Surgical Aspects. The Netherlands: Kugler Publications, 2003. S. 119 - 129. ISBN. – 9789062997008

[125] Brinkmann, R. Roider, J. Birngruber, R. Selective retina therapy (SRT): A review on methods, techniques, preclinical and first clinical results. Bulletin de la Societe belge d'ophtalmologie, 2006. Vol. 302:4. pp. 51 - 69. ISSN: 0081-0746

[126] Fuisting, B. Gisbert, R. Transpupillary thermotherapy (TTT) – Review of the clinical indication spectrum. Medical Laser Application, 2010. Vol. 25:4. pp. 214 - 222. ISSN: 1615-1615

[127] Brinkmann, R. Koinzer, S. Schlott, K. Ptaszynski, L. Bever, M. Baade, A. Luft, S. Miura, Y. Roider, J. Birngruber, R. Real-time temperature determination during retinal photocoagulation on patients. Journal of Biomedical Optics, 2012. Vol. 17:6. ISSN: 1083-3668

[128] Fuisting, B. Richard, G. Transpupillary thermotherapy (TTT) – Review of the clinical indicationspectrum. Medical Laser Application, 2010. Vol. 25:4. pp. 214-222. ISSN: 1615-1615

[129] Kozak, I. Luttrull, J. Modern retinal laser therapy. Saudi Journal of Ophthalmology, 2015. Vol. 29:2. pp. 137 -146. ISSN 1319-4534

[130] Desmettre, T. Maurage, C. Mordon, S. Heat Shock Protein Hyperexpression on Chorioretinal Layers After Transpupillary Thermotherapy. Investigative Ophthalmology & Visual Science, 2001. Vol. 42. pp. 2976-2980. ISSN: 1552-5783

[131] Desmettre, T. Maurage, C. Mordon, S. Transpupillary Thermotherapy (TTT) With Short Duration Laser Exposures Induce Heat Shock Protein (HSP) Hyperexpression on Choroidoretinal Layers. Lasers in Surgery and Medicine, 2003. Vol. 33:2. pp. 102-107. ISSN: 1096-9101

[132] Sramek, C. Mackanos, M. Spitler, R. Leung, L. Nomoto, H. Contag, C. Palanker, D. Non-damaging Retinal Phototherapy: Dynamic Range of Heat Shock Protein Expression. Investigative Ophthalmology & Visual Science, 2011. Vol. 52. pp. 1780-1787. ISSN: 1552-5783

[133] Kim, J. Park, K. Kim, Y. Park, H. Kim, D. Thermal Injury Induces Heat Shock Protein in the Optic Nerve Head In Vivo. Investigative Ophthalmology & Visual Science, 2006. Vol. 47. pp. 4888-4894. ISSN: 1552-5783

[134] She, X. Li, X. Yu, W. Subthreshold transpupillary thermotherapy of the retina and experimental choroidal neovascularization in a rat model. Graefe's Archive for Clinical and Experimental Ophthalmology, 2006. Vol. 244:9. pp. 1143-1151. ISSN: 1435-702X

[135] Kern, K. Mertineit, C. Brinkmann, R. Miura, Y. Expression of heat shock protein 70 and cell death kinetics after different thermal impacts on cultured retinal pigment epithelial cells. Experimental Eye Research, 2018. Vol. 170. pp. 117-126. ISSN: 0014-4835

[136] Wang, J. Huie, P. Dalal, R. Lee, S. Tan, G. Lee, D. Lavinsky, D. Palanker, D. Heat shock protein expression as guidance for the therapeutic window of retinal laser therapy. Proceedings of SPIE, 2016. Vol. 9693. ISSN: 1996-756X

[137] Inagaki, K. Shuo, T. Katakura, K. Ebihara, N. Murakami, A. Ohkoshi, K. Sublethal Photothermal Stimulation with a Micropulse Laser Induces Heat Shock Protein Expression in ARPE-19 Cells. Journal of Ophthalmology, 2015. Vol. 2015. Article ID 729792. ISSN: 2090-0058

[138] Virgili, G. Michelessi, M. Parodi, M. Bacherini, D. Evans, J. Laser Treatment of Drusen to Prevent Progression to Advanced Age-Related Macular Degeneration. Cochrane Database of Systematic Reviews 2015, Issue 10. Article number: CD006537. DO1 10.1002/14651858.CD006537.pub3.

[139] Shiber, A. Ravid, T. Chaperoning Proteins for Destruction: Diverse Roles of Hsp70 Chaperones and their Co-Chaperones in Targeting Misfolded Proteins to the Proteasome. Biomolecules, 2014. Vol. 4:3. pp. 704-724

[140] Zhang, J. Sun, Y. Hussain, A. Marshall, J. Laser-Mediated Activation of Human Retinal Pigment Epithelial Cells and Concomitant Release of Matrix Metalloproteinases.

Investigative Ophthalmology & Visual Science, 2012. Vol. 53. pp. 2928-2937. ISSN: 1552-5783

[141] Jobling, A. Guymer, R. Vessey, A. Greferath, U. Mills, S. Brassington, L. Aung, K. Trogrlic, L. Plunkett, M. Fletcher, E. Nanosecond laser therapy reverses pathologic and molecular changes in age-related macular degeneration without retinal damage. The FASEB Journal, 2015. Vol. 29. pp. 696-710. ISSN: 1530-6860

[142] Richert, E. Koinzer, S. Tode, J. Schlott, K. Brinkmann, R. Hillenkam, J. Klettner, A. Roider, J. Release of Different Cell Mediators During Retinal Pigment Epithelium Regeneration Following Selective Retina Therapy. Investigative Ophthalmology & Visual Science, 2018. Vol. 59. pp. 1323-1331. ISSN: 1552-5783

[143] Li, Z. Song, Y. Chen, X. Chen, Z. Ding, Q. Biological Modulation of Mouse RPE Cells in Response to Subthreshold Diode Micropulse Laser Treatment. Cell Biochemistry and Biophysics, 2015. Vol. 73:2. pp. 545-552. ISSN: 1559-0283

[144] Cordeiro, S. Seyler, S. Sindl, J. Milenkovic, V. Strauss, O. Heat-Sensitive TRPV Channels in Retinal Pigment Epithelial Cells: Regulation of VEGF-A Secretion. Investigative Ophthalmology & Visual Science, 2010. Vol. 51. pp. 6001-6008. ISSN: 1552-5783

[145] Faby, H. Hillenkamp, J. Roider, J. Klettner, A. Hyperthermia-induced upregulation of vascular endothelial growth factor in retinal pigment epithelial cells is regulated by mitogen-activated protein kinases. Graefe's Archive for Clinical and Experimental Ophthalmology, 2014. Vol. 252:11. pp. 1737-1745. ISSN: 1435-702X

[146] Iwami, H. Pruessner, J. Shraki, K. Brinkmann, R. Miura, Y. Protective effect of a laser-induced sub-lethal temperature rise on RPE cells from oxidative stress. Experimental Eye Research, 2014. Vol. 124. pp. 37-47. ISSN: 0014-4835

[147] Cillà, S. Vezzola, D. Farruggio, S. Vujosevic, S. Clemente, N. Raina, G. Mary, D. Casini, G. Rossetti, L. Avagliano, L. Martinelli, C. Bulfamante, G. Grossini, E. The subthreshold micropulse laser treatment of the retina restores the oxidant/antioxidant balance and counteracts programmed forms of cell death in the mice eyes. Acta Ophthalmologica, 2018. Vol. 97:4. pp. e559-e567. ISSN: 1755-3768

[148] Treumer, F. Klettner, A. Baltz, J. Hussain, A. Miura, Y. Brinkmann, R. Roider, J. Hillenkamp, J. Vectorial release of matrix metalloproteinases (MMPs) from porcine RPE-choroid explants following selective retina therapy (SRT): Towards slowing the macular ageing process. Experimental Eye Research, 2012. Vol. 97:1. pp. 63-72. ISSN: 0014-4835

[149] Sims, J. McCready, J. Jay, D. Extracellular Heat Shock Protein (Hsp) 70 and Hsp90a Assist in Matrix Metalloproteinase-2 Activation and Breast Cancer Cell Migration and Invasion. Plos One, 2011. Vol. 6:4. ISSN: 1932-6203

[150] Wang, J. Quan, Y. Dalal, R. Palanker, D. Comparison of Continuous-Wave and Micropulse Modulation in Retinal Laser Therapy. Investigative Ophthalmology & Visual Science, 2017. Vol. 58. pp. 4722-4732. ISSN: 1552-5783

[151] Sramek, C. Paulus, Y. Nomoto, H. Huie, P. Brown, J. Palanker, D. Dynamics of retinal photocoagulation and rupture. Journal of Biomedical Optics, 2009. Vol. 14:3. ISSN: 1560-2281

[152] Sramek, C. Mackanos, M. Spitler, R. Leung, L. Nomoto, H. Contag, C. Palanker, D. Non-damaging Retinal Phototherapy: Dynamic Range of Heat Shock Protein Expression. Investigative Ophthalmology & Visual Science, 2011. Vol. 52. pp. 1780-1787. ISSN: 1552-5783

[153] Barbe, M. Tytell, M. Gower, D. Welch, W. Hyperthermia Protects Against Light Damage in the Rat Retina. Science, 1988. Vol. 241:4874. pp. 1817-1820. ISSN: 1095-9203

[154] Tytell, M. Barbe, M. Brown, I. Induction of Heat Shock (Stress) Protein 70 and Its mRNAin the Normal and Light-Damaged Rat Retina After Whole Body Hyperthermia. Journal of Neuroscience Research, 1994. Vol. 38. pp. 19-31. ISSN: 1097-4547

[155] Kawana, K. Miyamoto, Y. Tanonaka, K. Han-no, Y. Yoshida, H. Takahashi, M. Takeo, S. Cytoprotective Mechanism of Heat ShockProtein 70 against Hypoxia/ReoxygenationInjury. Journal of Molecular and Cellular Cardiology, 2000. Vol. 32:12. pp. 2229-2237. ISSN: 0022-2828

[156] Gowda, A. Yang, C. Asimakis, G. Rastegar, S. Motamedi, M. Heat Shock Improves Recovery and Provides Protection Against Global Ischemia After Hypothermic Storage. The Annals of Thoracic Surgery, 1998. Vol. 66:6. pp. 1991-1997. ISSN: 0003-4975

[157] Rordorf, G. Koroshetz, W. Bonventre, J. Heat shock protects cultured neurons from glutamate toxicity. Neuron, 1991. Vol. 7:6. pp. 1043-1051. ISSN: 0896-6273

[158] Rylander, M. Diller, K. Wang, S. Aggrawal, S. Correlation of HSP70 Expression and Cell Viability Following Thermal Stimulation of Bovine Aortic Endothelial Cells. Journal of Biomechanical Engineering, 2005. Vol. 127:5. pp. 751-757. ISSN: 0148-0731

[159] Du, S. Zhang, Q. Zhang, S. Wang, L. Lian, J. Heat shock protein 70 expression induced by diode laser irradiation on choroid-retinal endothelial cells in vitro. Molecular Vision, 2012. Vol. 18. pp. 2380-2387. ISSN: 1090-0535

[160] Creel, D. The Electroretinogram and Electro-oculogram: Clinical Applications. Webvision. Moran Eye Center, 7.6.2019.
Available at: https://webvision.med.utah.edu/book/electrophysiology/the-electroretinogram-clinical-applications/

[161] Perlman, I. The Electroretinogram: ERG. Webvision. Moran Eye Center, 18.11.2018. Available at: https://webvision.med.utah.edu/book/electrophysiology/the-electroretinogram-erg/

[162] Vinberg, F. Ionic Mechanisms in Mouse Rod Photoreceptor Signaling. Doctoral Dissertation. Aalto University, School of Science, Department of Biomedical Engineering and Computational Science. Espoo. 2011. pp. 41-43

[163] Green, D. Kapousta-Bruneau, N. A dissection of the electroretinogram from the isolated rat retina with microelectrodes and drugs. Visual Neuroscience, 1999. Vol. 16. pp. 727-741. ISSN: 1469-8714

[164] Pepperberg, D. Brown, P. Lurie, M. Dowling, J. Visual pigment and photoreceptor sensitivity in the isolated skate retina. Journal of General Physiology, 1978. Vol. 71:4. pp. 369-396. ISSN: 1540-7748

[165] Pitkänen, M. Kaikkonen, O. and Koskelainen, A. A Novel Method for Mouse Retinal Temperature Determination Based on ERG Photoresponses. Ann. Biomed. Eng., 2017. Vol. 45:10. pp. 2360–2372, 2017.

[166] Lipman, N. Jackson, L. Trudel, J. Weis-Garcia, F. 2005. Monoclonal Versus Polyclonal Antibodies: Distinguishing Characteristics, Applications, and Information Resources. ILAR Journal. Vol. 46:3. pp. 258-268. ISSN: 1930-6180

[167] Koivunen, M. Krogsrud, R. 2006. Principles of Immunochemical Techniques Used in Clinical Laboratories. Lab Medicine. Vol 37:8. pp. 490-497. ISSN: 1943-7730

[168] Lichtman, J. Conchello, J. Fluorescence microscopy. Nature Methods, 2005. Vol. 2:12. pp. 910-919. ISSN: 1548-7091

[169] Schacht, V. Kern, J. Basics of Immunohistochemistry. Journal of Investigative Dermatology, 2015. Vol. 135. ISSN: 0022-202X

[170] Warford, A. Akbar, H. Riberio, D. Antigen retrieval, blocking, detection and visualisation systems in immunohistochemistry: A review and practical evaluation of tyramide and rolling circle amplification systems. Methods, 2014. Vol. 70:1. pp. 28-33. ISSN: 1046-2023

[171] Shi, S. Cote, R. Taylor, C. Antigen Retrieval Immunohistochemistry: Past, Present, and Future. Journal of Histochemistry & Cytochemistry, 1997. Vol. 45. pp. 327-343. ISSN: 1551-5044

[172] Ramos-Vara, J. Technical Aspects of Immunohistochemistry. Veterinary Pathology, 2005. Vol. 42. pp. 405-426. ISSN: 1544-2217

[173] Ravikumar, S. Surekha, R. Thavarajah, R. Mounting media: An overview. Journal of Dr. NTR University of Health Sciences, 2014. Vol. 3:5. pp. 1-8. ISSN: 2277-8632

[174] Kaikkonen, O. A Device for Controlled Heating of Mouse Retinal Pigment Epithelium. Master's thesis. Aalto University School of Science Department of Neuroscience and Biomedical Engineering. Espoo. 2018.

[175] The Jackson Laboratory. Life Span as a Biomarker [Website]. [13.1.2019] Available at: https://www.jax.org/research-and-faculty/research-labs/the-harrison-lab/gerontology/life-span-as-a-biomarker

[176] Kalloniatis, M. Luu, C. Temporal Resolution. Webvision. Moran Eye Center, 2.2.2019. Available at: https://webvision.med.utah.edu/book/part-viii-psychophysics-of-vision/temporal-resolution/

[177] André H, Tunik S, Aronsson M, Kvanta A. Hypoxia-inducible factor-1alpha is associated with sprouting angiogenesis in the murine laser-induced choroidal neovascularization model. Invest Ophthalmol Vis Sci. 2015. 56:11. pp. 6591-6604. ISSN: 1552-5783

[178] Songwon, S. A Review and Comparison of Methods for Detecting Outliers in Univariate Data Sets. Master's Thesis. University of Pittsburgh. 2006. Available at: http://d-scholarship.pitt.edu/7948/1/Seo.pdf

[179] Steiger, J. Tests for Comparing Elements of a Correlation Matrix. Psychological Bulletin, 1980. Vol. 87:2. pp. 245-251. ISSN: 1939-1455

[180] Williams, M. Pinto, L. Gherson, J. The Retinal Pigment Epithelium of Wild Type (C57BL/6J + / +) and Pearl Mutant (C57BL/6J pe/pe) Mice. Investigative Ophthalmology & Visual Science May, 1985. Vol. 26. pp. 657-669. ISSN: 1552-5783

[181] Howell, W. Rapp, L. Williams, T. Distribution of melanosomes across the retinal pigment epithelium of a hooded rat: implications for light damage. Investigative Ophthalmology & Visual Science, 1982. Vol. 22. pp. 139-144. ISSN: 1552-5783

[182] Gabel, V. Bringruber, R. Hillenkamp, F. Visible and near infrared light absorption in pigment epithelium and choroid. International Congress Series No. 450. XXIII Concilium Ophthaimologicum, Kyoto, 1978. Elsevier. ISBN 0 444 90060 8

[183] Sarna, T. Burke, J. Korytowski, W. Rózanowska, M. Skumatz, C. Zareba, A. Zareba, M. Loss of melanin from human RPE with aging: possible role of melanin photooxidation. Experimental Eye Research, 2003. Vol. 76:1. pp. 89-98. ISSN: 0014-4835

[184] Sramek, C. Paulus, Y. Nomoto, H. Huie, P. Brown, J. Palanker, D. Dynamics of retinal photocoagulation and rupture. Journal of Biomedical Optics, 2009. Vol. 14:3. ISSN: 1560-2281

[185] Ikeda, W. Nakatani, T. Uemura, A. Cataract-preventing contact lens for in vivo imaging of mouse retina. BioTechniques, 2018. Vol. 65:2. pp. 101-104. ISSN: 1940-9818

[186] Semenyuk, V. Prediction of temperature and damage in an irradiated human eye during retinal photocoagulation. International Journal of Heat and Mass Transfer, 2018. Vol. 126. pp. 306-316. ISSN: 0017-9310

[187] Baade, A. Burchard, C. Lawin, M. Koinzer, S. Schmarbeck, B. Schlott, K. Miura, Y. Roider, J. Birngruber, R. Brinkmann, R. Power-controlled temperature guided retinal laser therapy. Journal of Biomedical Optics, 2017. Vol. 22:11. ISSN: 1560-2281

[188] Kandulla, J. Elsner, H. Birngruber, R. Brinkmann, R. Noninvasive optoacoustic online retinal temperature determination during continuous-wave laser irradiation. Journal of Biomedical Optics, 2006. Vol. 11:4. ISSN: 1560-2281

[189] Cain, C. Welch, A. Measured and predicted laser-induced temperature rises in the rabbit fundus. Investigative Ophthalmology & Visual Science, 1975. Vol. 13. pp. 60-70. ISSN: 1552-5783

[190] Priebe, L. Cain, C. Welch, A. Temperature Rise Required for Production of Minimal Lesions in the Macaca Mulatta Retina. American Journal of Ophthalmology, 1975. Vol. 79:3. pp. 405-413. ISSN: 0002-9394

[191] Schulte, P. Healy, T. Fangue, N. Thermal Performance Curves, Phenotypic Plasticity, and the Time Scales of Temperature Exposure. Integrative and Comparative Biology, 2011. Vol. 51: 5. pp. 691-702. ISSN: 1557-7023

[192] Kingsolver, J. The Will-Temperatured Biologist. The American Naturalist, 2009. Vol. 174:6. pp. 755-768. ISSN: 0003-0147

[193] Nymark, S. Private discussion on November 8, 2018. Tampere University

Appendix

This appendix contains larger versions of the images of stained and flat-mounted RPEs after heating with treatment factors 2, 2.5 and 3 presented in the body text. In these figures, the arrow indicates the location of the optic disk. The right eye of the mouse was always treated and the left eye acted as a control.

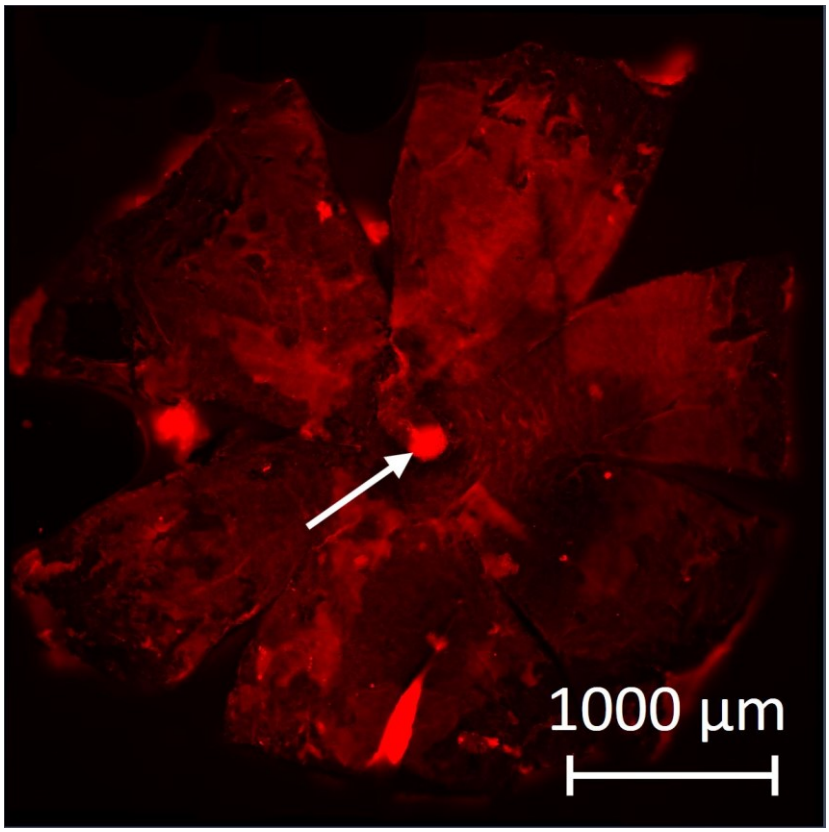

Figure A1. *Stained and flat-mounted RPE after heating with treatment factor 2. HSPA staining of the control eye. This figure is the same as Figure 24 A presented in the body text.*

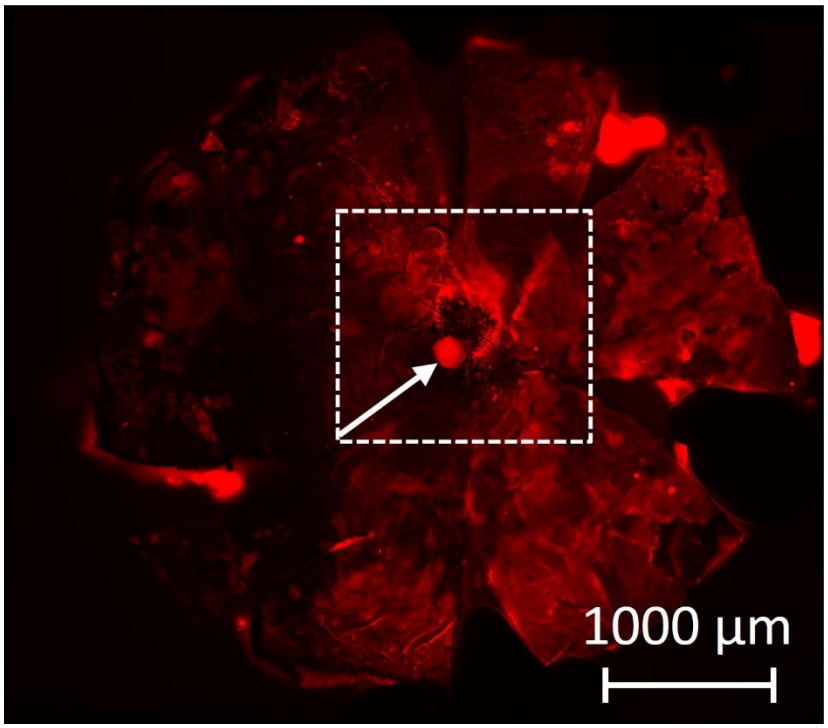

Figure A2. *Stained and flat-mounted RPE after heating with treatment factor 2. HSPA staining of the treated eye. This figure is the same as Figure 24 B presented in the body text.*

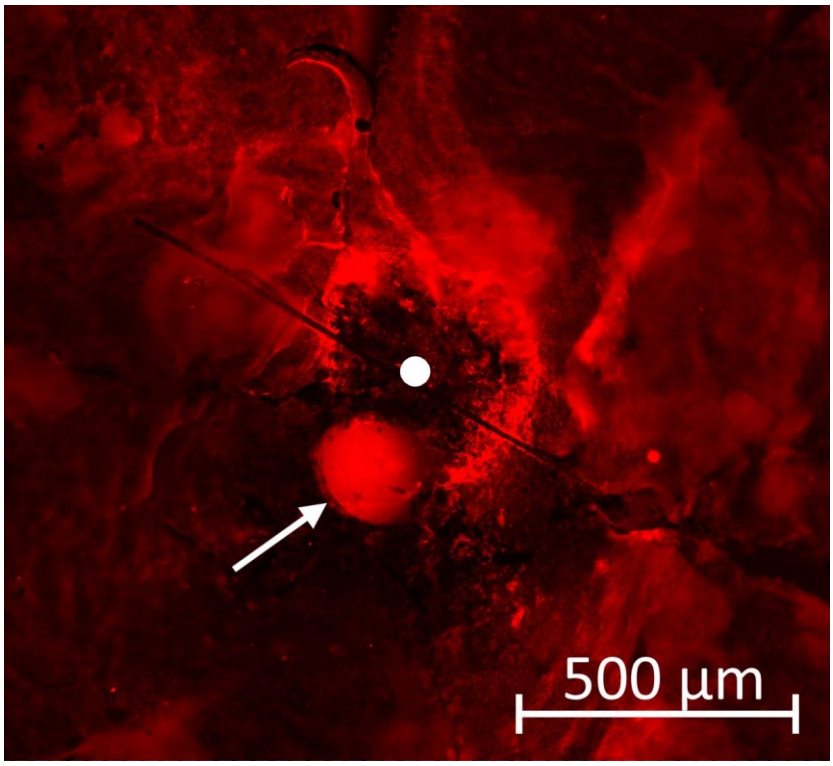

Figure A3. *Stained and flat-mounted RPE after heating with treatment factor 2. Close-up image of the heated area. Image borders are indicated with a dashed rectangle in Figure A2. This figure is the same as Figure 24 C presented in the body text.*

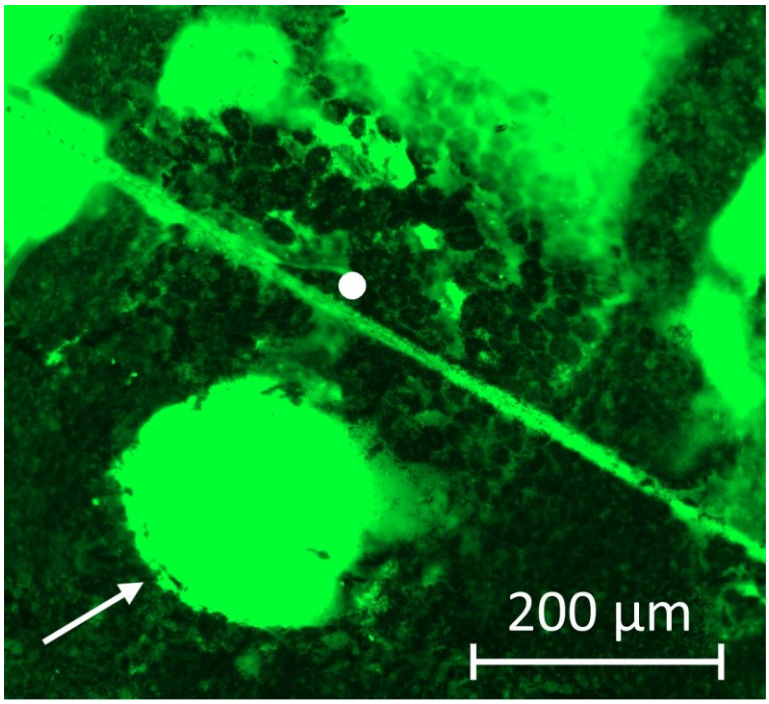

Figure A4. *Stained and flat-mounted RPE after heating with treatment factor 2. Phalloidin staining of the center of heated area. The location of the white dot is the same as in Figure A3. This figure is the same as Figure 24 D presented in the body text.*

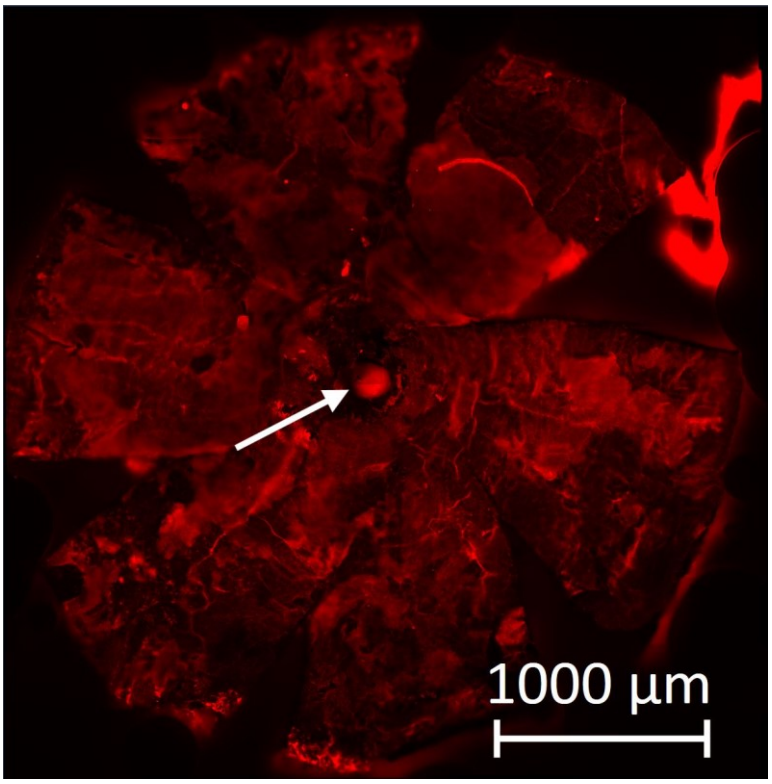

Figure A5. *Stained and flat-mounted RPE after heating with treatment factor 2.5. HSPA staining of the control eye. This figure is the same as Figure 25 A presented in the body text.*

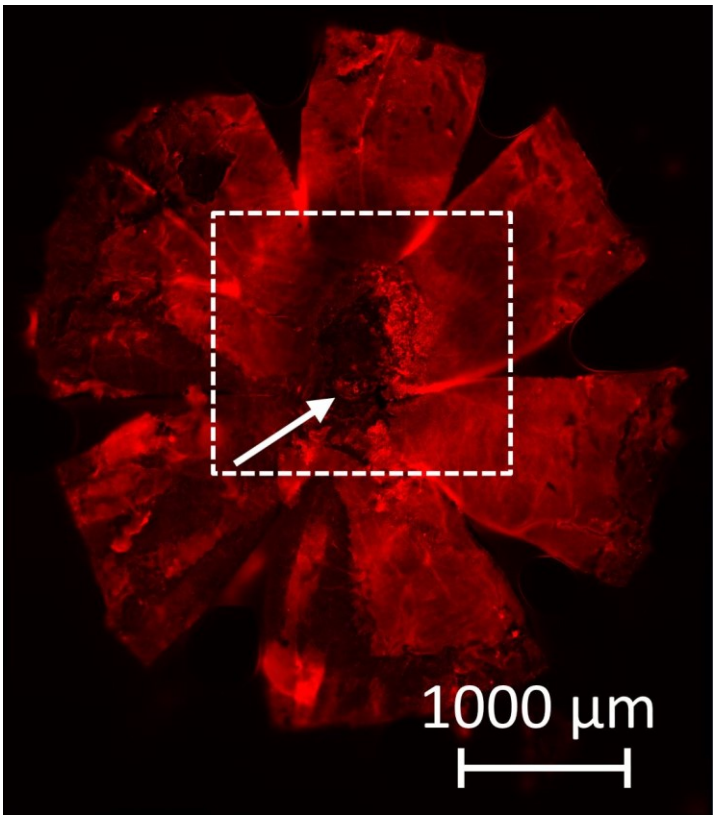

Figure A6. *Stained and flat-mounted RPE after heating with treatment factor 2.5. HSPA staining of the treated eye. This figure is the same as Figure 25 B presented in the body text.*

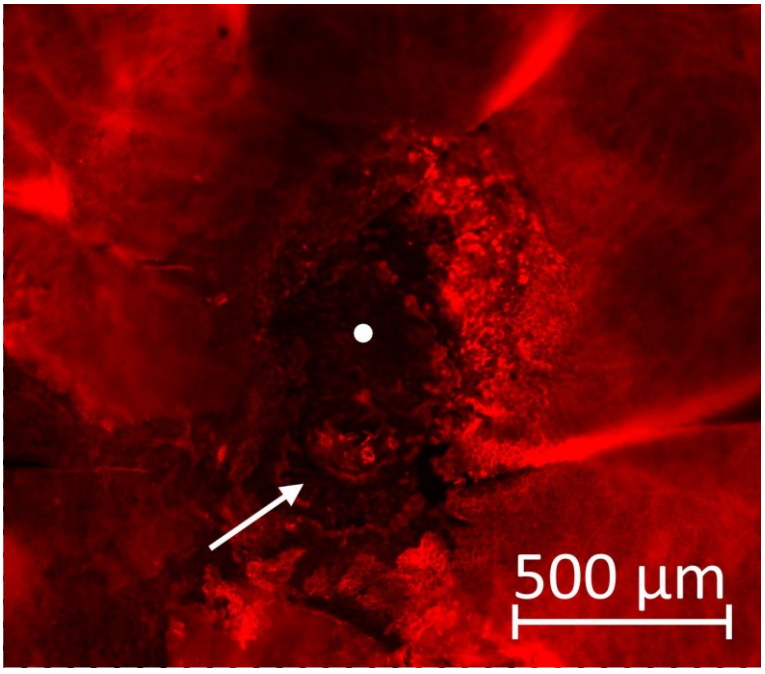

Figure A7. *Stained and flat-mounted RPE after heating with treatment factor 2.5. Close-up image of the heated area. Image borders are indicated with a dashed rectangle in Figure A6. This figure is the same as Figure 25 C presented in the body text.*

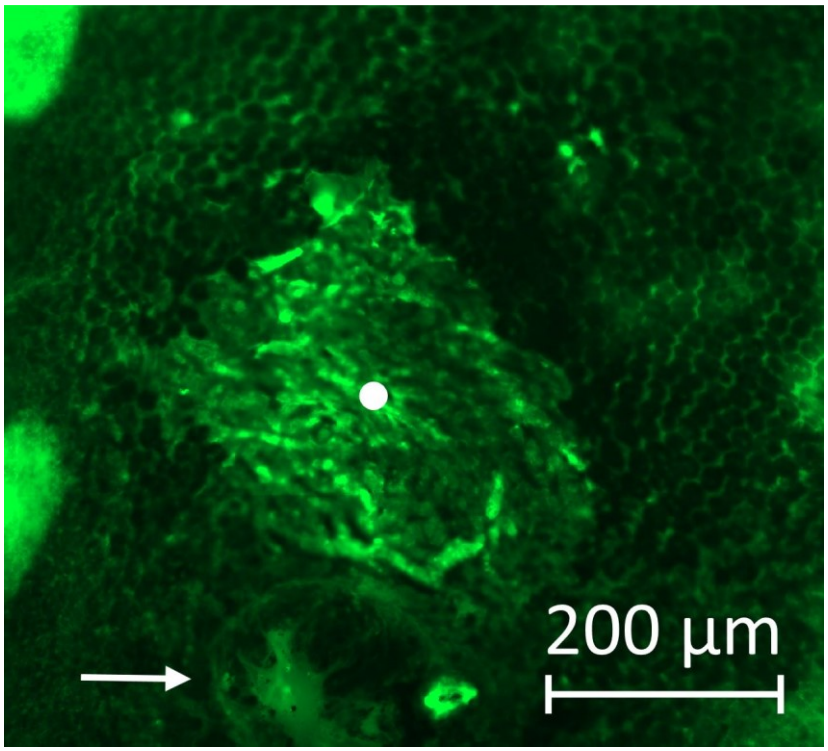

Figure A8. *Stained and flat-mounted RPE after heating with treatment factor 2.5. Phalloidin staining of the center of heated area. The brighter area at the center of the figure is probably neural retina that was not properly removed during dissection. The location of the white dot is the same as in Figure A7. This figure is the same as Figure 25 D presented in the body text.*

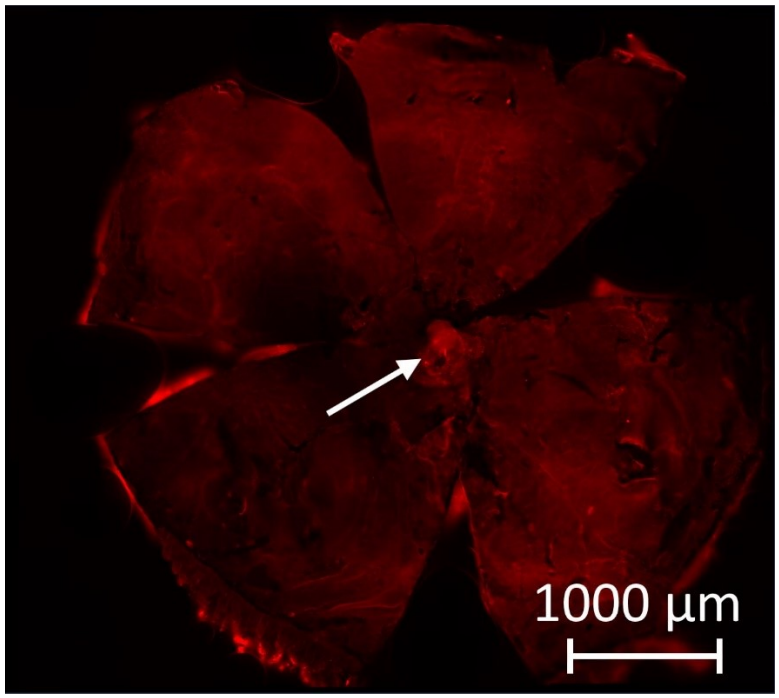

Figure A9. *Stained and flat-mounted RPE after heating with treatment factor 3. HSPA staining of the control eye. This figure is the same as Figure 26 A presented in the body text.*

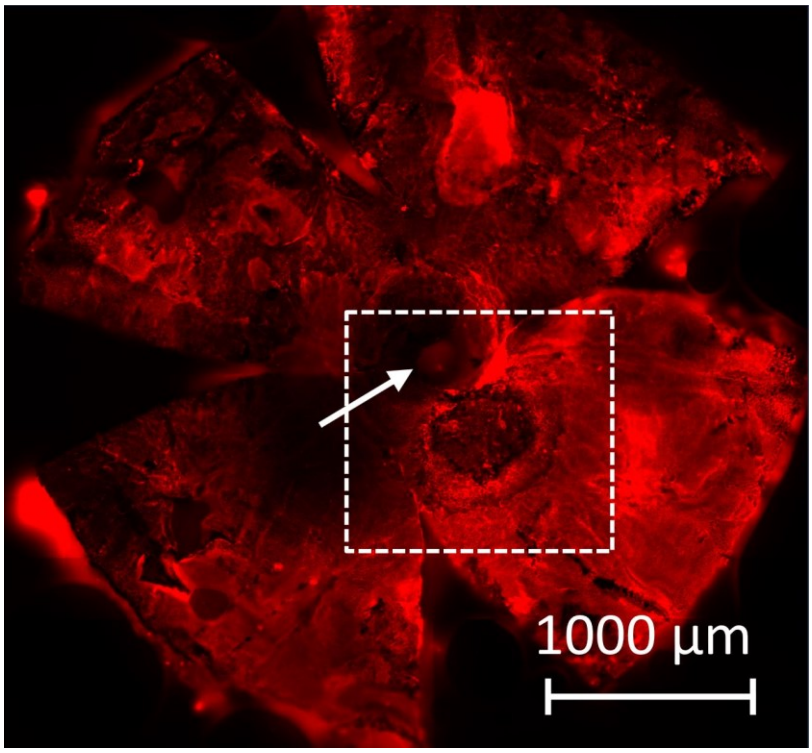

Figure A10. *Stained and flat-mounted RPE after heating with treatment factor 3. HSPA staining of the treated eye. This figure is the same as Figure 26 B presented in the body text.*

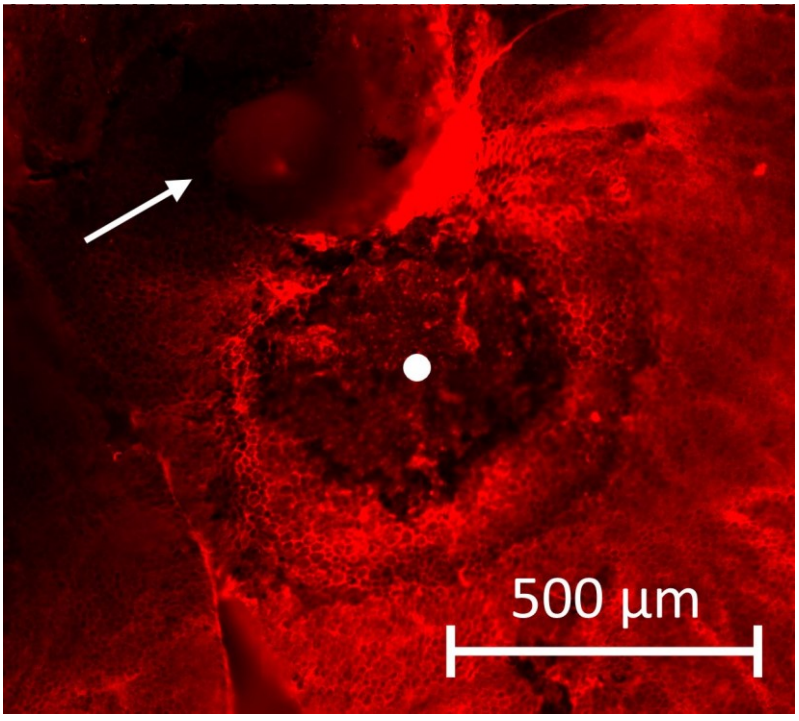

Figure A11. *Stained and flat-mounted RPE after heating with treatment factor 3. Close-up image of the heated area. Image borders are indicated with a dashed rectangle in Figure A10. This figure is the same as Figure 26 C presented in the body text.*

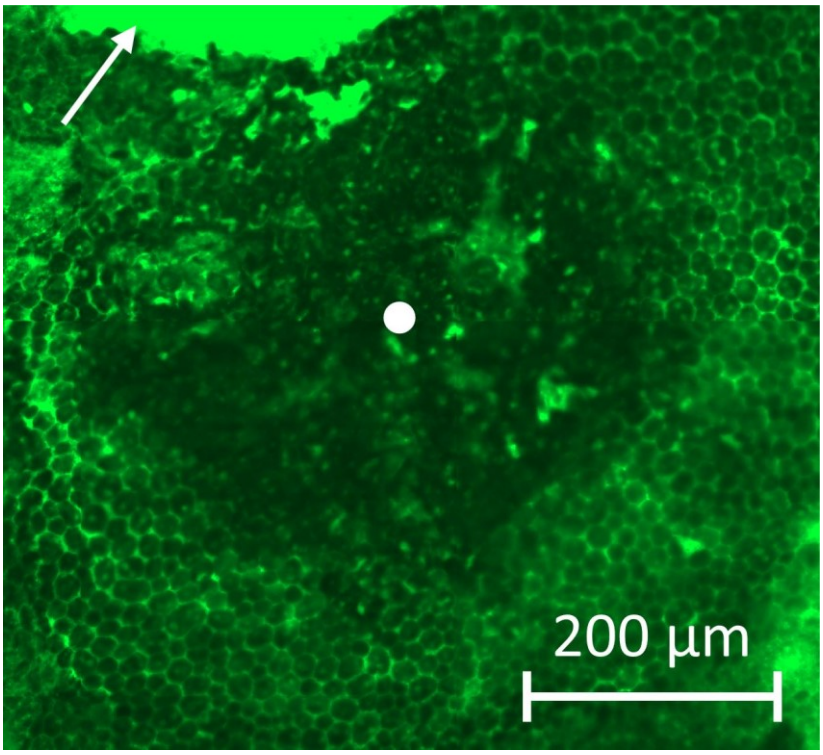

Figure A12. *Stained and flat-mounted RPE after heating with treatment factor 3. Phalloidin staining of the center of heated area. The location of the white dot is the same as in Figure A11. This figure is the same as Figure 26 D presented in the body text.*